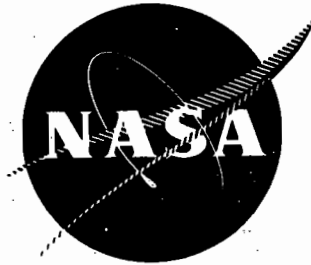


PAUL WILBUR

NASA CR - 135019

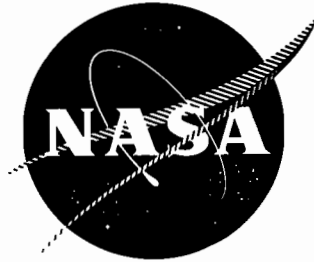


DOUBLE ION PRODUCTION IN MERCURY THRUSTERS

PREPARED FOR
LEWIS RESEARCH CENTER
NATIONAL AERONAUTICS AND SPACE ADMINISTRATION
Grant NGR-06-002-112

by
Ralph R. Peters

Approved by
Paul J. Wilbur
April 1976
Department of Mechanical Engineering
Colorado State University
Fort Collins, Colorado

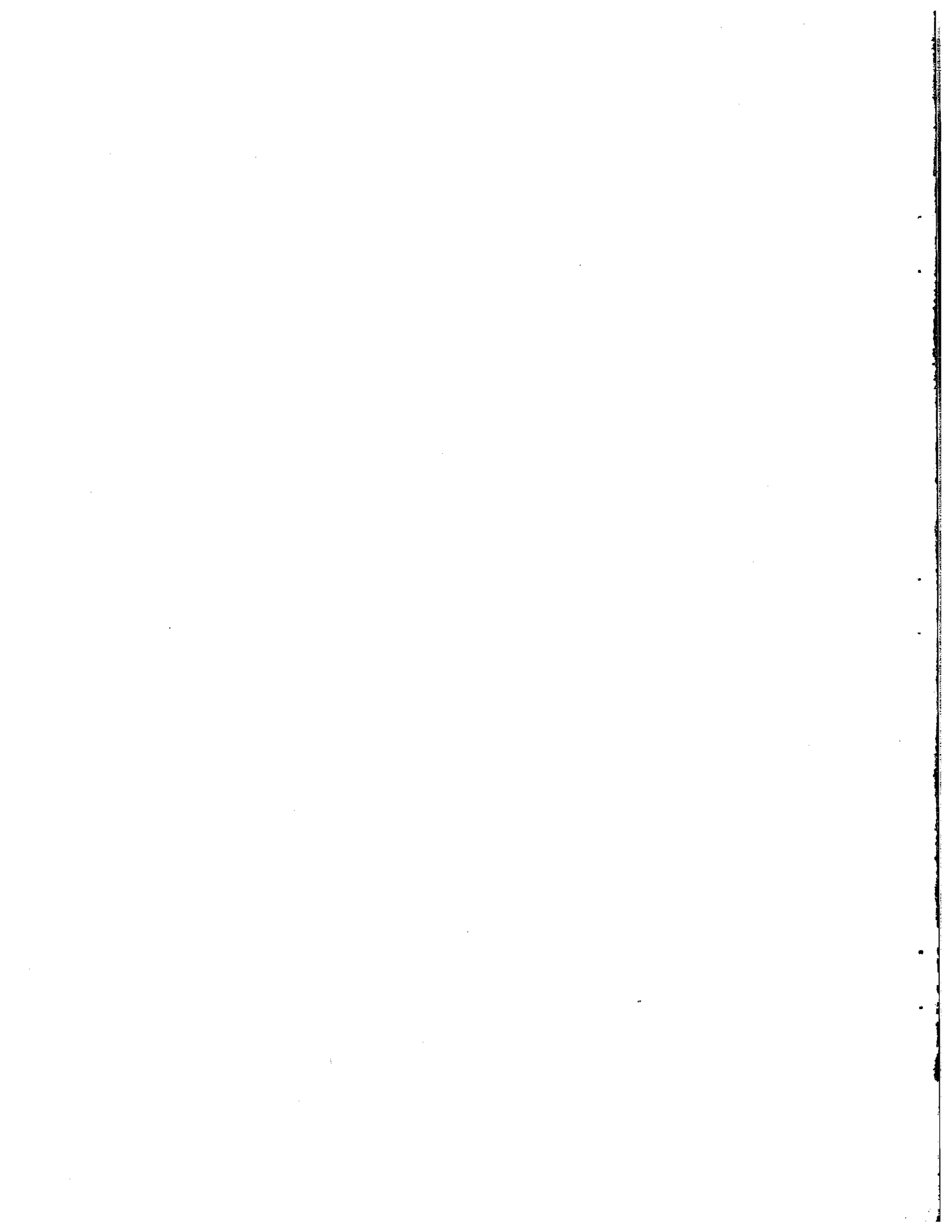


DOUBLE ION PRODUCTION IN MERCURY THRUSTERS

PREPARED FOR
LEWIS RESEARCH CENTER
NATIONAL AERONAUTICS AND SPACE ADMINISTRATION
Grant NGR-06-002-112

by
Ralph R. Peters

Approved by
Paul J. Wilbur
April 1976
Department of Mechanical Engineering
Colorado State University
Fort Collins, Colorado



1. Report No. NASA CR - 135019		2. Government Accession No.		3. Recipient's Catalog No.	
4. Title and Subtitle DOUBLE ION PRODUCTION IN MERCURY THRUSTERS				5. Report Date May, 1976	
				6. Performing Organization Code	
7. Author(s) Ralph R. Peters and Paul J. Wilbur				8. Performing Organization Report No.	
9. Performing Organization Name and Address Department of Mechanical Engineering Colorado State University Fort Collins, Colorado 80523				10. Work Unit No.	
				11. Contract or Grant No. NGR-06-002-112	
12. Sponsoring Agency Name and Address National Aeronautics and Space Administration Washington, D. C. 20546				13. Type of Report and Period Covered	
				14. Sponsoring Agency Code	
15. Supplementary Notes Grant Monitor - William Kerslake, NASA Lewis Research Center, Cleveland, Ohio 44135. This report is a reproduction of the M.S. Thesis of Mr. Ralph R. Peters. It is submitted to the sponsor and to the distribution list in this form both as a presentation of the technical material, and as an indication of the academic program supported by this Grant.					
16. Abstract <p>Significant densities of doubly charged ions exist in the discharge chambers of electron bombardment ion thrusters. These ions are undesirable because they are a major plasma constituent effecting the sputtering damage which limits thruster lifetime. It would be desirable to reduce their density while maintaining good thruster performance. The development of a model which predicts the doubly charged ion density is discussed. The accuracy of the model is shown to be good for two different thruster sizes and a total of 11 different cases. The model indicates that in most cases more than 80% of the doubly charged ions are produced from singly charged ions. This result can be used to develop a much simpler model which, along with correlations of the average plasma properties, can be used to determine the doubly charged ion density in ion thrusters with acceptable accuracy. Two different techniques which can be used to reduce the doubly charged ion density, while maintaining good thruster operation, are identified as a result of an examination of the simple model. First, the electron density can be reduced and the thruster size then increased to maintain the same propellant utilization. Second, at a fixed thruster size, the plasma density, temperature and energy can be reduced and then to maintain a constant propellant utilization the open area of the grids to neutral propellant loss can be reduced through the use of a small hole accelerator grid. The reduction in the values of the plasma properties causes a decrease in the doubly charged ion density.</p>					
17. Key Words (Suggested by Author(s)) Electrostatic Thruster Mercury Discharge Chamber Model				18. Distribution Statement Unclassified - Unlimited	
19. Security Classif. (of this report) Unclassified		20. Security Classif. (of this page) Unclassified		21. No. of Pages 85	22. Price*

* For sale by the National Technical Information Service, Springfield, Virginia 22161

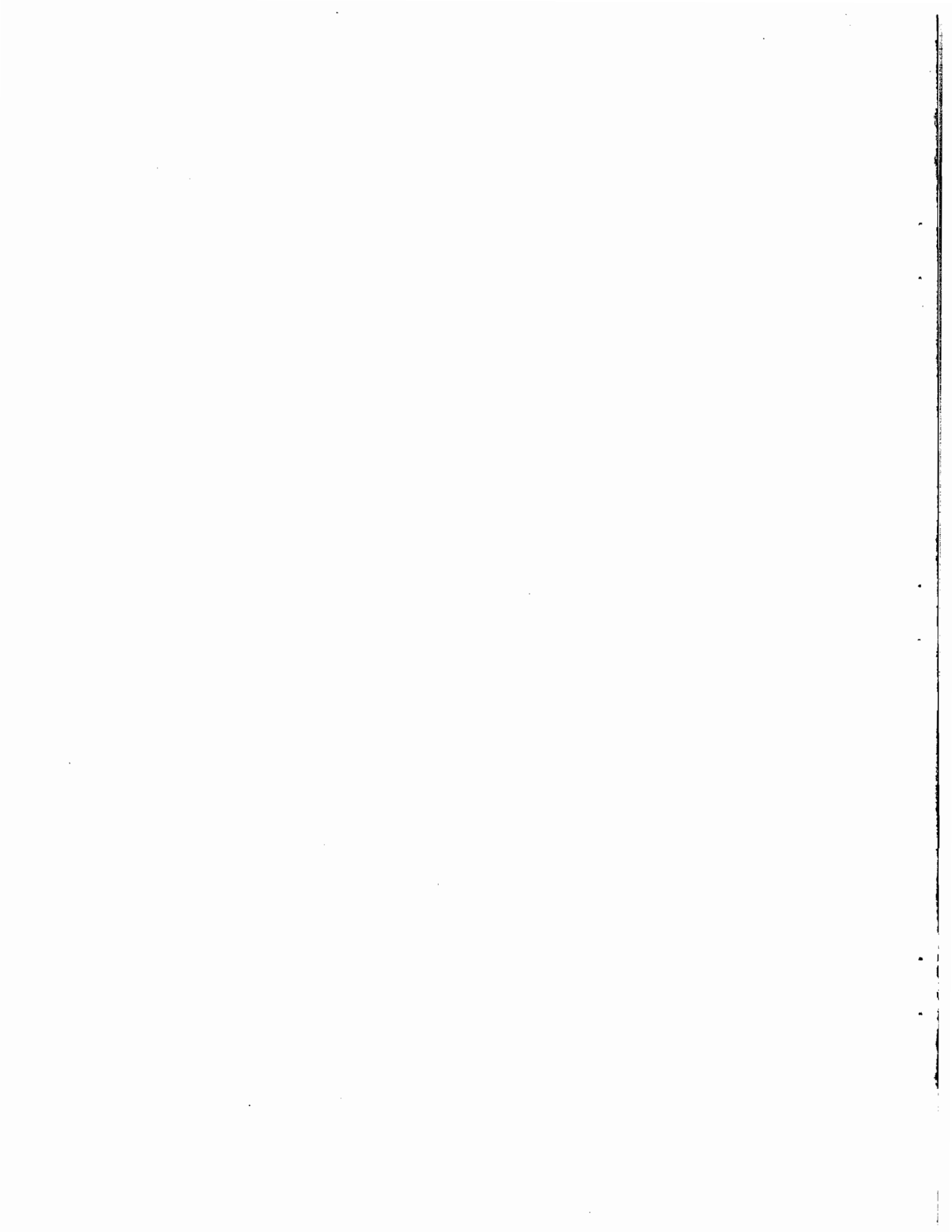
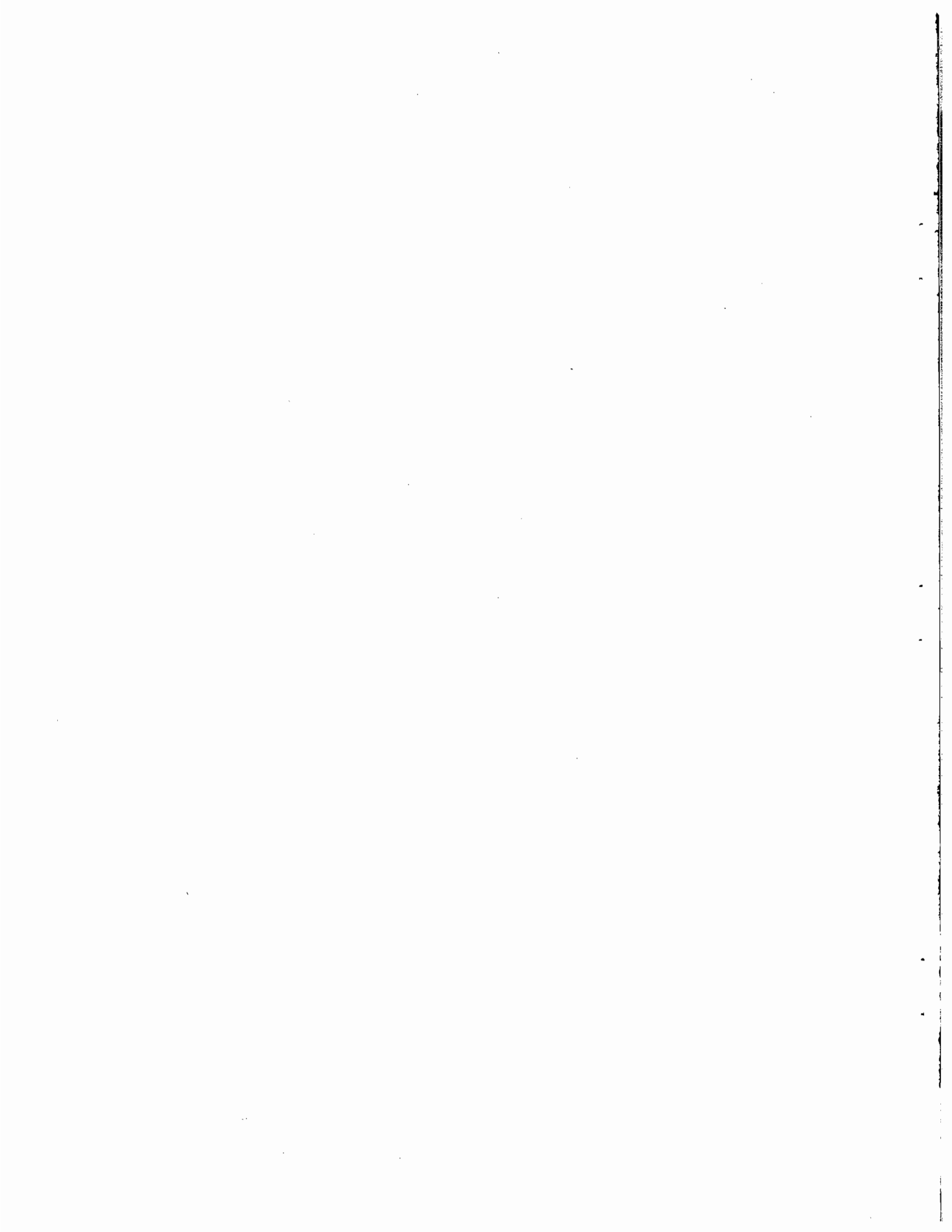


TABLE OF CONTENTS

	<u>Page</u>
ABSTRACT	i
TABLE OF CONTENTS	ii
LIST OF TABLES	iii
LIST OF FIGURES	iii
INTRODUCTION	1
THRUSTER OPERATION	2
THEORETICAL MODEL	6
Introduction	6
Electron Bombardment Reactions	10
Migration Losses	16
Photon Diffusion Losses	19
Determination of Specie Densities	21
EXPERIMENTAL PROCEDURES AND RESULTS	24
RESULTS AND DISCUSSION	32
SIMPLIFIED MODEL	39
CONCLUSIONS	55
REFERENCES	56
APPENDIX A: Listing of the Computer Program HG	58
APPENDIX B: Listing of the Computer Program PROP	73

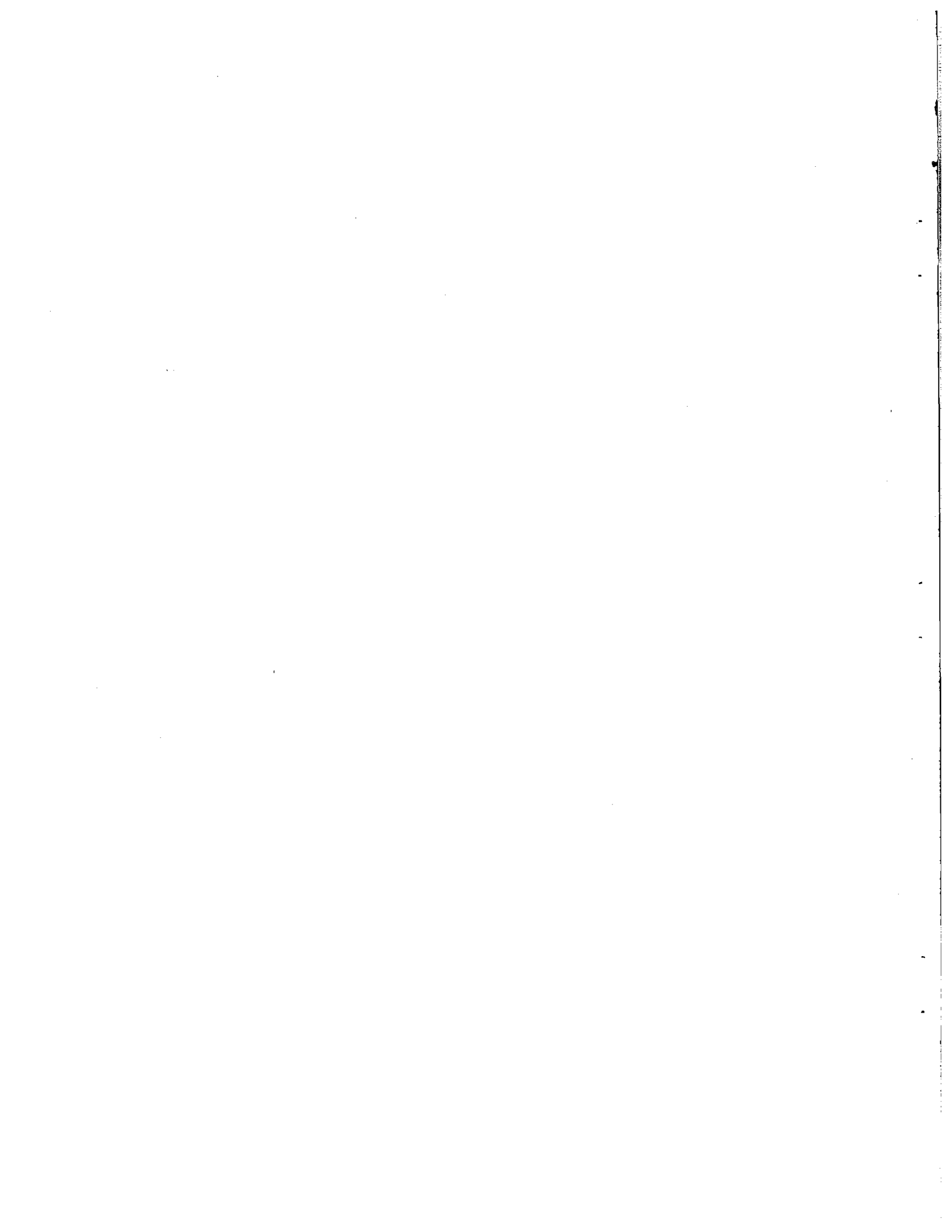


LIST OF TABLES

<u>Table Number</u>	<u>Page</u>
I Thruster Sizes, Configurations and Conditions	26
II Experimental Results	29
III Predicted Densities and Reaction Rates	36
IV Determination of the Double Ion Density Using the Simplified Model	51

LIST OF FIGURES

<u>Figure Number</u>	<u>Page</u>
1 Electron Bombardment Ion Thruster Schematic	3
2 Discharge Chamber Reaction Schematic	7
3 Mercury Cross Sections	12
4 Plasma Property Profiles, 15 cm Thruster - SERT II Grids - 37 V Anode Voltage	28
5 Double-to-Single Ion Density Ratio in a 15 cm Diameter Thruster	33
6 Double-to-Single Ion Density Ratio in a 30 cm Diameter Thruster	34
7 Rate Factors for $Hg^+ \rightarrow Hg^{++}$	41
8 Maxwellian Electron Temperature Correlation	43
9 Primary Electron Energy Correlation	45
10 Electron Density Correlation	47
11 Primary Electron Density Correlation	48
12 Uniformity Factor Correlation	49



INTRODUCTION

Electron bombardment ion thrusters are presently being considered for use in deep space probes and for satellite stationkeeping functions. These devices which have the advantage of very high specific impulses also have the attendant disadvantage of low thrust densities. This low thrust characteristic necessitates thruster operation for long periods of time in order to accomplish typical missions (of the order of 10,000 hours). Thruster lifetimes can be limited by the erosion of ion chamber component parts with most of this erosion (or sputtering damage) being caused by doubly charged ions. Long thruster lifetimes therefore require control of doubly charged ion densities.

Many experiments could be performed to determine how the thruster should be operated so that thruster performance would be good and the doubly charged ion density would be reduced to an acceptable level. However, these experiments would have the disadvantage of being time consuming and costly and the results might be applicable to one size and type of thruster only. Instead a theoretical model could be developed which would accurately predict the doubly charged ion density over a wide range of conditions and thruster sizes. This model could be applied at low cost to determine the factors affecting the doubly charged ion density and how they should be adjusted to reduce the double ion density. It should also indicate what effects these changes would have on thruster performance. Such a model has been developed for electron bombardment ion thrusters and has been verified experimentally for thrusters which use mercury propellant. A discussion of the model's development and verification is presented in this paper along with some results and conclusions based upon the model.

THRUSTER OPERATION

Many of the assumptions and approximations used in the development of the model are based upon a knowledge of thruster operation. This section will briefly discuss thruster operation so that the development of the model in the next section will be more easily understood. An ion thruster has two basic tasks to perform:

- 1) Ionization of the neutral propellant atoms.
- 2) Acceleration of the ions to high velocities producing thrust.

These two topics will form the basis for the discussion of thruster operation.

Figure 1 shows a schematic for a typical electron bombardment ion thruster. The specific type shown has a strongly divergent magnetic field which is presently the most common type. However, the operation of all types of electron bombardment ion thrusters is very similar⁽¹⁾. Electrons are emitted from the cathode and are drawn toward the anode which is biased 30-40V positive with respect to the cathode. These electrons (called primary electrons) are injected into the primary electron region with an energy slightly less than that associated with the 30-40V anode voltage. Electrons in this region are kept from going immediately to the anode by a magnetic field set up between the cathode pole piece and the anode pole piece but collisions eventually facilitate electron diffusion across these magnetic field lines so that they can be collected by the anode. As a result of the magnetic field containment the electron density is much higher ($\approx 10^{11} \text{cm}^{-3}$) within this region than it is outside of it. The primary electron region's boundary is defined by the surface of revolution of the critical (magnetic) field line and the screen grid. Because the strength of the magnetic field

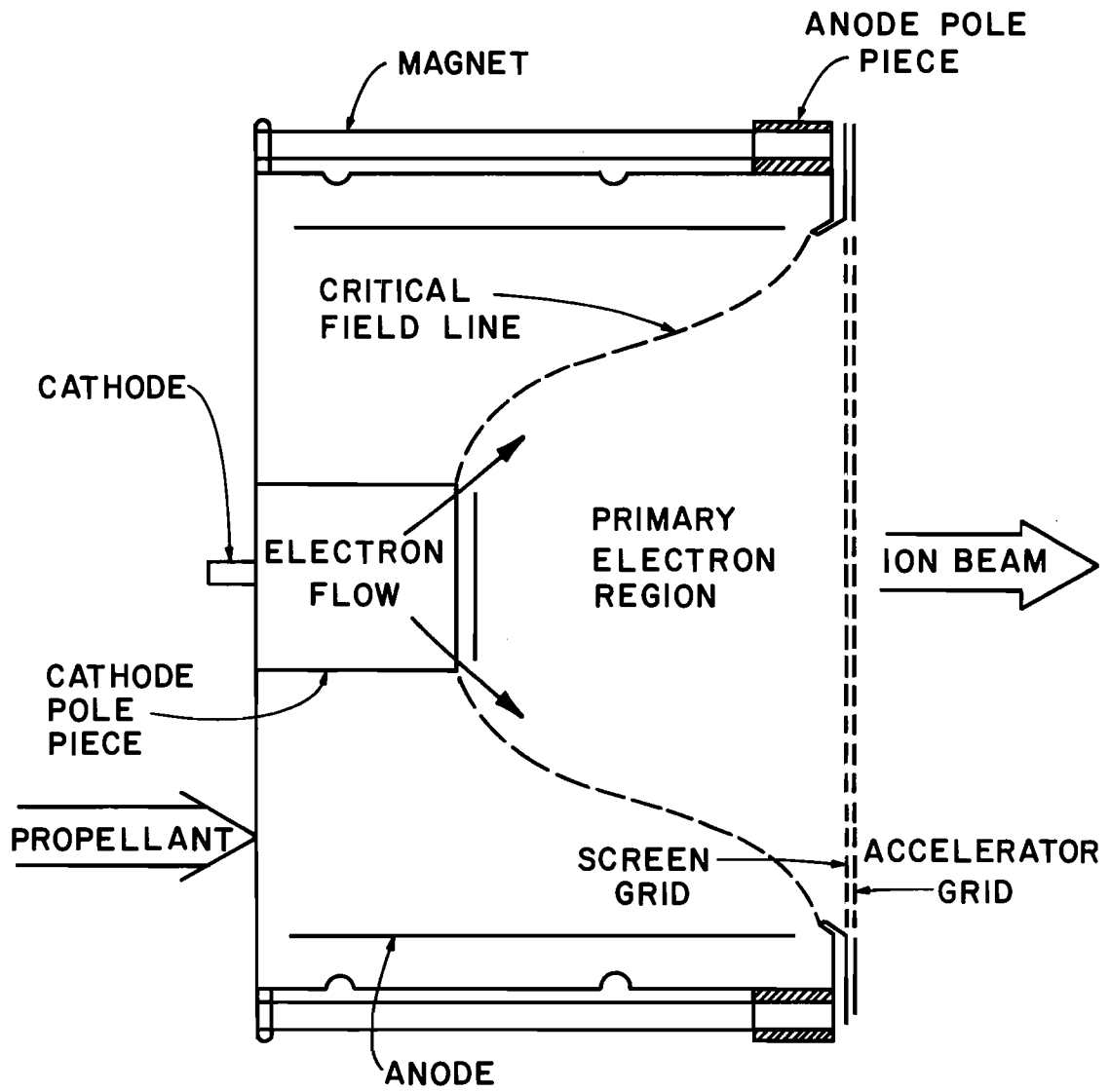


Figure 1 Electron Bombardment Ion Thruster Schematic

is fairly low within it, a fairly uniform electron density exists throughout the entire region.

Neutral propellant (e.g. mercury) is injected into the upstream end of the discharge chamber at low pressure (10^{-4} torr). Most of the interactions between electrons and neutral propellant atoms take place in the primary electron region because higher electron densities and energies exist there. Electrons bombard the neutral atoms occasionally knocking an outer shell electron loose from the atom forming a singly charged ion. The production of a mercury single ion requires more than 10 eV of energy from the incident electron. This electron and the ejected electron then share the remainder of the energy which the incident electron carried originally. This reaction results in the replacement of one high energy electron with two lower energy electrons which rapidly randomize with similarly generated electrons to form a Maxwellian electron group. Ions are extracted from the plasma through holes in the screen and accelerator grids as a result of the large potential difference applied across these two grids. The rate of ion loss through the grids times the ionic charge is called the beam current.

Electron bombardment of atoms and ions also produces doubly charged ions. Many of these ions are extracted from the discharge chamber by the grids, however, some of them go to the walls. As ions near the walls (the cathode pole piece, screen grid, etc.) they are accelerated to high velocities by an electric field that exists at the plasma boundary. When these high velocity ions strike the walls they can knock atoms loose (sputter atoms) from the walls of the discharge chamber. The energy that doubly charged ions possess upon striking the

walls is twice that of singly charged ions, therefore the sputtering damage caused by a double ion is much greater than that caused by a single ion. Double ions are thought to cause most of the sputtering damage even though their density is typically an order of magnitude less than that of the single ions.

THEORETICAL MODEL

Introduction

In order to develop a simple model for determining the double ion density in the discharge chamber only those ionic and atomic species which were considered significant in determining the double ion density were included. The significant species were selected as those which have substantial electron impact cross sections of formation over the electron energy range of interest so that large numbers of these excited atoms or ions will be produced. These states also have sufficiently long effective lifetimes so that they can participate in production processes before they decay. Only those reactions which lead directly or indirectly to the production of double ions were included.

Figure 2 is a discharge chamber reaction schematic showing these dominant species and the reactions in which each specie can participate. The model has been developed for thrusters using mercury propellant but the general procedure is valid for thrusters using other propellants.

The symbols used in Figure 2 represent the following species:

Hg^0 - neutral ground state mercury

Hg^m - metastable neutral mercury (6^3P_0 and 6^3P_2 states)

Hg^r - resonance state neutral mercury (6^3P_1 and 6^1P_1 states)

Hg^+ - singly ionized ground state mercury

Hg^{m+} - singly ionized metastable mercury ($6^2D_{3/2}$ and $6^2D_{5/2}$ states)

Hg^{++} - doubly ionized ground state mercury

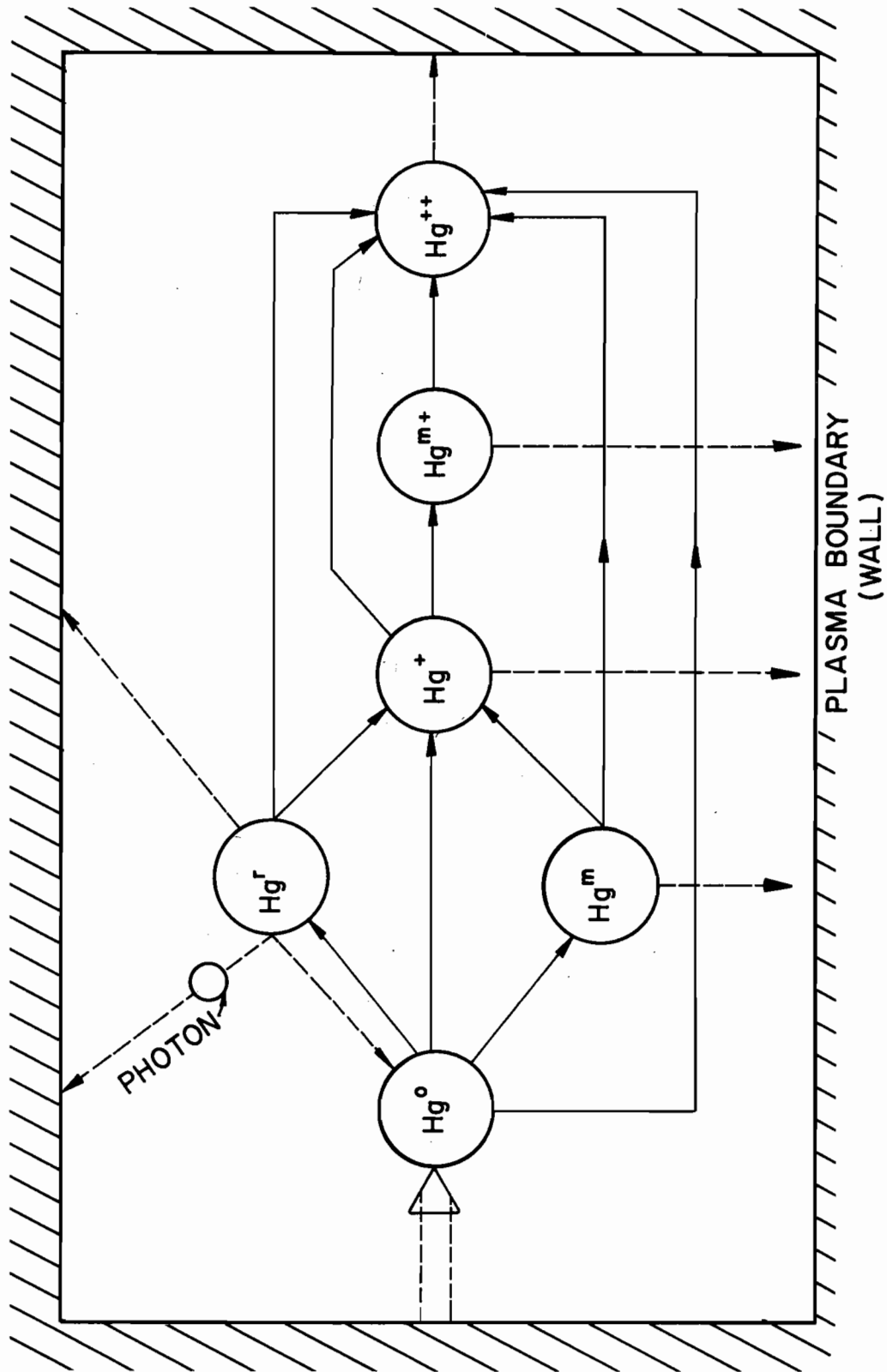


Figure 2 Discharge Chamber Reaction Schematic

The arrows in Figure 2 indicate the various interaction routes considered in this analysis. Three different types of reactions are indicated in this figure. The first type of reaction occurs when an electron interacts with an atom or ion producing a more highly excited specie. This reaction is indicated in Figure 2 by an arrow going from one specie to another more highly excited specie (e.g. the production of double ions from single ions). The production of a highly excited specie also represents a loss mechanism for the less excited specie. The reverse reaction in which, for example, an ion captures an electron is improbable because the reaction requires three bodies to simultaneously collide.

The second type of process is that of an atom or ion going to a plasma boundary. Such a boundary could be either the discharge chamber wall on which the atom or ion would be de-excited or it could be a grid aperture in which case the atom or ion would be extracted from the discharge region. In either case this represents a loss rate for any of the excited states. These losses to the boundary are indicated in Figure 2 by the dotted lines to the wall of the chamber. The large arrow back to the neutral ground state represents the resupply of neutral ground state atoms either from the walls or from the propellant supply system.

A third type of reaction shown in Figure 2 is relevant only to the two resonance states. The resonance states differ from metastable states in that they have a very short lifetime before they de-excite spontaneously by emitting a photon of light. However, the energy of this photon is such that it is readily absorbed by a nearby neutral ground state atom producing another resonance state atom. Since the

transport time of the photon is small compared to the excited state lifetime the excited state can be considered to exist continuously. Eventually the photon can diffuse to a boundary where it will be lost; this is equivalent to the loss of a resonance state atom. This loss mechanism is represented in Figure 2 by a dotted line conveying a photon to the wall and a branching line going from the resonance atom to the neutral ground state atom.

Figure 2 also shows the dominant routes for the production and loss of all of the excited atoms and ions considered. For example, ground state single ions can be produced as a result of electron bombardment of neutral ground state, resonance state, and metastable state atoms and these single ions can be lost as a result of single ion migration to the plasma boundary and the production of metastable single ions and double ions by electron bombardment.

When equilibrium conditions exist in the discharge chamber the rate of production of each specie must equal its loss rate. If, for example, the production rate of single ions increases, the single ion density must also increase to keep the loss rate (which is directly proportional to the single ion density) equal to the higher production rate. This example illustrates the fact that the equilibrium density of any specie is determined by the associated production and loss rates. If equations determining the production and loss rates could be derived, these equations could then be solved for the equilibrium density of any specie under consideration. The remainder of this section is concerned with deriving equations for the production and loss mechanisms indicated in Figure 2 and then solving these equations for the equilibrium densities of the various states.

Electron Bombardment Reactions

The first reaction to be considered is the one which produces excited atoms or ions by electron bombardment from less excited atoms or ions. The total rate of production of any specie γ from specie α (and hence the loss rate of α due to this reaction) is given by:

$$R_{\alpha}^{\gamma} = \int_{\text{Plasma Volume}} \int_{E=0}^{E=\infty} n_{\alpha} \sigma_{\alpha}^{\gamma}(E) v_e(E) dn_e dV \quad (1)$$

where n_{α} is the density of specie α at some point \vec{r} in the plasma, $\sigma_{\alpha}^{\gamma}(E)$ is the cross section for the production of γ from α at the electron energy E ⁽²⁻⁶⁾, v_e is the electron velocity at energy E , dn_e is the density of electrons with energies between E and $E + dE$ at \vec{r} , and dV is the infinitesimal volume element. The distribution of electrons over the energy spectrum of an ion thruster was assumed to be composed of a Maxwellian electron group which is described by a temperature (T_{mx} -- eV) and a density (n_{mx} -- cm^{-3}) and a monoenergetic group (primary electrons) which is described by an energy (ξ_{pr} -- eV) and a density (n_{pr} -- cm^{-3}). This type of electron distribution is generally accepted as appropriate for electron bombardment thruster plasmas.^(1,7)

Substituting this electron distribution into Equation (1) and combining terms to form new functions results in the following equation.

$$R_{\alpha}^{\gamma} = \int_{\text{Volume}} n_{\alpha} [n_{pr} P_{\alpha}^{\gamma}(\xi_{pr}) + n_{mx} Q_{\alpha}^{\gamma}(T_{mx})] dV \quad (2)$$

where

$$P_{\alpha}^{\gamma}(\xi_{pr}) = v_e(\xi_{pr}) \sigma_{\alpha}^{\gamma}(\xi_{pr}) \quad (3)$$

and

$$Q_{\alpha}^Y(T_{MX}) = \int_{E=0}^{E=\infty} \sigma_{\alpha}^Y(E) v_e(E) \frac{dn_{MX}(E)}{n_{MX}} \quad (4)$$

" $[dn_{MX}(E)/n_{MX}]$ " is the Maxwellian distribution function and the other terms are as defined previously.

Where possible the cross sections (σ_{α}^Y) required for Equations (3) and (4) were selected from experimental data.^(2,3,4) If experimental data were not available, theoretical cross sections were either obtained from the literature⁽⁵⁾ or calculated using the Gryzinski approximation.⁽⁶⁾ The Gryzinski approximation was modified for the cases of the metastable single ion production cross sections to reflect the significant value of the cross sections near the threshold. The cross sections used are presented in Figure 3 along with references indicating their origin.

Using integral equations like Equation (2) in the model would be inconvenient because it would then be very difficult to solve for the density of specie α (n_{α}) since n_{α} appears within the integral. For this reason it would be desirable to convert Equation (2) into a simple algebraic equation. Fortunately the plasma is fairly uniform in the primary electron region which is where most of the reactions take place. This suggests using average properties in Equation (2) to obtain the following result.

$$R_{\alpha}^Y = n_{\alpha}^* [n_{pr}^* P_{\alpha}^Y(\epsilon_{pr}^*) + n_{MX}^* Q_{\alpha}^Y(T_{MX}^*)] \Psi \quad (5)$$

The asterisks indicate volume averaged quantities and Ψ is the volume of the primary electron region.

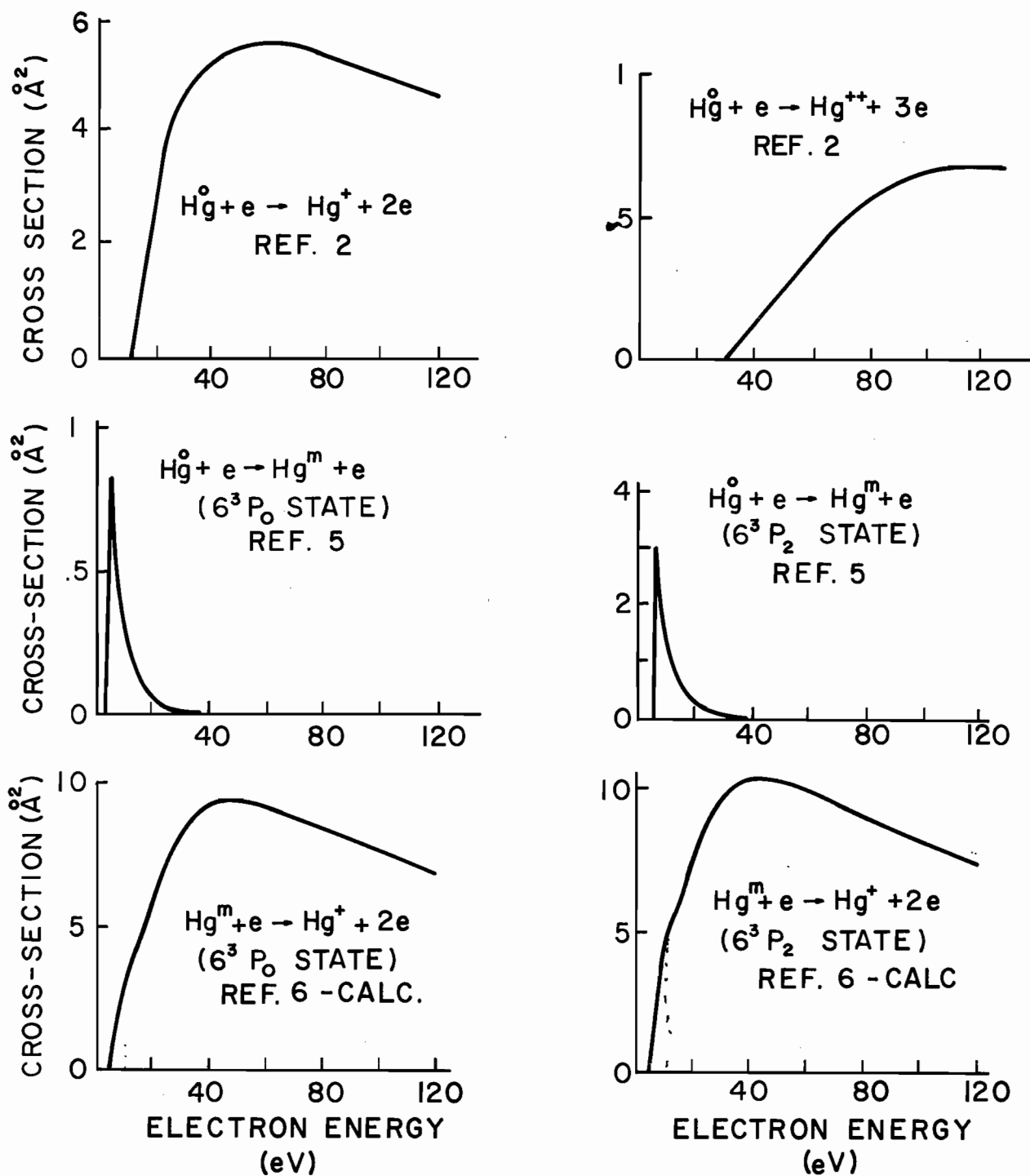


Figure 3 Mercury Cross Sections

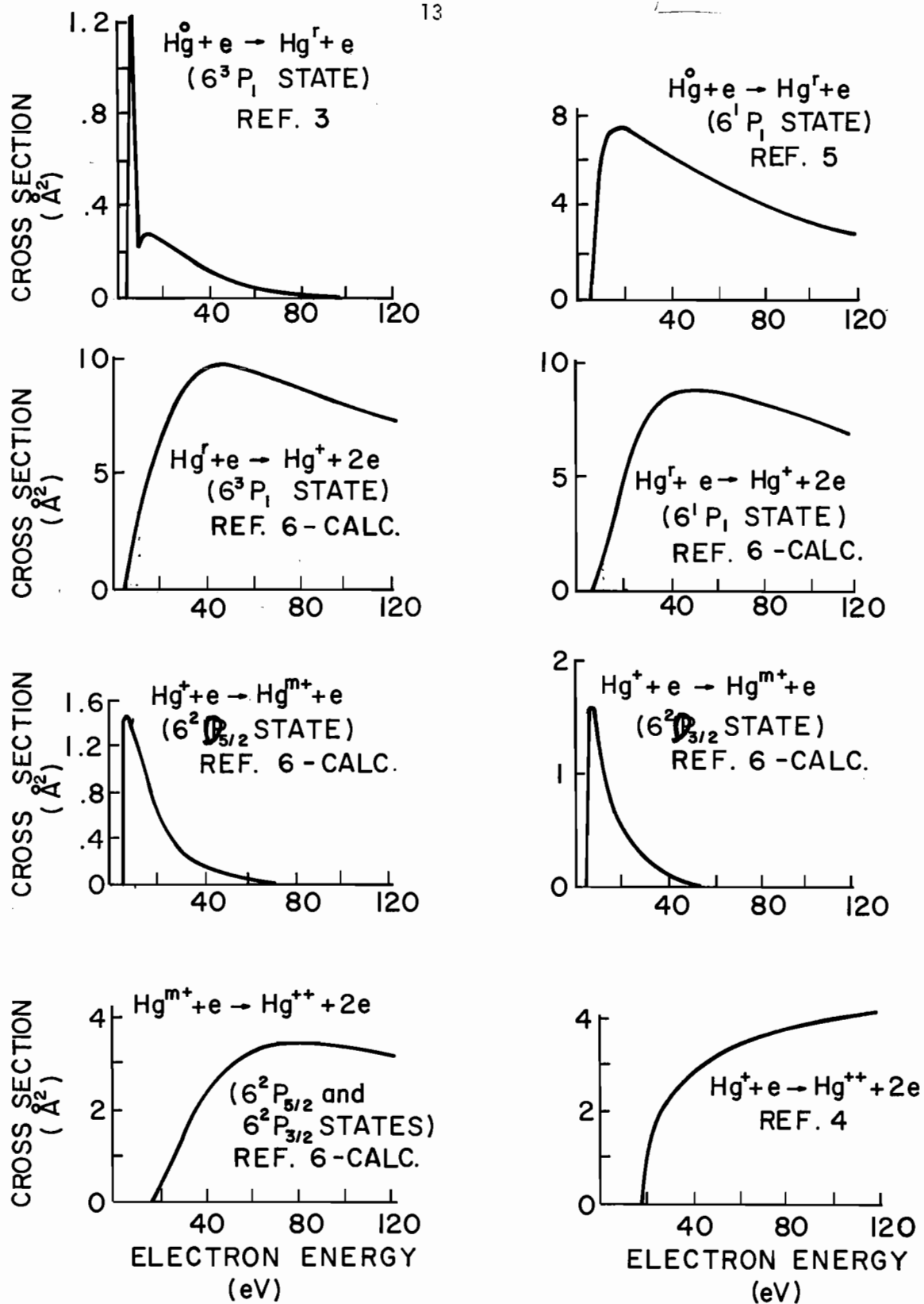


Figure 3 Mercury Cross Sections (continued)

In order to use Equation (5) to evaluate all of the production rates the volume averaged plasma properties (n_{pr}^* , n_{mx}^* , ξ_{pr}^* , T_{mx}^*) must be determined. Comparing Equations (2) and (5) the following definitions of the volume averaged properties must apply.

$$n_{\alpha}^* n_{pr}^* P_{\alpha}^{\gamma}(\xi_{pr}^*) \Psi = \int_{\text{Volume}} n_{\alpha} n_{pr} P_{\alpha}^{\gamma}(\xi_{pr}) d\Psi \quad (6)$$

$$n_{\alpha}^* n_{mx}^* Q_{\alpha}^{\gamma}(T_{mx}^*) \Psi = \int_{\text{Volume}} n_{\alpha} n_{mx} Q_{\alpha}^{\gamma}(T_{mx}) d\Psi \quad (7)$$

These two equations show that the volume averaged plasma properties will be weighted in some manner. In order to evaluate the integrals, species α and γ must be chosen. The only specie density (n_{α}) that can be determined readily is the single ion density because plasma neutrality requires it to be approximately equal to the electron density. Specie γ must also be chosen in order to determine what P_{α}^{γ} and Q_{α}^{γ} to use. Figure 2 shows only two choices are possible--the singly ionized metastable states and the doubly ionized ground state. Since the whole purpose of the model is to determine the double ion density, specie γ was chosen as the doubly ionized ground state. Using these choices for species α and γ , Equations (6) and (7) were rewritten in the following form where the electron density (n_e) has been used to approximate the single ion density.

$$n_e^* n_{pr}^* P_{+}^{++}(\xi_{pr}^*) \Psi = \int_{\text{Volume}} n_e n_{pr} P_{+}^{++}(\xi_{pr}) d\Psi \quad (8)$$

$$n_e^* n_{mx}^* Q_{+}^{++}(T_{mx}^*) \Psi = \int_{\text{Volume}} n_e n_{mx} Q_{+}^{++}(T_{mx}) d\Psi \quad (9)$$

The volume averaged values of the primary electron energy (ξ_{pr}^*) and the Maxwellian electron temperature (T_{mx}^*) were defined as shown in Equations (10) and (11). These definitions were chosen because they give reasonable values for the properties involved (i.e. these volume averaged values can't be greater than the peak values, which was possible with some of the other definitions).

$$P_+^{++}(\xi_{pr}^*) = \frac{\int_{\text{Volume}} n_e n_{pr} P_+^{++}(\xi_{pr}) d\psi}{\int_{\text{Volume}} n_e n_{pr} d\psi} \quad (10)$$

$$Q_+^{++}(T_{mx}^*) = \frac{\int_{\text{Volume}} n_e n_{mx} Q_+^{++}(T_{mx}) d\psi}{\int_{\text{Volume}} n_e n_{mx} d\psi} \quad (11)$$

Equations (8) - (11) along with Equation (12), which says the volume averaged electron density is the sum of the volume averaged primary and Maxwellian electron densities, can be combined to obtain the following definitions of the remaining volume averaged plasma properties.

$$n_e^* = n_{pr}^* + n_{mx}^* \quad (12)$$

$$n_e^* = \left[\int_{\text{Volume}} n_e^2 d\psi \right]^{1/2} / \psi^{1/2} \quad (13)$$

$$n_{pr}^* = \frac{\int_{\text{Volume}} n_e n_{pr} d\psi}{\left[\int_{\text{Volume}} n_e^2 d\psi \right]^{1/2} \psi^{1/2}} \quad (14)$$

$$n_{mx}^* = \frac{\int_{\text{Volume}} n_e n_{mx} d\psi}{\left[\int_{\text{Volume}} n_e^2 d\psi \right]^{1/2} \psi^{1/2}} \quad (15)$$

This concludes the mathematical development for electron bombardment reactions.

The volume averaged plasma properties must be evaluated in order to use Equation (5) to calculate the production rates. The plasma properties (n_{pr} , n_{mx} , ξ_{pr} , T_{mx}) are measured at many points inside the discharge chamber by a Langmuir probe. This data is then used to evaluate the integrals in Equations (10), (11) and (13)-(15) numerically yielding the needed volume averaged plasma properties.

Migration Losses

The second type of process to be considered is that of an excited atom or ion going to the plasma boundary. The equation for the plasma boundary loss rate of a specie α is given by:

$$R_{l\alpha} = \int_{\text{plasma boundary}} n_{\alpha} v_{\alpha} dA \quad (16)$$

where n_{α} is the density of specie α at the boundary, v_{α} is its average velocity toward the plasma boundary, and dA is the infinitesimal area. For neutral particles assumed to have a temperature equal to the discharge chamber wall temperature and having a mass " m_0 " the average velocity toward the boundary (v_0) is equal to one-fourth the average thermal speed

$$v_0 = \frac{1}{4} \sqrt{\frac{8k T_{\text{wall}}}{\pi m_0}} \quad (17)$$

where k is the Boltzmann constant.

For ions this velocity is determined by the Bohm criterion^(8,9) and is given by

$$v_q = \sqrt{\frac{T_{mx} q}{m_i} \left(1 + \frac{n_{pr}}{n_{mx}}\right)} \quad (18)$$

where q is the ion charge (coul) and m_i is the ion mass (kg), and T_{mx} , n_{pr} and n_{mx} are as defined previously.

Since the integral equation used to define production rates has been reduced to an algebraic equation in terms of average properties Equation (16) should also be simplified in this manner. Because the migration loss is a surface phenomenon, however, it is necessary to use surface averaged densities and velocities based on surface average properties to obtain

$$R_{l\alpha} = n_{\alpha}^s v_{\alpha}^s A \quad (19)$$

where A is the total surface area of the primary electron region and the superscript "s" designates values based on surface averaged properties. Equation (19) could be made more convenient for use in the model if it were based on volume averaged properties as Equation (5) is. Equation (19) was for this reason rewritten in terms of volume averaged densities as follows

$$R_{l\alpha} = n_{\alpha}^* v_{\alpha}^* A/F_{\alpha} \quad (20)$$

where v_{α}^* is $v_{\alpha}(T_{mx}^*, n_{pr}^*/n_{mx}^*)$ and F_{α} is a plasma uniformity factor given by Equation (21) which relates the volume and surface averaged density-velocity product.

$$F_{\alpha} = \frac{n_{\alpha}^* v_{\alpha}^*}{n_{\alpha}^s v_{\alpha}^s} = \frac{n_{\alpha}^* v_{\alpha}^*}{\left[\int_{\text{plasma boundary}} n_{\alpha} v_{\alpha} dA \right]} / A \quad (21)$$

This concludes the mathematical development for the migration loss of excited species, but some additional discussion and quantification of the uniformity factor F_{α} is necessary before it can be used in Equation (20). The evaluation of F_{α} for neutral excited states is difficult because it is difficult to measure their densities. The migration of excited neutrals to the plasma boundary is however a minor loss mechanism compared to the losses due to the conversion of neutral excited atoms into single ions. Therefore F_{α} for neutral excited states can be set equal to unity without introducing a significant error into the total loss rate calculation. In the case of ions, however, migration to the boundary is a major loss mechanism and F_{α} must be evaluated in order to obtain accurate results. For the singly ionized ground state the approximation, $n_{+} = n_{e}$, can again be used in order to evaluate F_{+} using Equation (21). The uniformity factor for the singly ionized metastable states was set to unity since these states have a very minor effect on the double ion density. The determination of F_{++} is based on the observation⁽¹⁰⁾ that the volume averaged double ion density (n_{++}^*) is proportional to the volume averaged electron density squared (n_e^*)². It has been assumed that this proportionality holds locally and this results in the following definition of F_{++} .

$$F_{++} = \frac{(n_e^*)^2 v_{++}^*}{\left[\int_{\text{plasma boundary}} n_e^2 v_{++} dA \right]} / A \quad (22)$$

Photon Diffusion Losses

The third type of process to be considered is the loss of resonance state atoms due to photon diffusion to the walls of the discharge chamber. From diffusion theory the rate of photon loss across any plasma boundary and hence the rate of resonance state atom loss by this mechanism is given by the equation

$$R_{\ell r} = \int_{\text{plasma boundary}} D \Delta n_p \, dA = DA[\Delta n_p] \quad (23)$$

In this equation n_p is the photon density and D is the photon diffusion coefficient which is given by

$$D = \frac{1}{3\tau(n_0^* \sigma_c)^2} \quad (24)$$

" τ " in this equation is the average lifetime of the resonance state atom, n_0^* is the neutral ground state atom density, and σ_c is the cross section for absorption of the photons by neutral ground state atoms. (11)

The second equality in Equation (23) reflects the fact that average properties are being used in this analysis. The photon density has been assumed constant up to a point one photon mean free path from the boundary. From this point the density is assumed to decay linearly to zero at the boundary. This assumption yields the following conservative estimate for the photon loss rate

$$R_{\ell r} = DA n_p^* / \ell_f \quad (25)$$

where ℓ_f is the mean free path for photon absorption $(\frac{1}{n_0^* \sigma_c})$. This

approximation is valid when the photon mean free path is much less than the characteristic dimension of the plasma, a condition that is readily satisfied for this case where the photon mean free paths are very small ($l_f < .1$ cm).

Since the neutral density is assumed uniform over the discharge region the photon density profile is similar to the resonance state atom density profile and the following approximation between the photon and resonance state atom density at any location in the plasma applies:

$$n_p = n_r \beta \quad (26)$$

β is a proportionality constant that can be thought of as the ratio of the probability that a photon will be "free" in the plasma to the probability that it will be "bound" forming a resonance state atom. This ratio of probabilities can also be expressed as the ratio of the average lifetime of a free photon ($\frac{1}{*}$) to the resonance state atom lifetime (τ). Therefore, β is given by:

$$\beta = \frac{1}{*}{cn_0\sigma_c \tau} \quad (27)$$

where c is the speed of light and the other quantities have already been defined. Combining Equations (25), (26 and (27) one obtains the following equation for the loss rate of resonance state atoms due to photon diffusion:

$$R_{lr} = \frac{n_r^*}{3c} A \left[\frac{1}{*\tau n_0 \sigma_c} \right]^2 \quad (28)$$

Determination of Specie Densities

The equations derived so far in this section can now be combined to determine the equilibrium density of each specie included in the model. Equations of the form of (5) and (20) -- and (28) for the case of resonance state atoms -- along with the values for the volume averaged plasma properties and the plasma uniformity factors can be used to determine the rates of production and loss for each specie in the plasma. The steady state density of these species can then be calculated by equating their total production rates to their total loss rates. For example, the 6^3P_0 metastable atom density is determined by equating the production rate of this metastable atomic state from neutral ground state atoms to the sum of the associated loss rates due to 1) migration to the wall, 2) production of single ions, and 3) the production of double ions, that is

$$n_o^* [n_{pr}^* P_o^m(\xi_{pr}^*) + n_{mx}^* Q_o^m(T_{mx}^*)] \psi = \frac{n_m^* v_m^* A}{F_m} \quad (29)$$

$$+ n_m^* [n_{pr}^* P_m^+(\xi_{pr}^*) + n_{mx}^* Q_m^+(T_{mx}^*)] \psi + n_m^* [n_{pr}^* P_m^{++}(\xi_{pr}^*) + n_{mx}^* Q_m^{++}(T_{mx}^*)] \psi .$$

Solving this for the metastable atom density ratio one obtains

$$\frac{n_m^*}{n_o^*} = [n_{pr}^* P_o^m(\xi_{pr}^*) + n_{mx}^* Q_o^m(T_{mx}^*)] / \left\{ \frac{v_m^*}{\psi/A F_m} + [n_{pr}^* P_m^+(\xi_{pr}^*) + n_{mx}^* Q_m^+(T_{mx}^*)] + [n_{pr}^* P_m^{++}(\xi_{pr}^*) + n_{mx}^* Q_m^{++}(T_{mx}^*)] \right\} \quad (30)$$

where n_m^* is the volume average metastable state density and v_m^* is the average velocity of metastable neutral atoms toward the boundary. A similar type of equation can be derived for each of the other excited states but they are all as complex or more complex than Equation (30).

For example, the equation for the doubly ionized ground state density has eight terms in the numerator. Each of these terms has the same form as the bracketed quantities in the numerator of Equation (30).

The quantity Ψ/A in the denominator of Equation (30) has an interesting physical interpretation. It is contained in a term which represents the loss rate per unit volume of metastable state atoms to the plasma boundary. This term shows the manner in which the size and shape of the primary electron region enters into the model. For a large thruster Ψ/A will be large and an ion or excited neutral must, on the average, travel great distances to reach the plasma boundary, and so the loss rate per unit volume of these species will be small. For a small thruster Ψ/A will be small and on the average the ions and excited species are near the boundary and can reach it readily resulting in a large loss rate of these species per unit volume.

At this point only the relative density of each excited specie (n_{α}^*/n_0^*) can be calculated. However one additional fact can be added to the model, the requirement that the plasma be neutral (i.e., $n_e^* = n_+^* + n_{m+}^* + 2n_{++}^*$). This requirement when added to the relative density equations of the ionized states implies unique single, metastable single and double ion densities. These in turn imply a unique neutral atom density and hence a unique density for each specie considered in the analysis. One must however iterate to arrive at these densities because a neutral ground state atom density must be assumed initially to determine photon loss rates from Equation (28). At the conclusion of the analysis then the calculated ground state atom density must agree with the assumed value.

A computer program has been written which calculates the densities of all the species considered in the model. The densities are calculated by using relative density equations similar to Equation (30) and the plasma neutrality condition. The input needed to make these calculations includes the volume averaged plasma properties, the plasma uniformity factors and the volume-to-surface area ratio of the primary electron region. A listing of this computer program entitled "HG" is included as Appendix A.

EXPERIMENTAL PROCEDURES AND RESULTS

The model developed in the previous section will predict the specie densities if the volume averaged plasma properties, uniformity factors and geometric quantities, which are collectively called the input parameters, are known. In order to verify the accuracy of the model, data must be gathered so that the model's input parameters can be determined. These input parameters can be used by the model to predict the specie densities which can then be compared to the measured densities to determine the model's accuracy. The model's accuracy has been determined by comparing the measured and predicted double ion densities since the double ion density is the model's main concern.

In order to test the accuracy of the model over a wide range of conditions data were used from different thrusters and operating conditions. The 15 cm diameter SERT II thruster was operated with two different grid sets and at three different power levels in each of these configurations. Data were collected at each condition allowing the accuracy of the model to be verified at six different points. Data for the 30 cm diameter thruster were also obtained from Hughes Research Laboratories⁽¹²⁾ so that the model could be verified over a wider range of thruster sizes, configurations, and operating conditions. Both thrusters have strongly divergent magnetic fields. Their general configuration and manner of operation have been described in the "Thruster Operation" section. More detailed thruster specifications, etc. are available in the literature.^(9, 13, 14)

The data gathering procedure for the 15 cm thruster will be used to illustrate the general manner in which the needed data were obtained.

Before the gathering of data could begin thruster operation and flow rates were kept stable for approximately thirty minutes. This insured thruster conditions would change little in the twenty minute period during which the data were obtained. Table I lists the conditions and configurations at which the 15 cm thruster was operated at C.S.U. along with those for the 30 cm thruster as obtained from Hughes Research Laboratories. This table indicates the changes in configuration for both thrusters resulted from using different grid types. The SERT II grids, listed in Table I, are flat grids with hole diameters of $\approx .4$ cm and in operation are separated by a gap of .23 cm. The high perveance dished grids are dished slightly to prevent the grids from shorting during operation due to their thermal expansion. Their hole diameter is smaller (.25 cm) as is their separation gap (.079). More detailed specifications for the two grid types can be found in Reference 9. The EM (Engineering Model) grids are similar to the high perveance dished grids described above. The SHAG (Small Hole Accelerator Grids) grids have an accelerator hole diameter that is $\approx 70\%$ of the EM grids' accelerator hole diameter. This smaller hole size reduces the loss of neutral propellant. These two grid types are described in more detail in References 15 and 16. Table I shows, for example, that the 15 cm thruster with the SERT II grids was operated at one condition where the amount of current collected at the anode (I_{arc}) was 1.7A, while the voltage difference between the anode and cathode (V_{arc}) was 37.2 V and the ion current through the grids (I_{beam}) was 0.258 A.

The values of the volume averaged plasma properties and the uniformity factors must be known in order to calculate the theoretical double ion density. In order to determine the values of these average

Table I
 Thruster Sizes, Configurations and Conditions

Thruster Diameter (cm)	Grid Type	Anode Current (I_{arc} --A)	Anode Voltage (V_{arc} --V)	Ion Beam Current (I_{beam} --A)	Mass Flow Rate (A)
15.	SERT II	1.00	33.	.180	.310
15.	SERT II	1.70	37.2	.258	.307
15.	SERT II	2.05	42.6	.272	.308
15.	Dished	3.02	32.2	.499	.735
15.	Dished	4.06	37.5	.654	.725
15.	Dished	4.13	40.4	.622	.650
30.	EM	5.0	37.	1.0	1.25
30.	EM	7.5	37.	1.5	1.76
30.	EM	10.0	37.	2.0	2.29
30.	SHAG	9.5	30.	1.5	1.74
30.	SHAG	11.7	30.	2.0	2.30

plasma properties, the primary and Maxwellian electron densities and energies must be determined everywhere in the discharge chamber. The plasma properties at some point in the plasma can be measured using a Langmuir probe and analyzed using the procedure described in Reference 17. The plasma properties at sixteen different points in the plasma were measured, for each 15 cm thruster condition listed in Table I, using the movable Langmuir probe and associated circuitry described in Reference 18. The results of a typical survey (15 cm thruster - SERT II grids -37 V anode voltage) are plotted in Figure 4. This figure shows the spatial variation of the Maxwellian electron temperature, primary electron energy and the primary and Maxwellian electron densities in the discharge chamber. The Maxwellian electron temperature is seen to average approximately 9 eV over the primary electron region defined by the critical field line while the primary electron energy averages about 30 eV. The average Maxwellian electron density is about 10^{11}cm^{-3} while the average primary electron density is approximately 10^{10}cm^{-3} over the same region. The electron densities and energies are seen to be fairly uniform in the primary electron region but drop off rapidly outside this region. Using data similar to that plotted in Figure 4, Equations (10)-(15) and (21) were evaluated numerically by the computer program "PROP" (listed in Appendix B) to obtain the volume averaged properties and uniformity factors for each case. The results are listed in Table II along with the volume-to-surface area ratio of the primary electron region (V/A) and the thruster operating specifications which are reproduced from Table I. The average values which resulted from an examination of Figure 4 ($T_{mx} \approx 9 \text{ eV}$, $\xi_{pr} \approx 30 \text{ eV}$, $n_{mx} \approx 10^{11}\text{cm}^{-3}$, $n_{pr} \approx 10^{10}\text{cm}^{-3}$) are seen to

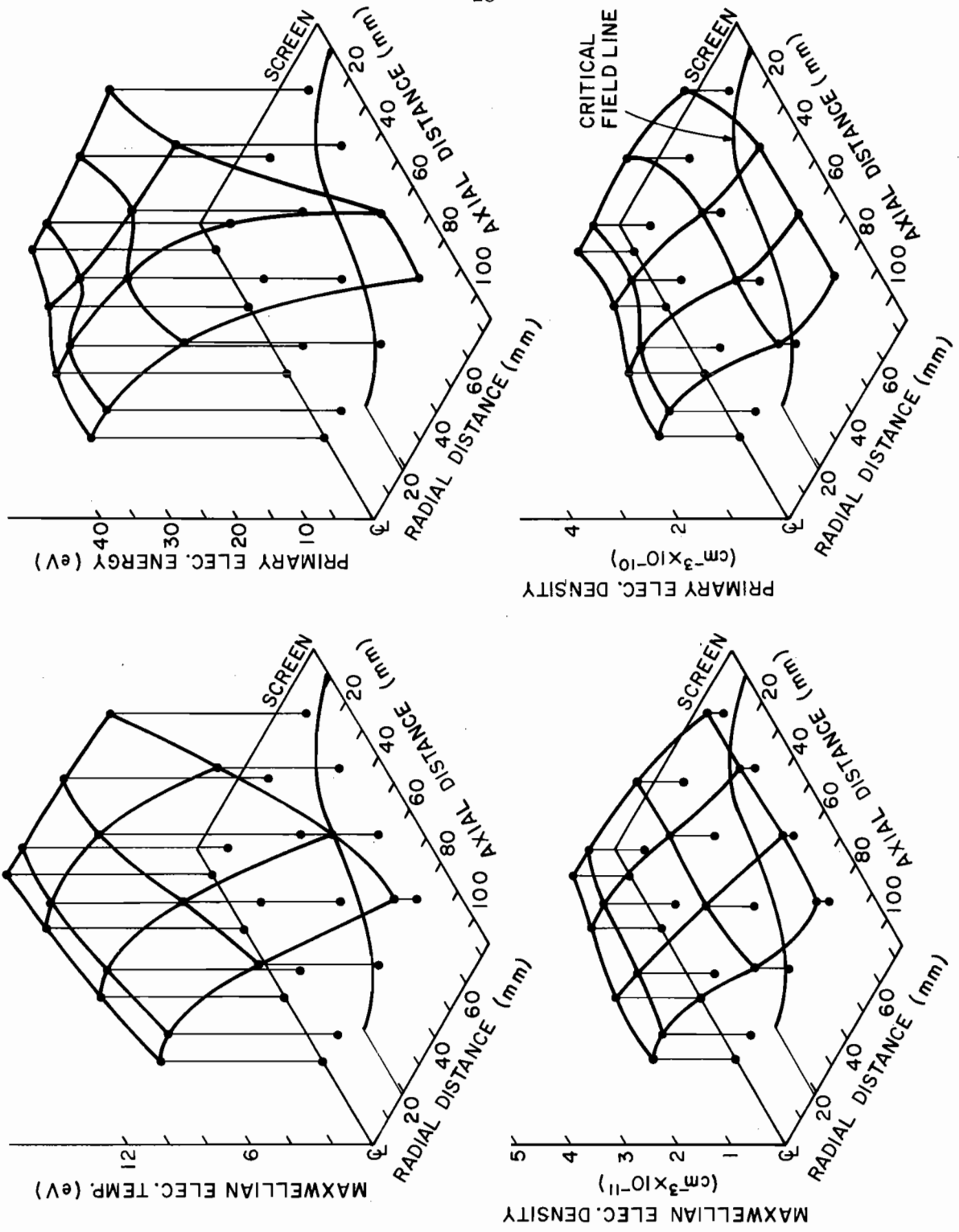


Figure 4 Plasma Property Profiles, 15 cm Thruster - SERT II Grids - 37 V Anode Voltage

Table II

Experimental Results

	15.	15.	15.	15.	15.	15.	15.	30.	30.	30.	30.	30.
Thruster Diameter (cm)												
Grid Type		SERT II			HIGH PERVEANCE DISHED			EM	EM	EM	SHAG	SHAG
Anode Current (I_{arc})	1.0	1.7	2.05	3.02	4.06	4.13	5.0	7.5	10.0	10.0	9.5	11.7
Anode Voltage (V_{arc})	33.	37.2	42.6	32.2	37.5	40.4	37.	37.	37.	37.	30.	30.
Beam Current (I_{beam})	.180	.258	.272	.499	.654	.622	1.0	1.5	2.0	1.5	2.0	2.0
Mass Flow Rate (A)	.310	.307	.308	.735	.725	.650	1.25	1.76	2.29	1.74	2.30	2.30
Operating Variables												
Plasma Volume to Surface Area Ratio (Ψ/A)	1.4	1.4	1.4	1.4	1.4	1.4	2.5	2.5	2.5	2.5	2.5	2.5
Average Maxwelllian Electron Temperature (T_{mx}^*)	4.2	9.1	12.2	4.3	7.1	10.2	3.3	3.6	3.8	3.0	2.9	2.9
Average Primary-to-Maxwelllian Electron Density Ratio (n_{pr}^*/n_{mx}^*)	.034	.083	.166	.017	.042	.134	.50	.35	.25	.19	.22	.22
Average Primary Electron Energy (ξ_{pr}^*)	27.5	29.6	38.4	21.5	23.4	31.0	25.4	25.5	27.2	19.6	19.7	19.7
Average Electron Density ($n_e^* \times 10^{-10} \text{ cm}^{-3}$)	9.80	9.10	8.07	36.0	24.3	18.2	7.51	8.97	16.4	8.3	12.8	12.8
Uniformity Factor F_+	2.3	2.1	2.3	2.0	1.9	1.8	1.5	1.5	1.5	1.8	1.7	1.7
Uniformity Factor F_{++}	3.1	2.5	2.6	2.5	2.1	2.0	1.8	1.9	1.8	2.5	2.1	2.1
Input Parameters												
Measured Double-to-Single Ion Current Ratio (I_{++}/I_+)	.024	.073	.12	.036	.081	.18	.080	.125	.167	.062	.080	.080

agree well with the volume averaged values listed in Table II ($T_{mx}^* = 9.1$ eV, $\xi_{pr}^* = 29.6$ eV, $n_{mx}^* = 8.4 \times 10^{10} \text{cm}^{-3}$, $n_{pr}^* = 7.0 \times 10^9 \text{cm}^{-3}$). F_+ and F_{++} , which are defined as the ratio of the volume average ion flux to the average flux at the surface of the primary electron region, are seen to have values of 2.1 and 2.5 respectively for the case being discussed. The average plasma properties listed in Table II are observed to cover a wide range in plasma conditions; a situation which is desirable for verification of the model.

The double ion density inside the discharge chamber must also be determined. This can be accomplished indirectly by determining the double-to-single ion density ratio (n_{++}/n_+) in the discharge chamber and the single ion density. The single ion density can be determined with sufficient accuracy by equating the single ion density to the electron density. The value of the double-to-single ion density ratio can be determined from measurements of the ratio of the double ion current to the single ion current in the exhaust beam (I^{++}/I^+), and the equation

$$n_{++}/n_+ = \frac{I^{++}}{I^+ 2\sqrt{2}} \quad (31)$$

The quantity $2\sqrt{2}$ accounts for charge and Bohm criterion velocity differences between double and single ions.

The quantity " I^{++}/I^+ " was measured using a mass spectrometer.⁽¹⁹⁾

The methods used for data acquisition and analysis using such a device are described in Reference 20 for the 15 cm thruster data and in Reference 19 for the 30 cm thruster. The results obtained are listed in the last row of Table II. They show, for example, a double-to-single ion current ratio of 7.3% for the 15 cm thruster - SERT II grid - 37 V

anode voltage case. The general trend observed from these data is that an increase in power input (I_{arc} times V_{arc}) for a certain thruster configuration results in an increase in the ratio I^{++}/I^+ .

RESULTS AND DISCUSSION

The values of the average plasma properties, listed in Table II, are observed to vary over large ranges. For example, the average Maxwellian electron temperature ranges from a low value of 3.3 eV to a high value of 12.2. Similarly the average primary-to-Maxwellian electron density ratio varies from 0.02 to 0.50. This large variation is considered sufficient to allow a general decision to be made about the accuracy of the model. Comparisons of the experimental and theoretical values of the double-to-single ion density ratio have been used to verify the model's accuracy because this quantity (n_{++}/n_+) was determined experimentally. The theoretical and experimental values of the double-to-single ion density ratio are plotted as a function of propellant utilization in Figures 5 and 6. The curves labeled "THEORETICAL" result from predictions made by the model using the "Input Parameters" listed in Table II. The curves labeled "EXPERIMENTAL" result from measurements of the ratio I^{++}/I^+ made using the mass spectrometer. The trends exhibited by the THEORETICAL and EXPERIMENTAL curves are very similar and the agreement between the THEORETICAL and EXPERIMENTAL values of the double-to-single ion density ratio is good for plasma physics work with the average error being 3%. The maximum error of 40% is observed at low double-to-single ion density ratios in the 30 cm thruster. These error values indicate the model is accurate over a wide range of plasma conditions and thruster configurations.

Since the model has been shown to be accurate in its predictions of the double-to-single ion density ratio over a wide range of conditions there is a distinct possibility that the specie densities and

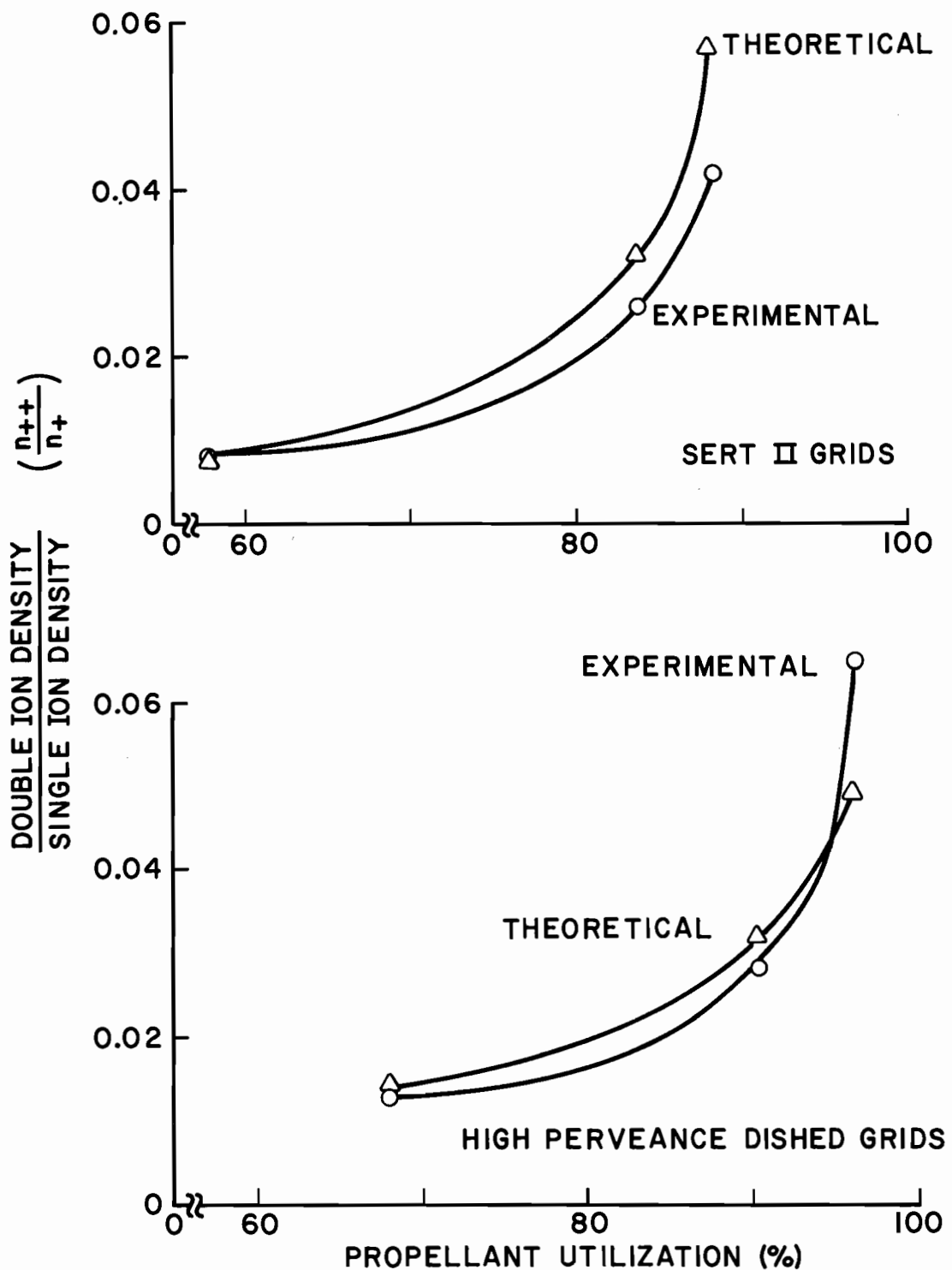


Figure 5 Double-to-Single Ion Density Ratio in a 15 cm Diameter Thruster

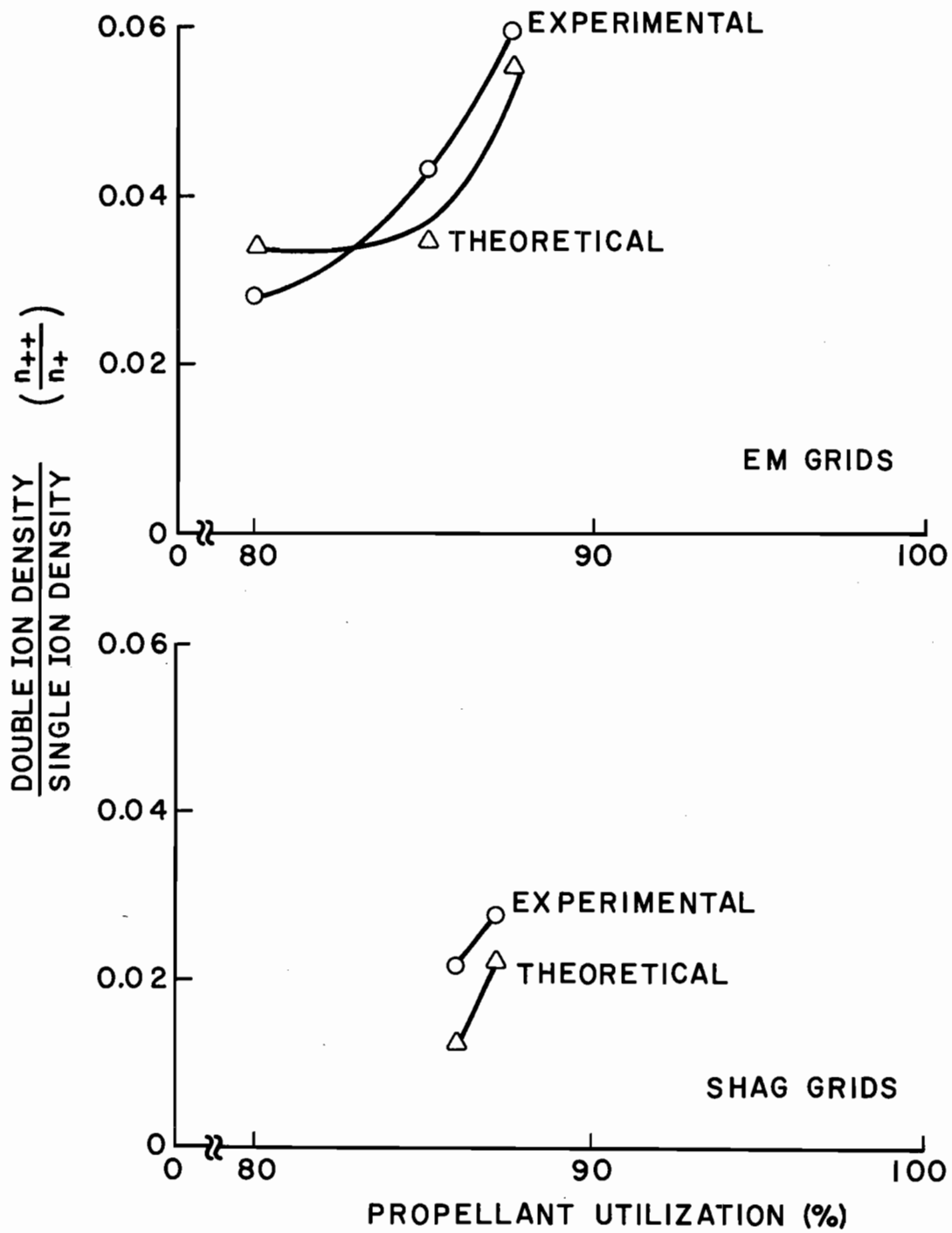


Figure 6 Double-to-Single Ion Density Ratio in a 30 cm Diameter Thruster

reaction rates used to predict the double-to-single ion density ratio are also accurate. The remainder of this section will examine the model's predictions of these specie densities and reaction rates. These quantities are listed in Table III along with the thruster operating variables and the model's input parameters which were reproduced from Table II.

The section in Table III titled "Calculated Normalized Densities" lists the model's predictions of the normalized densities of the states considered in the model where the normalized density of some specie is defined as the specie density divided by the total heavy particle density. The sum of the normalized densities for any thruster condition should therefore equal unity. Table III shows, for example, that the 15 cm diameter thruster operating with SERT II grids at 37 V anode voltage would be predicted to have 68% neutral ground state atoms, 19% neutral resonance state atoms, 6.9% singly charged ground state ions and .2% doubly charged ground state ions. The normalized density of the single ions agrees fairly well in all cases with the 10% value quoted as typical in the literature.⁽¹⁾ As expected the neutral ground state atoms are the most numerous.

These normalized density trends can be explained in terms of variations of plasma properties. For example, the normalized single ion density increases with increasing power input (I_{arc} times V_{arc}) to the thruster in all cases. This occurs because an increase in the values of the volume averaged plasma properties causes the ratio of the production rate of single ions to the total neutral density to increase. The increase in the ratio indicates a smaller total neutral density is

Table III
Predicted Densities and Reaction Rates

Operating Variables	Thruster Diameter (cm)	15.	15.	15.	15.	15.	15.	30.	30.	30.	30.	30.
	Grid Type	SERT II			HIGH PERVEANCE DISHED			EM	EM	EM	SHAG	SHAG
	Anode Current (I_{arc} --A)	1.0	1.7	2.05	3.02	4.06	4.13	5.0	7.5	10.0	9.5	11.7
	Anode Voltage (V_{arc} --V)	33.	37.2	42.6	32.2	37.5	40.4	37.	37.	37.	30.	50.
	Beam Current (I_{beam} --A)	.180	.258	.272	.499	.654	.622	1.0	1.5	2.0	1.5	2.0
	Mass Flow Rate (A)	.310	.307	.308	.735	.725	.650	1.25	1.76	2.29	1.74	2.30
Input Parameters	Plasma Volume to Surface Area Ratio (V/A --cm)	1.4	1.4	1.4	1.4	1.4	1.4	2.5	2.5	2.5	2.5	2.5
	Average Maxwellian Electron Temperature (T_{mx} --eV)	4.2	9.1	12.2	4.3	7.1	10.2	3.3	3.6	3.8	3.0	2.9
	Average Primary-to-Maxwellian Electron Density Ratio (n_{pr}^+/n_{mx}^+)	.034	.083	.166	.017	.042	.134	.50	.35	.25	.19	.22
	Average Primary Electron Energy (e_{pr} --eV)	27.5	29.6	38.4	21.5	23.4	31.0	25.4	25.5	27.2	19.6	19.7
	Average Electron Density ($n_e^+ \times 10^{-10} \text{ cm}^{-3}$)	9.80	9.10	8.07	36.0	24.3	18.2	7.51	8.97	16.4	8.3	12.8
	Uniformity Factor F_+	2.3	2.1	2.3	2.0	1.9	1.8	1.5	1.5	1.5	1.8	1.7
	Uniformity Factor F_{++}	3.1	2.5	2.6	2.5	2.1	2.0	1.8	1.9	1.8	2.5	2.1
Calculated Normalized Densities	Measured Double-to-Single Ion Current Ratio (I^{++}/I^+)	.024	.073	.12	.036	.081	.18	.080	.125	.167	.062	.080
	Neutral Ground State Atoms	.63	.68	.73	.42	.50	.57	.71	.67	.58	.65	.59
	Neutral Metastable State Atoms	.12	.063	.040	.15	.086	.048	.060	.075	.085	.11	.11
	Neutral Resonance State Atoms	.21	.19	.14	.32	.28	.25	.14	.16	.19	.18	.22
	Singly Charged Ground State Ions	.036	.069	.084	.094	.12	.12	.081	.084	.13	.052	.076
	Singly Charged Metastable Ions	.002	.002	.002	.015	.011	.006	.003	.004	.010	.003	.006
Doubly Charged Ground State Ions	.000	.002	.004	.002	.004	.007	.003	.003	.007	.001	.002	
Calculated Production Fractions of Double Ions from Single Ions	Neutral Ground State	.42(.39) ^a	.59(.23)	.70(.32)	.25(.17)	.40(.15)	.52(.29)	.66(.95)	.60(.91)	.52(.87)	.51(.87)	.47(.90)
	Neutral Metastable States	.29(.23)	.13(.19)	.08(.28)	.34(.10)	.19(.11)	.10(.25)	.12(.87)	.16(.79)	.19(.73)	.25(.69)	.24(.73)
	Neutral Resonance States	.29(.32)	.28(.22)	.22(.32)	.41(.13)	.41(.13)	.38(.28)	.22(.92)	.24(.87)	.29(.84)	.24(.78)	.29(.82)
	Neutral Ground State	.032(.26)	.15(.08)	.23(.31)	.012(0.)	.046(0.)	.09(.14)	.000(0.)	.000(0.)	.002(0.)	.001(0.)	.000(0.)
	Neutral Metastable States	.006(.26)	.014(.08)	.012(.31)	.004(0.)	.008(0.)	.008(.14)	.000(0.)	.000(0.)	.000(0.)	.000(0.)	.000(0.)
	Neutral Resonance States	.011(.26)	.040(.08)	.045(.31)	.009(0.)	.026(0.)	.039(.14)	.000(0.)	.000(0.)	.001(0.)	.000(0.)	.000(0.)
	Singly Charged Ionic State	.94(.62)	.78(.28)	.70(.35)	.95(.34)	.89(.21)	.84(.33)	.99(.99)	.99(.97)	.97(.95)	1.00(.95)	1.00(.97)
	Singly Charged Metastable Ionic States	.014(.72)	.013(.26)	.012(.41)	.025(.11)	.027(.07)	.022(.33)	.008(.99)	.010(.98)	.025(.97)	.001(.70)	.001(.76)
	Neutral Ground State											
	Neutral Metastable States											
	Neutral Resonance States											

^a Numbers in parenthesis are the fraction of the indicated interactions effected by primary electrons.

needed to maintain a specified single ion density and so the normalized single ion density increases as previously observed.

The last section in Table III shows the calculated production rates for singly and doubly charged ions through the various intermediate states. These production rates have been normalized by the total production rate of the specie indicated. The fraction of the associated interactions effected by the primary electrons is indicated in parenthesis. For example, at the 15 cm thruster's 37 V, SERT II grid operating point, 59% of the single ions are produced as a result of electron interaction with neutral ground state atoms and 28% resulted from electron bombardment of neutral resonance state atoms. The neutral ground state-to-single ionic state interactions were induced by primary electrons 23% of the time and by Maxwellian electrons the remainder (77%) of the time.

Thruster performance is determined primarily by the mechanism for the production and loss of single ions. The production of these ions is, according to this model, quite dependent on the neutral metastable and neutral resonance states which are ignored in most other analyses. The manner in which single ions are produced however differs a great deal between the two thrusters. In the 15 cm thruster most of the single ions are produced as a result of Maxwellian electron bombardment while primary electrons are unimportant because of their low densities. This indicates that for 15 cm thruster operation the primary electron region is the important reaction region because it is the region where high densities of high energy Maxwellian electrons occur. In the 30 cm thruster, however, relatively high primary electron densities exist and since the Maxwellian electron temperature is low most of the single ion

production results from primary electron bombardment. So for the 30 cm thruster the primary electron region is the important reaction region because it contains high densities of high energy primary electrons.

Table III indicates in all cases a large percentage of the double ions are produced from single ions. This is as one would expect because the minimum energy required to produce a double ion from a single ion is 18.7 eV while 29 eV is required to produce a double ion from a neutral ground state atom. As the power input to the thruster increases the number of electrons with energies greater than 29 eV increases causing the relative importance of the neutral-to-double transition to increase. The least energy is required for the production of double ions via singly ionized metastable states, but the densities of these states are so low that this production mechanism is unimportant.

SIMPLIFIED MODEL

In the previous section it has been shown that most double ions are produced as a result of electron bombardment of single ions. In order to simplify the analysis of the "Theoretical Model" section the other intermediate states for double ion production can therefore be ignored with no significant loss in the accuracy of the double ion density calculations. In the simplified model presented here the approximation is made that the total rate of production of double ions equals the rate of production of double ions from single ions. This production rate is given by:

$$R_p^{++} \approx R_{p_+}^{++} = n_+^* [n_{pr}^* P_+^{++}(\xi_{pr}^*) + n_{mx}^* Q_+^{++}(T_{mx}^*)] \psi \quad (32)$$

The total loss rate of double ions is given by the equation

$$R_{l_{++}} = \frac{n_{++}^* v_{++}^* A}{F_{++}} \quad (33)$$

Equating the loss and production rates and then solving the resultant equation for the double ion density one obtains

$$n_{++}^* = n_+^* \frac{[n_{pr}^* P_+^{++}(\xi_{pr}^*) + n_{mx}^* Q_+^{++}(T_{mx}^*)] \psi}{\frac{v_{++}^* A}{F_{++}}} \quad (34)$$

The approximation $n_e^* = n_+^*$ can now be used and Equation (18) can be substituted for the double ion velocity to obtain the following equation.

$$n_{++}^* = n_e^{*2} \frac{\psi}{A} F_{++} \frac{\left[\frac{n_{pr}^*}{n_e^*} P_+^{++}(\epsilon_{pr}^*) + \frac{n_{mx}^*}{n_e^*} Q_+^{++}(T_{mx}^*) \right]}{\left[n_{mx}^* q \left(1 + \frac{n_{pr}^*}{n_{mx}^*} \right) / m_i \right]^{1/2}} \quad (35)$$

*↑
double ioning*

The double ion density can now be determined for a given thruster operating condition using this equation and the plots of $P_+^{++}(\epsilon_{pr}^*)$ and $Q_+^{++}(T_{mx}^*)$ found in Figure 7 if the volume averaged plasma properties and the uniformity factor F_{++} are known. This equation will consistently predict lower double ion densities than the complete model since it ignores the production of double ions from neutral states and the singly ionized metastable states, but this error should generally be small. The error will be greatest for plasmas with high energy electrons which can produce double ions directly from neutral states.

The last section of Table III can be used to determine the magnitude of this error for the 11 cases considered in this study. Since the simplified model considers only the single-to-double transition the error associated with this approximation can be determined from the listed value of the percentage of double ions produced from single ions. For example, for the 15 cm-SERT II grid - 37 V anode voltage case the percentage of double ions produced from single ions is 78%. This means that the value of the double ion density predicted by the simplified model would be 78% of that predicted by the complete model. Examination of Table III indicates the double ion densities calculated using the simplified model will agree well with the complete model's predictions for all the 30 cm thruster conditions because in these cases the percentage of double ions produced from single ions is greater than 97%.

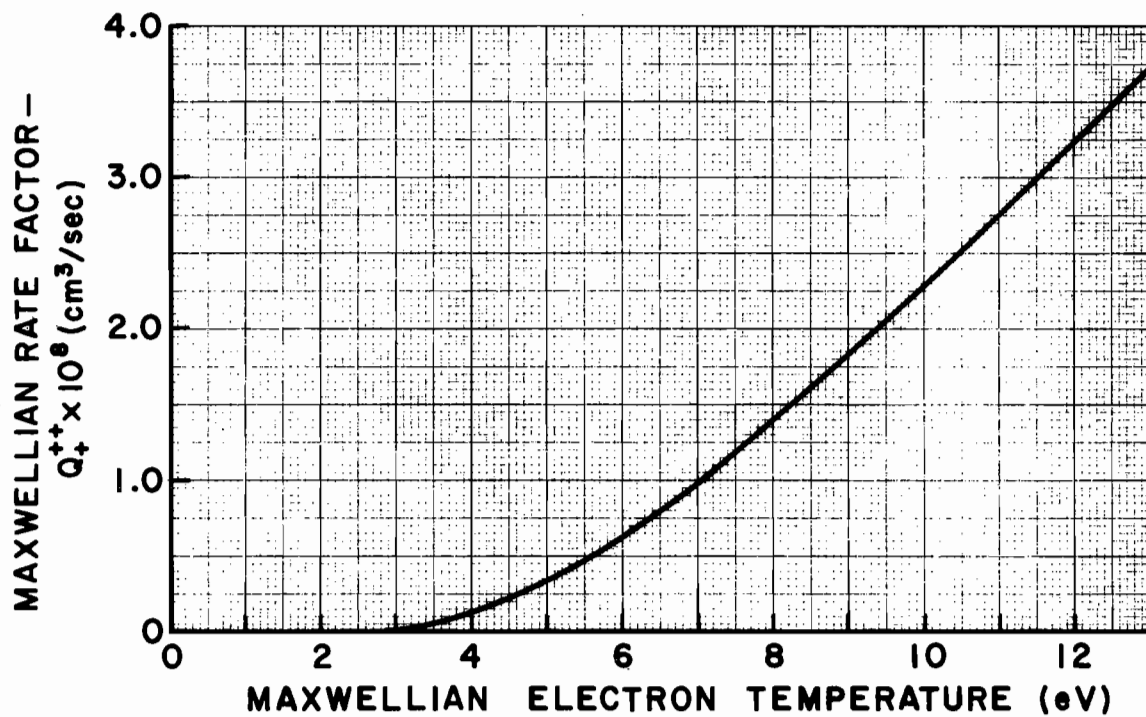
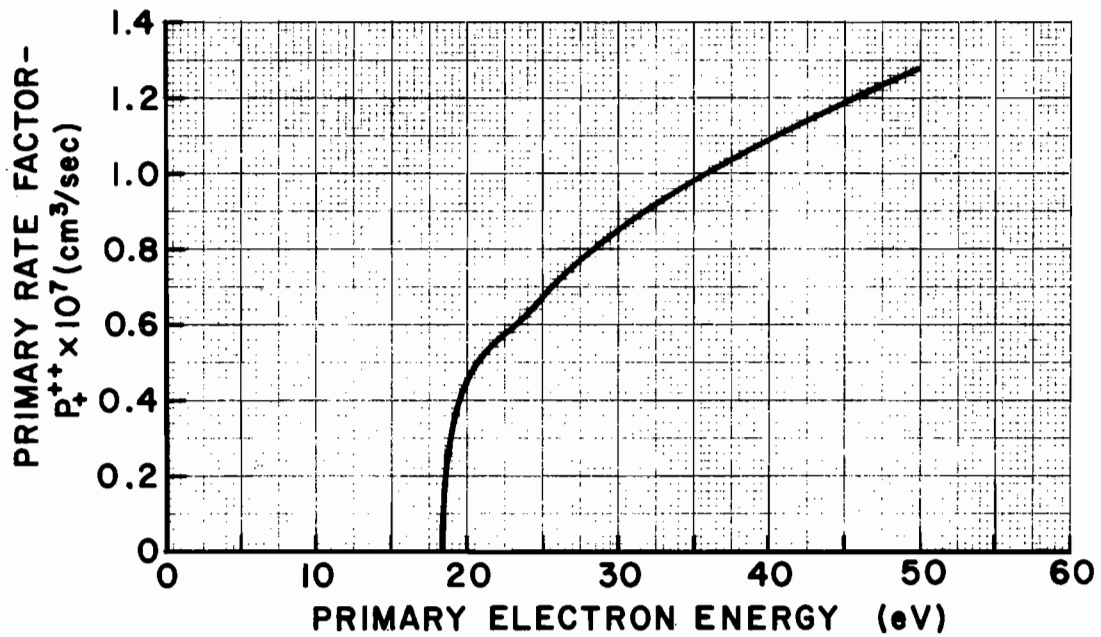


Figure 7 Rate Factors for $Hg^+ \rightarrow Hg^{++}$

In each of these cases few electrons have energies in excess of 29 eV (the minimum energy required for the neutral-to-double transition). The simplified model will however, according to Table III, yield results which are generally low for the 15 cm thruster data (e.g. 30% low for the SERT II grid - 42 V anode voltage condition) because in these cases sufficiently high Maxwellian electron temperatures exist to cause a relatively large percentage of the electrons to have energies in excess of 29 eV.

The most accurate way to determine the values of the average plasma properties required in Equation (35) would be to conduct a Langmuir probe survey of the discharge chamber under consideration to determine the plasma properties at many different points and to then use this information in Equations (10) to (15) and (21) to determine average plasma properties. The collection of the plasma property data is however costly and time consuming. For this reason average plasma property correlations were developed. The correlating parameters used are composed of thruster operating parameters (e.g. I_{arc}) and geometric properties (e.g. Ψ/A). Using the Maxwellian electron temperature data listed in Table III, for example, one obtains the correlation presented in Figure 8. The terms used in the correlating parameter are defined in Table III. The correlating parameter used in Figure 8 was determined by trial and error. The shape of a curve through the resultant data points was picked to match the trends observed in the data points. For example, the slope of the curve in the neighborhood of the low Maxwellian electron temperature points is seen to decrease. This agrees with the trend observed in the data and also agrees with a prediction, based on inelastic collision cross section data, which says a lower

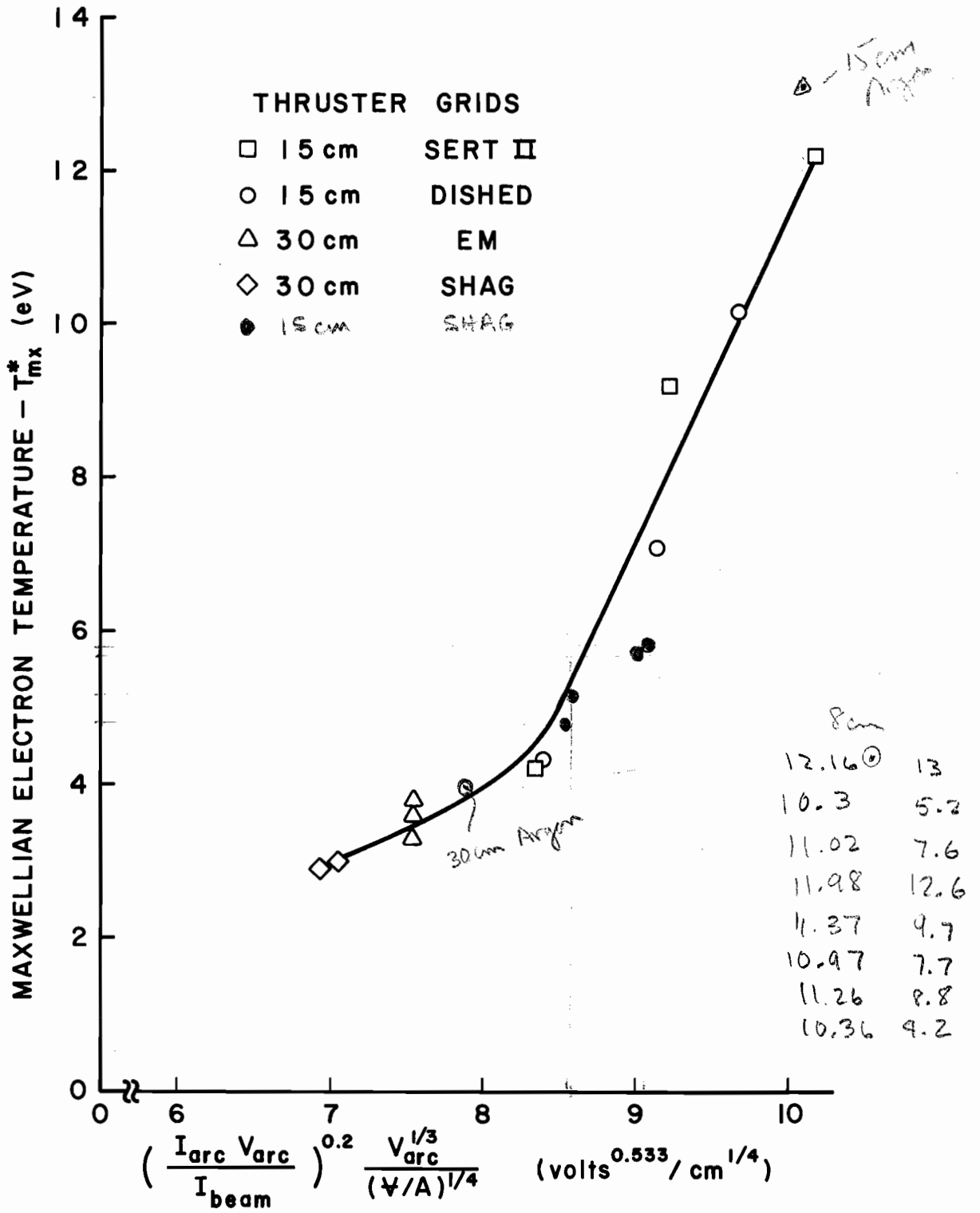


Figure 8 Maxwellian Electron Temperature Correlation

bound on the Maxwellian electron temperature should exist roughly in the neighborhood of 5 eV⁽¹⁾.

The correlation for the primary electron energy is shown in Figure 9. The correlating parameter contains the quantity η_c which is the corrected propellant utilization. The corrected utilization was used in the correlating parameter, instead of the measured propellant utilization, because a better fit of the data points resulted from its use. The propellant utilization (η) of an ion thruster depends upon the plasma properties, the effective open area for the loss of neutral atoms through the grids (A_0) and the effective open area for the loss of ions through the grids (A_+). The propellant utilization is defined by the equation

$$\eta = \frac{n_+ v_+ A_+}{n_+ v_+ A_+ + n_{ot} v_0 A_0} \approx 1 - \frac{n_{ot} v_0 A_0}{n_+ v_+ A_+} \quad (36)$$

where n_{ot} is the total neutral atom density. The primary energy (and other average plasma properties) of a given thruster correlate with the propellant utilization as defined above, but correlation between grid sets having different values of the ratio A_0/A_+ is poor. The problem caused by the utilization's dependence upon grid sets can be corrected by eliminating the ratio A_0/A_+ from Equation (36) and then substituting in its place the value of the ratio A_0/A_+ for some standard grid set. The resultant quantity is the corrected utilization and is defined by the equation

$$\eta_c = 1 - \frac{n_{ot} v_0}{n_+ v_+} \left[\frac{A_0}{A_+} \right]_{\text{standard}} \quad (37)$$

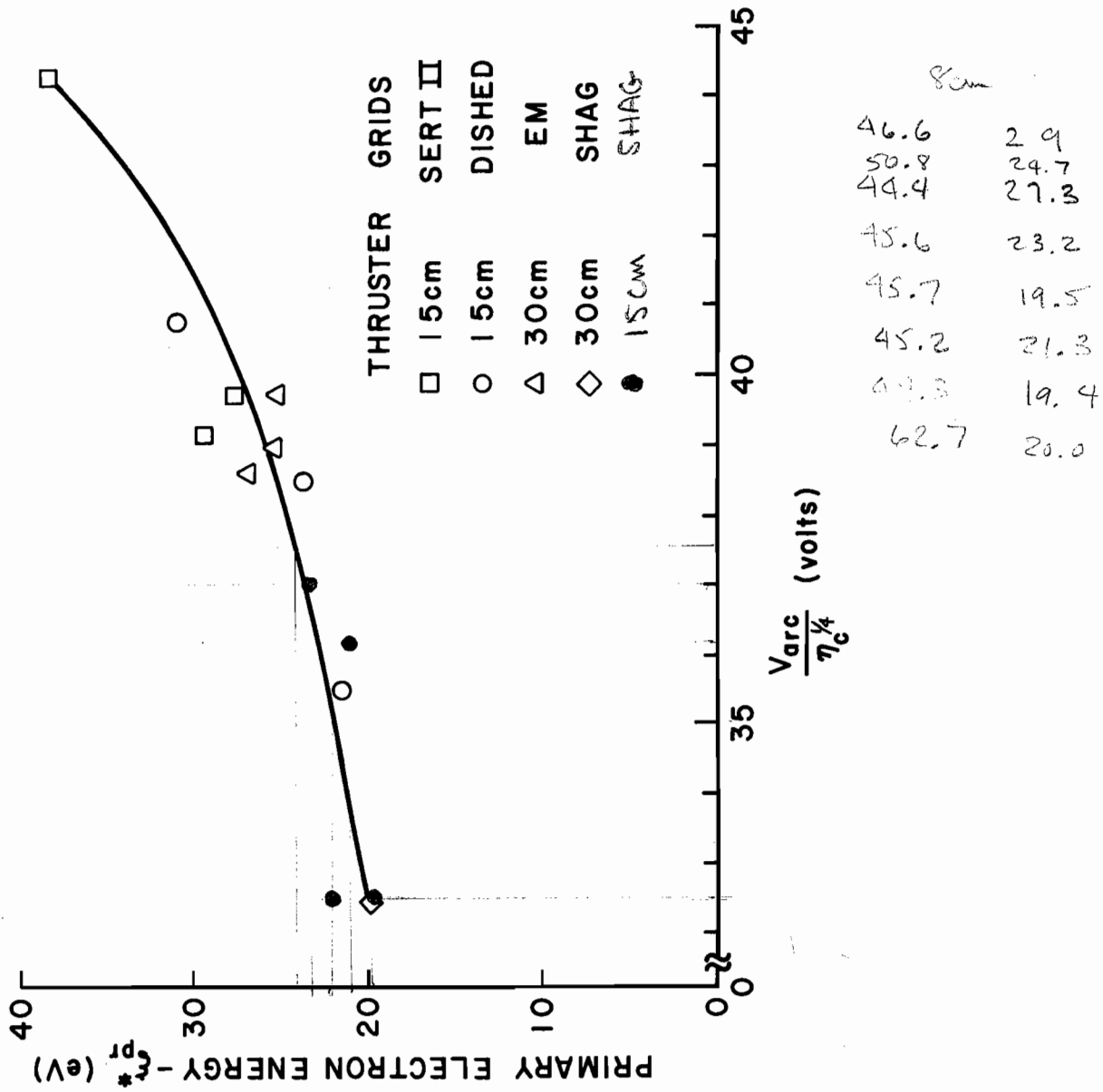


Figure 9 Primary Electron Energy Correlation

The open area for the loss of ions (A_+) from a thruster is proportional to the open area fraction of the screen grid (ϕ_s)⁽¹⁾. Equilibrium flow theory⁽¹⁾ can be used to determine that the open area for the loss of neutral atoms (A_0) is proportional to the quantity $(\phi_s \phi_a)/(\phi_s + \phi_a)$ where ϕ_a is the open area fraction of the accelerator grid. These two approximations can be used to define the ratio A_0/A_+ as follows

$$\frac{A_0}{A_+} = \left(\frac{\phi_s \phi_a}{\phi_s + \phi_a} \right) / \phi_s = \frac{\phi_a}{\phi_s + \phi_a} \quad (38)$$

If Equations (36) - (38) are combined the following result is obtained,

$$\eta_c = 1 - .5(1 - \eta) \frac{\phi_s + \phi_a}{\phi_a}, \quad (39)$$

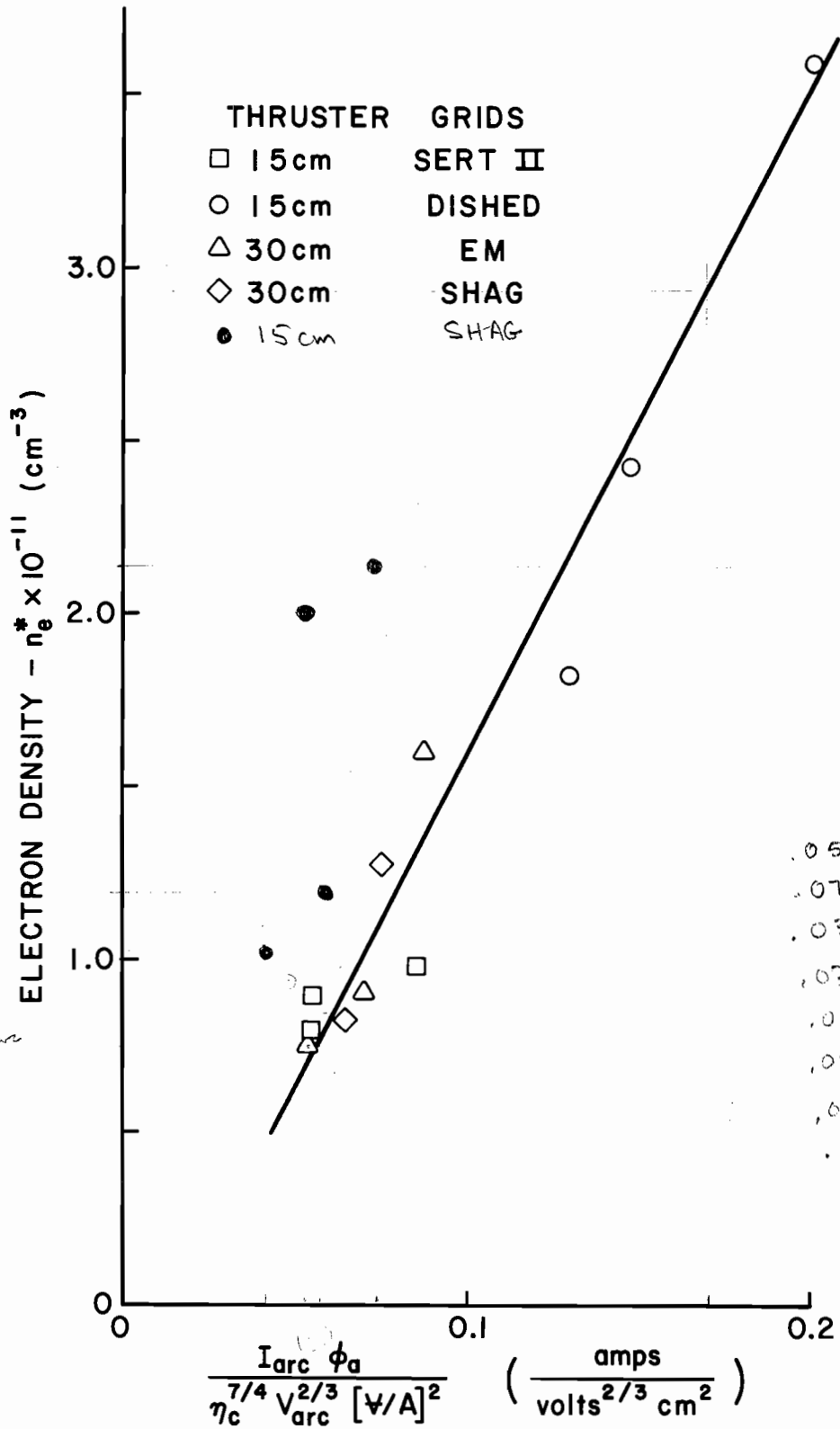
where the constant ".5" defines $\phi_a/(\phi_s + \phi_a)$ for the standard grid set.

Figures 10-12 show correlations for the remaining input parameters. These correlations were developed by trial and error in a manner similar to that used to obtain those in Figures 8 and 9. It should be noted that the correlation in Figure 11 is for the quantity $n_{pr}^* [V/A]^{-1.5}$ not the primary electron density (n_{pr}^*).

It should be understood that the correlations of Figures 8-12 are based on data obtained from strongly divergent magnetic field thrusters. The average plasma properties predicted using these figures may be inaccurate for other types of thrusters (e.g. multipole or radial field thrusters). Therefore Langmuir probe surveys should be made for these other types in order to obtain good estimates of the average plasma properties and hence accurate predictions of the double ion density.

ϕ_s 1
 ϕ_a 2
 25 3

RCL 1
 FMFE
 RCL 2
 +
 RCL 2
 :
 :
 :
 R/S - I_B
 FMFE
 R/S
 ÷
 ↓
 xzy
 -
 xzy
 -
 RCL 3
 y^x
 y_x
 R/S - V_{arc}
 x



8cm

.055	9.2×10^{10}
.072	8.5×10^{10}
.033	12.6
.034	12.5
.032	11.0
.033	11.8
.033	12.9
.27	20

Figure 10 Electron Density Correlation

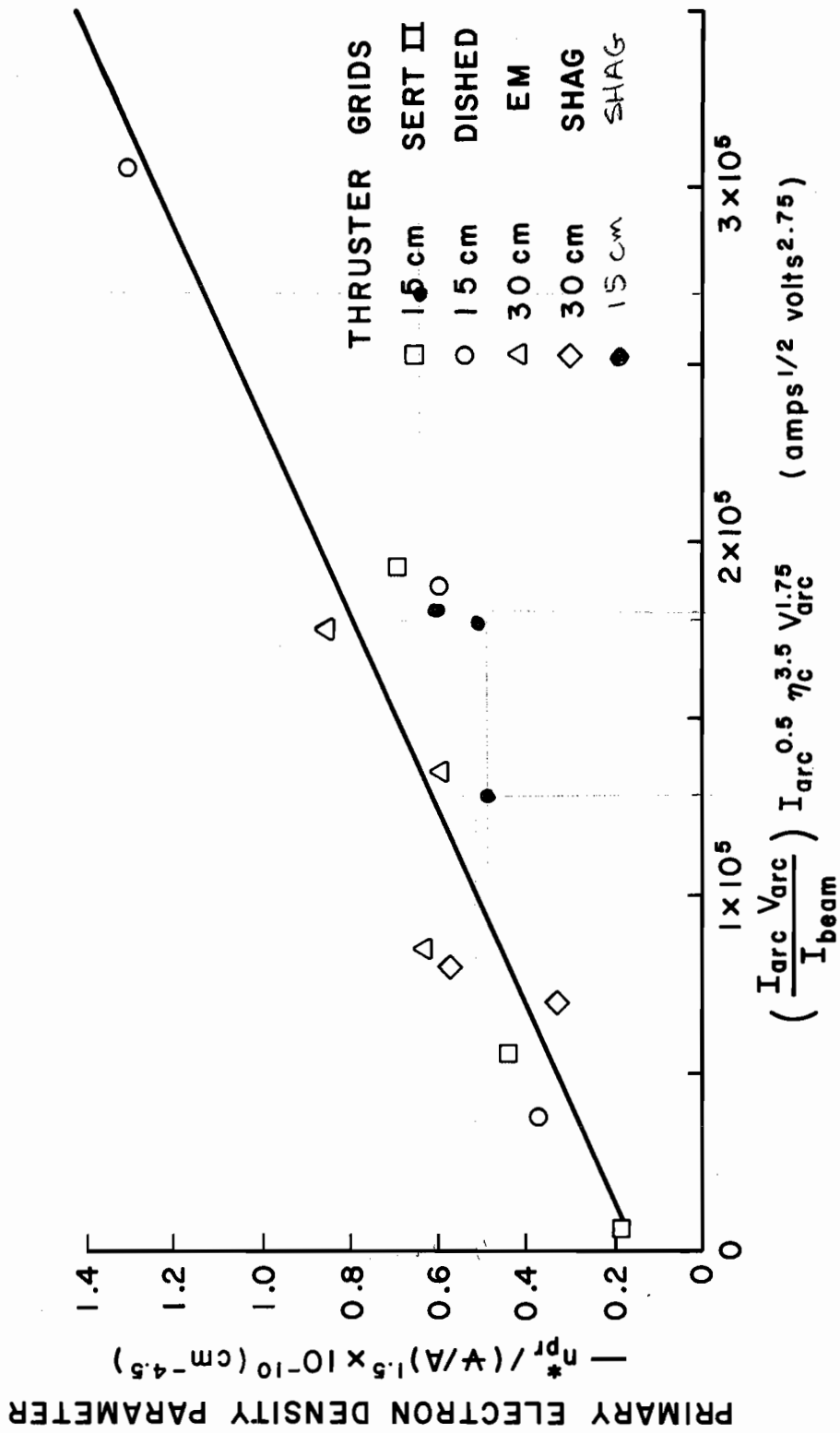


Figure 11 Primary Electron Density Correlation

Application of the simplified model can be best demonstrated through an example. Consider a 15 cm thruster operating at the conditions defined by the first section of Table IV. The corrected utilization (η_c) is first calculated using Equation (39) and a value of 68% is obtained. Next the correlating parameters are calculated. For example, the value of the correlating parameter

$$\left(\frac{I_{\text{arc}} V_{\text{arc}}}{I_{\text{beam}}} \right)^{.2} V_{\text{arc}}^{1/3} (\Psi/A)^{-1/4}$$

used in Figure 8 is $8.3 \frac{\text{volts}}{\text{cm}^{1/4}}^{.533}$. This value indicates the average Maxwellian electron temperature would be 4.6 eV. The remainder of the average plasma properties were determined in a similar manner. The results obtained are listed in the second section of Table IV. Using the values of the primary electron energy and the Maxwellian electron temperature one can enter Figure 7 and determine P_+^{++} (22 eV) and Q_+^{++} (4.6 eV). These quantities, together with the average densities, the uniformity factor and the volume-to-surface area ratio for this thruster are then substituted into Equation (35) to obtain the double ion density as shown in the last section of Table IV. The double ion density calculated using the simplified model is $6.2 \times 10^9 \text{ cm}^{-3}$ while the value calculated using the complete model is $5.2 \times 10^9 \text{ cm}^{-3}$. The major reason for the discrepancy is that the electron temperature in Table IV (4.6 eV) is larger than the value used by the complete model (4.3 eV). This higher electron temperature causes $Q_+^{++}(T_{\text{mx}}^*)$ to be too large and results in the over-estimate of the double ion density.

Table IV.

Determination of the Double Ion Density Using the Simplified Model

Measured Thruster Variables

(15 cm Thruster)

I_{arc}	= 3. amps	ϕ_s	= .67
V_{arc}	= 32.2 volt	ϕ_a	= .67
I_{beam}	= .499 amps	Ψ/A	= 1.4 cm
η	= .68		
η_c	= .68		

Approximate Plasma Properties

T_{mx}^*	= 4.6 eV	n_{pr}^*	= $4.64 \times 10^9 \text{ cm}^{-3}$
ξ_{pr}^*	= 22. eV	n_e^*	= $3.51 \times 10^{11} \text{ cm}^{-3}$
F_{++}	= 2.55	n_{mx}^*	= $n_e^* - n_{\text{pr}}^* = 3.46 \times 10^{11} \text{ cm}^{-3}$

Calculation of the Double Ion Density

$$\begin{aligned}
 n_{++}^* &= \frac{(3.51 \times 10^{11} \text{ cm}^{-3})^2 (1.4 \text{ cm}) (2.55)}{\left[9.6 \times 10^9 \frac{\text{cm}^2}{\text{sec}^2 \text{ eV}} (4.6 \text{ eV}) (1.013)\right]^{\frac{1}{2}}} \\
 &\times \left[.013 \left(.55 \times 10^{-7} \frac{\text{cm}^3}{\text{sec}}\right) + .987 \left(.23 \times 10^{-8} \frac{\text{cm}^3}{\text{sec}}\right)\right] \\
 &= 6.2 \times 10^9 \text{ cm}^{-3}
 \end{aligned}$$

An examination of Equation (35) will indicate some general trends which should be considered in the design and operation of electron bombardment thrusters. For example, the double ion density varies linearly with the volume-to-surface area ratio. Therefore if two thrusters have the same average plasma properties the larger thruster will have a higher double ion density. Equation (35) suggests it would be desirable to reduce the electron density since the double ion density is proportional to the square of the electron density. However, making arbitrary adjustments in the plasma properties to reduce the double ion density may have an adverse effect on other aspects of thruster performance which must also be considered. An examination of the effect of electron density on propellant utilization will indicate one of the effects such an adjustment would have. The propellant utilization previously defined in Equation (36), is reproduced below.

$$\eta = 1 - \frac{n_{ot}^* v_o A_o / A_+}{n_+ v_+} \quad (40)$$

The single ion density (n_+^*) can be approximated by the electron density (n_e^*). The total neutral density (n_{ot}^*) is the sum of the densities of all the neutral species and can be calculated using the equation

$$n_{ot}^* = n_o^* (1 + n_{mt}^* / n_o^* + n_{rt}^* / n_o^*) \quad (41)$$

where n_{mt}^* and n_{rt}^* are the total metastable and resonance states densities. The values of the ratios in Equation (41) can be calculated using equations similar in form to Equation (30). The neutral ground state density can be calculated using the equation

$$n_0^* = n_+^* (n_0^*/n_+^*) \approx n_e^* (n_0^*/n_+^*) \quad (42)$$

where the ratio (n_0^*/n_+^*) again takes a form similar to that of Equation (30). Combining these results into Equation (40) a result of the following form is obtained. "f" is a function of the Maxwellian electron temperature, primary electron energy, primary-to-Maxwellian electron density ratio and the uniformity factor F_+ . The dependence of the propellant utilization on the electron density and thruster parameters is explicitly shown.

$$\eta = 1 - \frac{A_0/A_+}{n_e^* \psi/A} f(T_{mx}^*, \epsilon_{pr}^*, n_{pr}^*/n_{mx}^*, F_+) \quad (43)$$

One can see that a reduction in the electron density to reduce the double ion density will also have the undesirable effect of reducing the propellant utilization. However, if some changes in thruster design are made along with a reduction in the electron density the propellant utilization can be held constant while the double ion density is reduced. For example, if a new thruster were being designed one might double the volume-to-surface area ratio by making the thruster larger than its predecessor. It could then be operated at one-half the electron density of the predecessor allowing the propellant utilization to remain constant while exhibiting half the double ion density in accordance with Equation (35).

It might also be desirable to reduce the double ion density of a certain size thruster while maintaining the same propellant utilization. The propellant utilization could be held constant by reducing both the ratio A_0/A_+ (which reduces the relative escape rate of neutrals) and

the electron density in a manner that keeps the ratio $(A_0/A_+)/n_e^*$ constant. According to Equation (35) this would result in a large reduction in the double ion density which varies as the square of the electron density. The data in Table III for the two 30 cm thruster configurations at 1.5 and 2.0 amps beam current can be used to determine if theory and experiment agree for this method of double ion density reduction. The only difference in these two thruster configurations is the open area fraction of the accelerator grid. The EM accelerator grid has an open area fraction (ϕ_a) of 45% while the open area fraction for the SHAG accelerator grid is 23%. Both sets have a 69% open area fraction for the screen grid. The value of the ratio A_0/A_+ can be calculated for both grid sets using Equation (38). For the EM grids the ratio A_0/A_+ has a value of .39 while for the SHAG grids the value of the ratio is .25. The change from EM grids to SHAG grids then allowed operation at a given propellant utilization to occur at a lower arc voltage and hence a lower electron densities and energies and as a result lower double ion densities. In this particular case the double-to-single ion density ratios dropped from 4.4% and 6.0% to 2.2% and 2.8% respectively at two different utilizations when the SHAG grids were used. The theoretical model predicted essentially the same quantitative changes.

CONCLUSIONS

A discharge chamber model for an electron bombardment ion thruster has been developed which considers metastable, resonance and ground state atomic and ionic production and loss mechanisms. The model can be used to predict doubly charged ion densities from plasma property information. These calculated double ion densities agree with measured values to within 40% for low values of the double-to-single ion density ratio ($n_{++}/n_+ < 2\%$) and to within 20% for the rest of the data. Correlations, which relate average plasma properties to thruster operating variables such as anode current, can be used to estimate the average plasma properties in strongly divergent magnetic field thrusters when the properties themselves are not available. Singly charged ions are produced, according to this analysis, in significant numbers in two step processes through intermediate metastable and resonance states in addition to direct ionization from the neutral ground state. Doubly charged ions are produced predominantly via the singly ionized ground state with direct ground state neutral-to-double ion production becoming more significant in plasmas with high Maxwellian electron temperatures and primary electron energies. A simplified model which considers only the singly ionized ground state in double ion production can be used to predict double ion densities that agree with the complete model's predictions to within 5% when primary electron energies and Maxwellian electron temperatures are less than 29 eV and 5 eV respectively. The recent experimental observation⁽¹²⁾ that the use of small hole accelerator grids in conjunction with lower anode voltages provides a means for reducing double ion densities in thrusters, without degrading performance, is supported by the model.

REFERENCES

1. Kaufman, H. R., "Technology of Electron-Bombardment Ion Thrusters," Advances in Electronics and Electron Physics, Vol. 36, Academic Press, 1974.
2. Kieffer, L. J., "Electron Impact Ionization Cross Section Data for Atoms, Atomic Ions and Diatomic Molecules," Rev. Mod. Physics, Vol. 38, No. 1, pp.15, 23, 1966.
3. Shpenik, O. B. and I. P. Azpesochnyi, "Excitation Cross Sections near the Threshold for Electron Atom Collisions," Optics and Spect., Vol. 23, pp.7-10, 1967.
4. Kupriyanov, S. E. and Z. Z. Latypov, "Ionization of Positive Ions by Electrons," Soviet Physics JETP, Vol. ~~19~~¹⁸, No. ~~8~~², pp. 558-559, ~~Sept.~~^{Feb.} 1964.
5. McConnell, J. C. and B. L. Moiseiwitsch, "Excitation of Mercury by Electrons," J. Phys. B., Vol. 1, No. 3, pp.409-412.
6. Gryzinski, Michal, "Classical Theory of Atomic Collisions. I. Theory of Inelastic Collisions," Phys. Rev., Vol. 138, No. 2A, p. A341, April 19, 1965.
7. Strickfaden, W. B. and K. L. Geiler, "Probe Measurements of the Discharge in an Operating Electron Bombardment Engine," AIAA Journal, Vol. 1, No. 8, pp. 1815-1823, August 1963.
8. Masek, T. D., "Plasma Properties and Performance of Mercury Ion Thrusters," AIAA Paper No. 69-256, March 3-5, 1969.
9. Wilbur, P. J., "Hollow Cathode Restartable 15 cm Diameter Ion Thruster," NASA CR-134532, December, 1973.
10. Peters, R. R. and P. J. Wilbur, "Double Ion Production in Mercury Thrusters," AIAA Paper 75-398, March 19-21, 1975.
11. Mitchell, A. C. G., "Resonance Radiation and Excited Atoms," Cambridge at the University Press, 1961.
12. Vahrenkamp, R. P., Personal Communication, January, 1976.
13. Bechtel, R. J., Csiky, G. A., and D. C. Byers, "Performance of a 15-centimeter Diameter, Hollow Cathode Kaufman Thruster," AIAA Paper No. 68-88, January 22-24, 1968.
14. Poeschel, R. L., King, H. J., and D. E. Schneider, "An Engineering Model 30 cm Thruster," AIAA Paper No. 73-1084, Oct. 31 - Nov. 2, 1973.

15. Poeschel, R. L., et al., "2.5 Kw Advanced Technology Ion Thruster," NASA CR-134687, August, 1974.
16. Poeschel, R. L., et al., "High Power and 2.5 Kw Advanced Technology Ion Thruster," Monthly Report No. 7, Contract NAS 3-19703, January, 1976.
17. Wilbur, P. J., "15 cm Diameter Ion Thruster Research," NASA CR-134755, December, 1974.
18. Wilbur, P. J., "An Experimental Investigation of a Hollow Cathode Discharge," NASA CR-130847, December, 1971.
19. Vahrenkamp, R. P., "Measurement of Doubly Charged Ions in the Beam of a 30 cm Mercury Bombardment Thruster," AIAA Paper No. 73-1057, Oct. 31 - Nov. 2, 1973.
20. Wilbur, P. J., "15 cm Mercury Ion Thruster Research," NASA CR-134905, December, 1975.

APPENDIX A

The computer program "HG", which can be used to predict the densities of excited atomic and ion states considered in the complete model, is listed below. The input parameters needed by this program can be approximated using the correlations in Figures 8-12. More accurate input parameters can be determined using the computer program "PROP", listed in Appendix B, and data obtained from a Langmuir probe survey of the discharge chamber. The computer program "HG" uses the equations developed in the "Theoretical Model" section and carries out the calculations in the manner suggested at the end of that section. Comment cards are included in the listing to indicate what calculations, etc. are to be carried in each section.

Values of the functions $P_{\alpha}^{\gamma}(\epsilon_{pr})$ and $Q_{\alpha}^{\gamma}(T_{mx})$ are listed immediately after the computer program listing. The particular initial state (α) and final state (γ) are indicated in the last twenty columns. For example, the label "HGM-HG+ 3P0" indicates the initial state for the reaction is the 6^3P_0 metastable state and the final state is the singly ionized ground state. The first seven cards listed with a particular identifying label contain the values for $P_{\alpha}^{\gamma}(\epsilon_{pr})$ while the second seven list values for $Q_{\alpha}^{\gamma}(T_{mx})$.

```

PROGRAM HG (INPUT,OUTPUT,PUNCH,TAP5=INPUT,TAP6=OUTPUT,TAPE8=PUNCHG 10
1H,FILMPL) HG 20
COMMON /A/ NP,NM,TEMP,PRINRG HG 30
COMMON /R/ UTT(4,25),PD(4,25),IK HG 40
DIMENSION A(8), R(3), C(3), D(3), E(3), SXO0M(2,2,21), SE00M(2,2,2HG 50
11), SX01(2,21), SE01(2,21), SX02(2,21), SE02(2,21), SX0M1(2,2,21),HG 60
2 SE0M1(2,2,21), SX11M(2,2,21), SF11M(2,2,21), SX12(2,21), SE12(2,2HG 70
31), RR(2), TR(2), SELM2(2,2,21), RA0M0(2), RA1M0(2), SX(2,21), SE(HG 80
42,21), P2(8), TI(8), X(8), Y(8), G(8), R(5), Z(8), H(8), SXOR(2,2,HG 90
521), SEOR(2,2,21), SXR1(2,2,21), SFR1(2,2,21), ER(2), TM(2), W(2),HG 100
6 Q(2), TK(2), XSM(2), XSMM(2), XPSM(2), XPSMM(2), FREE(2), PHLOSS(HG 110
72), TAU(2), XLAM(2), DPP(6,6), XNE(6), XL(3,6,10), PNE(6,10), SP(6HG 120
8,6), PZA(7), HA(7), PYP(30), PNO(4), SD(14,6,10), TTI(14,8), PP(10HG 130
9), PR(10), PXP(30), SX1M2(2,2,21), TMP(5), QT(8), QR(8) HG 140
REAL NP,NM HG 150
DATA X(1),TTI(1,1),TTI(2,1),TTI(3,1),TTI(4,1),TTI(5,1),TTI(6,1),TTI(HG 160
11(7,1),TTI(8,1),TTI(9,1),TTI(10,1),TTI(11,1),TTI(12,1),TTI(13,1),THG 170
2TI(14,1),TM,TR,TK,H(1),Z(1),Z(2)/10HPRI ENERGY,10HNEUT DENS.,10HNMHG 180
3/NO PERC,10HNR/NO PERC,10HN+/NO PERC,10HNM+/NO PER,10HN++/NO PER,1HG 190
40HN+/NOT ,10HN++/NOT ,10HBEAM MA. ,10HN+ CM-3 ,10HN++ CM-3HG 200
5 ,10HI ARC AMP.,10HEV/BFAMION,10H ,10H6 3P0 ,10H6 3PHG 210
62 ,10H6 3P1 ,10H6 1P1 ,10H6 2D 5/2 ,10H6 2D 3/2 ,10HHG 220
7N++/N+ ,10HPLOT WITH ,10HM CONSTANT/ HG 230
DATA EP,TAU,XLAM/5.545,6.7,.000000108,.0000000013,.00002537,.00001HG 240
1849/ HG 250
FR(A,8)=(A(1)*R(1)+A(2)*R(2))/(A(1)+A(2)) HG 260
C HG 270
C THIS PROGRAM IS SET UP FOR MERCURY ONLY HG 280
C SET UP OF THE PROGRAM HG 290
C HG 300
NMZ=10 HG 310
NNN=0 HG 320
DO 101 J=2,8 HG 330
H(I)=10H HG 340
101 X(I)=10H HG 350
DO 102 I=3,8 HG 360
102 Z(I)=10H HG 370
DO 103 J=1,14 HG 380
DO 103 I=2,8 HG 390
103 TTI(J,I)=10H HG 400
DO 104 I=1,8 HG 410
QT(I)=TTI(13,I) HG 420
104 QR(I)=10H HG 430
OR(1)=10HUTL. HG 440
NQ=2 HG 450
DO 105 I=1,3 HG 460
105 A(I)=1. HG 470
C HG 480
C READ IN THE INTEGRATED CROSS SECTIONS HG 490
C 1 -- INDICATES DATA FOR PRIMARY ELECTRONS HG 500
C 2--- INDICATES DATA FOR MAXWELLIAN ELECTRONS HG 510
C HG 520
C NEUTRAL TO SINGLE HG 530
C HG 540
C READ (5,168) ((SE01(J,I),SX01(J,I),I=1,21),J=1,2) HG 550
C HG 560
C NEUTRAL TO DOUBLE HG 570
C HG 580
C READ (5,168) ((SE02(J,I),SX02(J,I),I=1,21),J=1,2) HG 590
C HG 600
C SINGLE TO DOUBLE HG 610
C HG 620
C READ (5,168) ((SE12(J,I),SX12(J,I),I=1,21),J=1,2) HG 630
C HG 640
C NEUTRAL TO METASTABLE HG 650

```

C		HG	560
C	READ (5,168) (((SF00M(I,J,K),SX00M(I,J,K),K=1,21),J=1,2),I=1,2)	HG	670
C		HG	680
C	NEUTRAL TO RESONANCE	HG	690
C		HG	700
C	READ (5,168) (((SE0P(I,J,K),SX0P(I,J,K),K=1,21),J=1,2),I=1,2)	HG	710
C		HG	720
C	METASTABLE ATOM TO SINGLE	HG	730
C		HG	740
C	READ (5,168) (((SE0M1(I,J,K),SX0M1(I,J,K),K=1,21),J=1,2),I=1,2)	HG	750
C		HG	760
C	SINGLE METASTABLE TO DOUBLE	HG	770
C		HG	780
C	READ (5,168) (((SE1M2(I,J,K),SX1M2(I,J,K),K=1,21),J=1,2),I=1,2)	HG	790
C		HG	800
C	RESONANCE TO SINGLE	HG	810
C		HG	820
C	READ (5,168) (((SER1(I,J,K),SXR1(I,J,K),K=1,21),J=1,2),I=1,2)	HG	830
C		HG	840
C	SINGLE TO SINGLE METASTABLE	HG	850
C		HG	860
C	READ (5,168) (((SE11M(I,J,K),SX11M(I,J,K),K=1,21),J=1,2),I=1,2)	HG	870
C		HG	880
C	READ IN DATA	HG	890
C	ND-NO. OF DIFFERENT PRIMARY ENERGIES DESIRED FOR EACH ELECTRON DEN	HG	900
C	DP-(BELOW) DELTA PRIMARY ENERGY	HG	910
C	NS-NO. OF DIFFERENT ELECTRON DENSITIES USED PER RUN	HG	920
C	NRR-NO. OF RUNS	HG	930
C	IFLAG=1 NO INTERPOLATION FOR MASS FLOW RATE	HG	940
C		HG	950
C	READ (5,142) ND,NS,NRR,IFLAG	HG	960
C		HG	970
C	BEGIN THE RUNS	HG	980
C		HG	990
C	DP=10.	HG	1000
C	DO 138 IP=1,NRR	HG	1010
C		HG	1020
C	EQUIVALENT OPEN AREA FOR NEUTRALS AND CHARGED PARTICLES. VOLUME OF	HG	1030
C	PRIMARY ELECTRON REGION. NONUNIFORMITY PARAMETERS.	HG	1040
C		HG	1050
C	READ (5,141) OPN,OPC,VOL,F1,F2	HG	1060
C		HG	1070
C	NO. OF DIFFERENT MASS FLOW RATES DESIRED	HG	1080
C		HG	1090
C	NC=2	HG	1100
C		HG	1110
C	VALUES OF M	HG	1120
C		HG	1130
C	IF (IFLAG.EQ.1) GO TO 106	HG	1140
C	READ (5,141) (PNO(I),I=1,NC)	HG	1150
106	KKK=1	HG	1160
	XNI=.05	HG	1170
	DO 129 JJ=KKK,NS	HG	1180
	PRINRG=15.	HG	1190
	XN1=.05	HG	1200
	XNM=0.	HG	1210
	XN2=0.	HG	1220
C		HG	1230
C	PRIMARY ELECTRON VOLUME TO AREA, MAX. TEMPERATURE, DUMMY, PRIMARY/	HG	1240
C	MAXWELLIAN RATIO, ELECTRON DENSITY.	HG	1250
C		HG	1260
C	IF (JJ.NE.1) GO TO 107	HG	1270
	READ (5,143) VA,TEMP,DUMMY,DENR,ELDENS	HG	1280
	IF (IFLAG.EQ.1) PRINRG=DUMMY	HG	1290
	IF (IFLAG.EQ.1) GO TO 109	HG	1300
C		HG	1310

C	ELECTRON DENSITIES FOR ITERATION ON MASS FLOW RATE	HG	1320
C	RFAD (5,140) (TMP(L),L=1,NS)	HG	1330
	GO TO 109	HG	1340
107	ELDENS=TMP(JJ)	HG	1350
	GO TO 109	HG	1360
108	WRITE (6,139)	HG	1370
109	CONTINUE	HG	1380
	XNF(JJ)=FLDENS	HG	1390
	ELD=ELDENS/1.F18	HG	1400
	ENCODE (64,144,II) VA,ELD,TEMP,DENR	HG	1410
	DO 128 II=1,ND	HG	1420
	SEV=0.	HG	1430
	WRITE (6,145) VA,FLDENS,TEMP,PRINPG,DENR	HG	1440
	WRITE (6,146) VOL,OPN,OPC,F1,F2	HG	1450
	TOT=1.+1./DENR	HG	1460
	NP=ELDENS/TOT	HG	1470
	NM=FLDENS/TOT/DENR	HG	1480
	FFNL=20.*TEMP	HG	1490
	CALL YINTEG (SX02,SE02,1.,SUMM,PRSUMM)	HG	1500
C		HG	1510
C	CALCULATION OF METASTABLE/ NEUTRAL GROUND STATE RATIO	HG	1520
C		HG	1530
	DO 112 J=1,2	HG	1540
	DO 110 I=1,2	HG	1550
	DO 110 K=1,21	HG	1560
	SX(I,K)=SX00M(J,I,K)	HG	1570
110	SE(I,K)=SE00M(J,I,K)	HG	1580
	CALL YINTEG (SX,SE,1.,SUM,PRSUM)	HG	1590
	DO 111 I=1,2	HG	1600
	DO 111 K=1,21	HG	1610
	SX(I,K)=SX0M1(J,I,K)	HG	1620
111	SE(I,K)=SE0M1(J,I,K)	HG	1630
	CALL YINTEG (SX,SE,1.,SUM2,PRSUM2)	HG	1640
	WLOSS=230./VA/4.	HG	1650
	WALL=WLOSS	HG	1660
	RA0M0(J)=SUM/(WLOSS+SUM2+SUMM)	HG	1670
	WRITE (6,147) TM(J),RA0M0(J)	HG	1680
	WRITE (6,161)	HG	1690
	WRITE (6,163) SUM,PRSUM	HG	1700
	SEV=SEV+SUM*PRSUM	HG	1710
	WRITE (6,162)	HG	1720
	WRITE (6,167) WLOSS,SUM2,PRSUM2,SUMM,PRSUMM	HG	1730
	TT=WLOSS+SUM2+SUMM	HG	1740
	AA=WLOSS/TT	HG	1750
	AB=SUM2/TT	HG	1760
	AC=SUMM/TT	HG	1770
	WRITE (6,148) AA,AB,AC	HG	1780
112	CONTINUE	HG	1790
	SD(2,JJ,II)=(RA0M0(1)+RA0M0(2))*100.	HG	1800
C		HG	1810
C	CALCULATION AND ITERATION FOR RESONANCE/NEUTRAL, SINGLE/NEUTRAL, +	HG	1820
C	NEUTRAL DENSITY	HG	1830
C		HG	1840
	JKL=-1	HG	1850
	IFLAG=0	HG	1860
	I2=II-2	HG	1870
	I1=II-1	HG	1880
	IF (II.GT.2) XN1=(2.*SD(4,JJ,I1)-SD(4,JJ,I2))/100.	HG	1890
	XN1=XN1+XNM+XN2	HG	1900
	XSM(2)=0.	HG	1910
		HG	1920
C		HG	1930
C	GUESS NEUTRAL DENSITY	HG	1940
C		HG	1950
113	XNO=ELDENS/XNI/1000000.	HG	1960
C		HG	1970

C	CALCULATE RESONANCE/NEUTRAL RATIO	HG	1980
C		HG	1990
	DO 117 J=1,NQ	HG	2000
	IF (IFLAG.EQ.1) GO TO 116	HG	2010
	DO 114 I=1,2	HG	2020
	DO 114 K=1,21	HG	2030
	SX(I,K)=SXOR(J,I,K)	HG	2040
114	SE(I,K)=SEOR(J,I,K)	HG	2050
	CALL YINTEG (SX,SE,1.,XSM(J),XPSM(J))	HG	2060
	DO 115 I=1,2	HG	2070
	DO 115 K=1,21	HG	2080
	SX(I,K)=SYR1(J,I,K)	HG	2090
115	SE(I,K)=SER1(J,I,K)	HG	2100
	CALL YINTEG (SX,SE,1.,XSMM(J),XPSMM(J))	HG	2110
116	CONTINUE	HG	2120
	DVD=33963./XLAM(J)	HG	2130
	SIGMAC=.112/DVD*XLAM(J)**2/TAU(J)	HG	2140
	FRFE(J)=1./(XNO*SIGMAC)	HG	2150
	PHLOSS(J)=1./(9.E12*VA*(TAU(J)*XNO*SIGMAC)**2)	HG	2160
117	RR(J)=XSM(J)/(WALL+PHLOSS(J)+XSMM(J)+SUMM)	HG	2170
	IF (IFLAG.EQ.1) GO TO 118	HG	2180
	CALL YINTEG (SX01,SE01,1.,SUM1,PRSUM1)	HG	2190
	CALL SUMIT (SX0M1,SE0M1,2,RA0M0,TSUM1,B,C)	HG	2200
	W(?)=0.	HG	2210
	Q(?)=0.	HG	2220
118	CALL SUMIT (SXR1,SER1,NQ,RR,TSS,W,Q)	HG	2230
	IF (IFLAG.EQ.1) GO TO 119	HG	2240
C		HG	2250
C	CALCULATION OF SINGLE/NEUTRAL RATIO	HG	2260
C		HG	2270
	VP=SQRT(TEMP*4.8038E9*(1.+NP/NM))/100.	HG	2280
	WLOSS=VP/VA/F1	HG	2290
	CALL SUMIT (SX11M,SE11M,2,A,TSUM2,D,E)	HG	2300
	CALL YINTEG (SX12,SE12,1.,SUM2,PRSUM2)	HG	2310
119	RNIO=(SUM1+TSUM1+TSS)/(WLOSS+TSUM2+SUM2)	HG	2320
C		HG	2330
C	CHECK OF ERROR IN GUESS OF NEUTRAL DENSITY	HG	2340
C		HG	2350
	RNPO=RNIO+XN2+XNM	HG	2360
	ERRPOR=ARS((RNPO-XNI)/RNPO)	HG	2370
	XNI=RNIO+XN2+XNM	HG	2380
	XNI=RNIO	HG	2390
	JKL=JKL+1	HG	2400
	IFLAG=1	HG	2410
	IF (ERRPOR.GT..03) GO TO 113	HG	2420
C		HG	2430
C	NEUTRAL GROUND STATE ATOM DENSITY	HG	2440
C		HG	2450
	XNO=ELDENS/XNI/1000000.	HG	2460
	WRITE (6,149) XNO,JKL	HG	2470
	SD(3,JJ,II)=(RR(1)+RR(2))*100.	HG	2480
	SD(1,JJ,II)=XNO	HG	2490
	SD(4,JJ,II)=RNIO*100.	HG	2500
	XXA=100./(100.+SD(3,JJ,II)+SD(2,JJ,II))	HG	2510
	SD(7,JJ,II)=RNIO*XXA	HG	2520
	XNT=XNO*(1.+RA0M0(1)+RA0M0(2)+RR(1)+RR(2))	HG	2530
	XL(1,JJ,II)=XNT*5750.	HG	2540
C		HG	2550
C	PRINT OUT RESONANCE ATOM DENSITY RATIO	HG	2560
C		HG	2570
	DO 120 J=1,NQ	HG	2580
	WRITE (6,150) TR(J),RR(J),FREE(J)	HG	2590
	WRITE (6,161)	HG	2600
	WRITE (6,163) XSM(J),XPSM(J)	HG	2610
	SEV=SEV+XSM(J)*XPSM(J)	HG	2620
	WRITE (6,162)	HG	2630

```

1          WRITE (6,152) WALL,PHLOSS(J),XSMM(J),XPSMM(J),SUMM,PRSHG 2640
          UMM HG 2650
          TT=WALL+PHLOSS(J)+XSMM(J)+SUMM HG 2660
          AA=WALL/TT HG 2670
          AB=XSMM(J)/TT HG 2680
          AC=SUMM/TT HG 2690
          AD=PHLOSS(J)/TT HG 2700
          WRITE (6,151) AA,AD,AB,AC HG 2710
120        CONTINUE HG 2720
C          PRINT OUT SINGLE ION DENSITY RATIO HG 2730
C          WRITE (6,153) RNIO HG 2740
C          SD(10, JJ, II)=RNIO*XNO HG 2750
          PRIF=FR(B,C) HG 2760
          WRITE (6,161) HG 2770
          PRIG=FR(W,O) HG 2780
          PRIH=FR(D,E) HG 2790
          WRITE (6,164) SUM1,PRSUM1,TSUM1,PRIF,TSS,PRIG HG 2800
          SEV=SEV+SUM1*PRSUM1+TSUM1*PRIF+TSS*PRIG HG 2810
          TT=SUM1+TSUM1+TSS HG 2820
          AA=SUM1/TT HG 2830
          AB=TSUM1/TT HG 2840
          AC=TSS/TT HG 2850
          WRITE (6,154) AA,AB,AC HG 2860
          WRITE (6,162) HG 2870
          WRITE (6,167) WLOSS,SUM2,PRSUM2,TSUM2,PRIH HG 2880
          TT=SUM2+WLOSS+TSUM2 HG 2890
          AA=WLOSS/TT HG 2900
          AB=SUM2/TT HG 2910
          AC=TSUM2/TT HG 2920
          WRITE (6,148) AA,AB,AC HG 2930
C          CALCULATION OF SINGLE META/NEUTRAL RATIO HG 2940
C          DO 123 J=1,2 HG 2950
          DO 121 I=1,2 HG 2960
          DO 121 K=1,21 HG 2970
            SX(I,K)=SX11M(J,I,K) HG 2980
121          SE(I,K)=SE11M(J,I,K) HG 2990
          CALL YINTEG (SX,SE,RNIO,SUM1,PRSUM1) HG 3000
          DO 122 I=1,2 HG 3010
          DO 122 K=1,21 HG 3020
            SX(I,K)=SX1M2(J,I,K) HG 3030
122          SE(I,K)=SE1M2(J,I,K) HG 3040
          CALL YINTEG (SX,SE,1.,SUM2,PRSUM2) HG 3050
          WLOSS=VP/VA/F2 HG 3060
          RAIMO(J)=SUM1/(SUM2+WLOSS) HG 3070
          WRITE (6,155) TK(J),RAIMO(J) HG 3080
          WRITE (6,161) HG 3090
          WRITE (6,163) SUM1,PRSUM1 HG 3100
          SEV=SEV+SUM1*PRSUM1 HG 3110
          WRITE (6,162) HG 3120
          WRITE (6,166) WLOSS,SUM2,PRSUM2 HG 3130
          TT=WLOSS+SUM2 HG 3140
          AA=WLOSS/TT HG 3150
          AB=SUM2/TT HG 3160
          WRITE (6,148) AA,AB HG 3170
123        CONTINUE HG 3180
          XL(2, JJ, II)=(RNIO+RAIMO(1)+RAIMO(2))*VP*XNO*100. HG 3190
          XNM=RAIMO(1)+RAIMO(2) HG 3200
          IF (II.GT.1) XNM=2.*XNM-SD(5, JJ, 11)/100. HG 3210
C          CALCULATION OF DOUBLE/NEUTRAL RATIO HG 3220
C          CALL YINTEG (SXO2,SEO2,1.,SUM1,PRSUM1) HG 3230
          HG 3240
          HG 3250
          HG 3260
          HG 3270
          HG 3280
          HG 3290

```

	CALL YINTEG (SX12,SE12,PN10,SUM2,PRSUM2)	HG 3300
	CALL SUMIT (SX1M2,SE1M2,2,RA1M0,TSUM1,B,C)	HG 3310
	WLOSS=1.4142*VP/VA/F2	HG 3320
	RK=0.	HG 3330
	SD(5,JJ,II)=(RA1M0(1)+RA1M0(2))*100.	HG 3340
124	DO 124 I=1,2	HG 3350
	RK=RK+RA0M0(I)*SUMM	HG 3360
	RL=0.	HG 3370
125	DO 125 I=1,NQ	HG 3380
	RL=RL+RR(I)*SUMM	HG 3390
	R20=(SUM1+SUM2+TSUM1+RK+RL)/WLOSS	HG 3400
C		HG 3410
C	PREDICTION OF NEXT DOUBLE ION/NEUTRAL FOR USE IN PREDICTION	HG 3420
C	OF NEUTRAL DENSITY	HG 3430
C		HG 3440
	IF (II.EQ.1) GO TO 126	HG 3450
	I1=II-1	HG 3460
	XN2=(2.*R20-SD(6,JJ,I1))*01)*2.	HG 3470
	GO TO 127	HG 3480
126	XN2=2.*R20	HG 3490
127	CONTINUE	HG 3500
	SD(11,JJ,II)=R20*XN0	HG 3510
	SD(8,JJ,II)=R20*XXA	HG 3520
	XL(3,JJ,II)=R20*VP*1.4142*XN0*100.	HG 3530
	SD(6,JJ,II)=R20*100.	HG 3540
C		HG 3550
C	WRITE DOUBLE/NEUTRAL RATIO, ETC.	HG 3560
C		HG 3570
	WRITE (6,156) R20	HG 3580
	G(I1)=PRINRG	HG 3590
	PN=FR(B,C)	HG 3600
	WRITE (6,161)	HG 3610
	WRITE (6,165) SUM1,PRSUM1,SUM2,PRSUM2,TSUM1,PN,RK,PRSUMM	HG 3620
	SEV=SEV+SUM1*PRSUM1+SUM2*PRSUM2+TSUM1*PN+(RK+RL)*PRSUMM	HG 3630
	TT=SUM1+SUM2+TSUM1+RK+RL	HG 3640
	AA=SUM1/TT	HG 3650
	AB=SUM2/TT	HG 3660
	AC=TSUM1/TT	HG 3670
	AD=RK/TT	HG 3680
	AE=RL/TT	HG 3690
	WRITE (6,157) AA,AB,AC,AD	HG 3700
	WRITE (6,163) XL,PRSUMM	HG 3710
	WRITE (6,158) AF	HG 3720
	WRITE (6,162)	HG 3730
	WRITE (6,166) WLOSS	HG 3740
C		HG 3750
C	BEAM CURRENT	HG 3760
C		HG 3770
	XXXX=(XL(2,JJ,II)+XL(3,JJ,II)*2.)*1.6E-16*OPC	HG 3780
C		HG 3790
C	MASS LOSS RATE	HG 3800
C		HG 3810
	TOTLOSS=(XL(1,JJ,II)*OPN+(XL(2,JJ,II)+XL(3,JJ,II))*OPC)*1	HG 3820
1	.6E-16	HG 3830
	UTL=XXXX/TOTLOSS	HG 3840
	SD(9,JJ,II)=XXXX	HG 3850
		HG 3860
C	EV/ION	HG 3870
C		HG 3880
	EV=PRINRG*SEV/(XXXX/1.6E-16)*XN0*VOL	HG 3890
C		HG 3900
C	ARC CURRENT	HG 3910
C		HG 3920
	ARCI=SEV*VOL*XN0*1.6E-19+XXXX*.001	HG 3930
	SD(12,JJ,II)=ARCI	HG 3940
	SD(13,JJ,II)=EV	HG 3950

```

WRITE (6,159) XXXX,UTL,EV,ARCI
C
C CHECK FOR PLASMA NEUTRALITY
C
C EP=ABS((XNM+XN2+RNIO)/XNI-1.)
C IF (IFLAG.EQ.1.AND.EP.GT..03) GO TO 108
C PRINRG=PRINRG+DP
C IF (IFLAG.NE.0) GO TO 138
128 CONTINUE
129 CONTINUE
C
C INTERPOLATION FOR THE ELECTRON DENSITY WHICH YIELDS DESIRED MASS
C LOSS RATE
C
C DO 132 IY=1,NS
C
C LOSS RATE
C
C DO 131 JZ=1,ND
C DO 130 JY=1,NS
C PYP(JY)=(XL(1,JY,JZ)*OPN+(XL(2,JY,JZ)+XL(3,JY,JZ))*OP
C )*1.6E-16
130 CONTINUE
C WRITE (6,160) (PYP(JK),JK=1,NS)
C DO 131 JA=1,NC
C CALL AITKEN (PYP,XNF,NS,2,PNO(JA),PNE(JA,JZ))
C IF (PNE(JA,JZ).LT.0.) PNE(JA,JZ)=0.
131 CONTINUE
C
C CALCULATE N+/N+
C
C DO 132 IZ=1,ND
C DPP(IY,IZ)=SD(6,IY,IZ)/SU(4,IY,IZ)
132 CONTINUE
C CALL CRSPLT (PNO,DPP,XNE,PNE,G,X,H,Z,ND,NS,NC)
C
C INTERPOLATION OF PLASMA PROPERTIES ETC. FOR CONSTANT MASS LOSS RATE
C
C DO 135 IK=1,13
C DO 133 IE=1,8
133 Y(IE)=TTI(IK,IE)
C DO 134 IF=1,NS
C DO 134 IF=1,ND
134 DPP(IE,IF)=SD(IK,IF,IF)
C CALL CRSPLT (PNO,DPP,XNE,PNE,G,X,Y,Z,ND,NS,NC)
135 CONTINUE
C DO 137 L=1,NC
C DO 136 K=1,25
C PXP(K)=UTT(L,K)/PNO(L)
136 PYP(K)=PD(L,K)
C CALL MAPA (5,PXP,PYP,1,25,HL,HH,VL,VH,QR,QT,Z,1)
137 CALL MAPM (5,PXP,PYP,1,25,HL,HH,VL,VH,QR,QT,Z,1)
138 CONTINUE
C
C 139 FORMAT (2X,16HITERATION FOR N+)
C 140 FORMAT (8E10.4)
C 141 FORMAT (8F10.4)
C 142 FORMAT (16I5)
C 143 FORMAT (4F10.4,E10.2)
C 144 FORMAT (4HV/A=,F6.3,9X,3HED=,F6.3,3HE18,9X,2HT=,F4.1,9X,4HP/M=,F5.
C 12)
C 145 FORMAT (///,3X,14HVOL/ARFA(M+1)=,F7.4,5X,14HELEC DEN(M-3)=,E11.4,5HG
C 1X,14HELEC TEMP(EV)=,F7.3,5X,16HPR[. ENERGY(EV)=,F7.3,5X,6HNP/NM=,FHG
C 26.5)
C 146 FORMAT (/,10X,10HVOL (CM3)=,F10.3,10X,7HA-NEUT=,F10.3,10X,10HA-+
C 1CM2)=,F10.3,3X, 3HF1=,F6.2,3X, 3HF2=,F6.2)

```

```

147 FORMAT (///,20X,A10,5X,9HNMETA/NO=,F10.5) HG 4620
148 FORMAT (10X,F10.5,21X,2(F10.5,20X)) HG 4630
149 FORMAT (//,10X,23HNEUTRAL DENSITY (CM-3)=,E10.3,10X,15HNO. ITERATING 4640
      IONS=,I4) HG 4650
150 FORMAT (//,20X,A10,5X,8HNRES/NO=,F10.6,10X,20HMEAN FREE PATH (CM)=HG 4660
      1,F8.5) HG 4670
151 FORMAT (11X,F10.5,20X,3(F10.5,20X)) HG 4680
152 FORMAT (10X,F11.4,20X,F11.4,20X,2(E11.4,1X,E9.2,10X)) HG 4690
153 FORMAT (///,20X,6HN+/NO=,F10.5) HG 4700
154 FORMAT (10X,3(F10.5,20X)) HG 4710
155 FORMAT (//,20X,A10,5X,10HN+META/NO=,F10.5) HG 4720
156 FORMAT (///,20X,7HN++/NO=,F10.5) HG 4730
157 FORMAT (10X,4(F10.5,21X)./) HG 4740
158 FORMAT (10X,F10.5) HG 4750
159 FORMAT (/,5X,5HREAM=,F10.3,3HMA.,10X,12HUTILIZATION=,F10.6,10X,16HHG 4760
      1EV PER BEAM ION=,F10.5,10X,5HIARC=,F10.3) HG 4770
160 FORMAT (/,2X,3HM/A,8(3X,F10.1)) HG 4780
161 FORMAT (/,20X,49HNUMERATOR TERMS (1/SEC) FOLLOWED BY PRI. FRACTIONHG 4790
      1) HG 4800
162 FORMAT (/,20X,52HDENOMINATOR TERMS FOLLOWED BY PRI. FRACTION (IF AHG 4810
      1NY)) HG 4820
163 FORMAT (10X,F11.4,1X,E9.2) HG 4830
164 FORMAT (10X,3(F11.4,1X,E9.2,10X)) HG 4840
165 FORMAT (10X,4(E11.4,1X,E9.2,10X)) HG 4850
166 FORMAT (10X,F11.4,20X,F11.4,1X,E9.2,10X) HG 4860
167 FORMAT (10X,F11.4,20X,2(F11.4,1X,E9.2,10X)) HG 4870
168 FORMAT (3(F10.4,E10.3),20X) HG 4880
C HG 4890
      END HG 4900

SUBROUTINE CRSPLOT (PNO,DPP,XNE,PNE,G,X,H,Z,ND,NS,NC) CRS 10
C CRS 20
C THIS SUBROUTINE INTERPOLATES IN THE ARRAY DPP TO GET THE VALUES FOCRS 30
C CONSTANT MASS FLOW RATE (DET. BY PNE) AND THEN PLOTS THE RESULTS CRS 40
C CRS 50
C COMMON /R/ UTL(4,25),PD(4,25),IK CRS 60
C DIMENSION DPP(6,6), PNO(4), XNE(6), PNE(6,10), G(8), PYP(30), PXP(CRS 70
C 130), PP(30), SP(10,30), X(8), Y(8), H(8), Z(4) CRS 80
C CRS 90
C INTERPOLATION CRS 100
C CRS 110
C DO 102 KZ=1,ND CRS 120
C DO 101 KY=1,NS CRS 130
101 PYP(KY)=DPP(KY,KZ) CRS 140
C DO 102 KX=1,NC CRS 150
C CALL AITKEN (XNE,PYP,NS,2,PNE(KX,KZ),SP(KX,KZ)) CRS 160
C IF (PNE(KX,KZ).GT.1.E18) SP(KX,KZ)=0. CRS 170
C IF (PNE(KX,KZ).EQ.0.) SP(KX,KZ)=0. CRS 180
102 CONTINUE CRS 190
C CRS 200
C FIND MAX AND MIN CRS 210
C CRS 220
C DO 104 JO=1,NC CRS 230
C DO 103 JP=1,ND CRS 240
103 PP(JP)=SP(JO,JP) CRS 250
104 CALL MAPA (G,PP,1,ND,HL,HH,VL,VH,X,Y,TI,1) CRS 260
C CRS 270
C PLOT OF DATA CRS 280
C CRS 290
C CALL MAPA (1,PXP,PYP,1,25,HL,HH,VL,VH,X,Y,TI,1) CRS 300
C CALL MAPM (1,PXP,PYP,1,25,HL,HH,VL,VH,X,Y,TI,1) CRS 310
C DO 112 IA=1,NC CRS 320
C DO 105 IR=1,ND CRS 330
105 PP(IR)=SP(IA,IR) CRS 340
C CALL XINTERP (G,PP,PXP,PYP,ND,25,3) CRS 350
C XX=PNO(IA) CRS 360

```

	WRITE (6,113) XX	CRS 370
	WRITE (6,114) X(1),H(1)	CRS 380
	DO 106 IX=1,25	CRS 390
106	WRITE (6,115) PXP(IX),PYP(IX)	CRS 400
	WRITE (6,116) (PNE(IA,II),II=1,ND)	CRS 410
	WRITE (8,117) (G(IX),PP(IX),IX=1,ND)	CRS 420
C		CRS 430
C	PLOT OF UTILIZATION VERSUS DISCHARGE POWER	CRS 440
C		CRS 450
	IF (IK.EQ.9.OR.IK.EQ.13) GO TO 107	CRS 460
	GO TO 111	CRS 470
107	IF (IK.FQ.13) GO TO 109	CRS 480
	DO 108 L=1,25	CRS 490
108	UTL(IA,L)=PYP(L)	CRS 500
	GO TO 111	CRS 510
109	DO 110 L=1,25	CRS 520
110	PD(IA,L)=PYP(L)	CRS 530
111	CONTINUE	CRS 540
	CALL MAPM (2,PXP,PYP,1,25,HL,HH,VL,VH,X,H,Z,1)	CRS 550
112	CALL MAPA (2,PXP,PYP,1,25,HL,HH,VL,VH,X,H,Z,1)	CRS 560
	CALL MAPA (4,PXP,PYP,1,25,HL,HH,VL,VH,X,H,Z,1)	CRS 570
	CALL MAPM (4,PXP,PYP,1,25,HL,HH,VL,VH,X,H,Z,1)	CRS 580
	RETURN	CRS 590
C		CRS 600
113	FORMAT (//,20X,13HPICKED VALUE=,2X,E10.3,9HMILLIAMPS)	CRS 610
114	FORMAT (/,10X,A10,20X,A10)	CRS 620
115	FORMAT (12X,F4.3,18X,F11.4,10X,E11.4)	CRS 630
116	FORMAT (/,5X,10HELEC.DENS.,8(2X,E10.3))	CRS 640
117	FORMAT (8F10.3)	CRS 650
C		CRS 660
	END	CRS 670
	SUBROUTINE XINTERP (X,Y,XI,YI,NIN,NOUT,INTERP)	INT 10
C		INT 20
C	THIS SUBROUTINE RETURNS -NOUT- POINTS WHICH ARE INTERPOLATED TO	INT 30
C	THE -INTERP- DEGREE FROM -X,Y-	INT 40
C		INT 50
	DIMENSION X(NIN), Y(NIN), XI(NOUT), YI(NOUT)	INT 60
	DX=(X(NIN)-X(1))/FLOAT(NOUT-1)	INT 70
	XX=X(1)	INT 80
	DO 101 I=1,NOUT	INT 90
	XI(I)=XX	INT 100
	CALL AITKFN (X,Y,NIN,INTERP,XX,YY)	INT 110
	IF (YY.LT.0.) YY=0.	INT 120
	YI(I)=YY	INT 130
101	XX=XX+DX	INT 140
	RETURN	INT 150
C		INT 160
	END	INT 170
	SUBROUTINE YINTEG (SIGMA,SIGNRG,PROP.SUM,PRSUM)	NTG 10
C		NTG 20
C	EVALUATION OF REACTION RATE	NTG 30
C		NTG 40
	COMMON /A/ NP,NM,T,PRINRG	NTG 50
	DIMENSION SIGMA(2,21), SIGNRG(2,21), SX(21), SE(21)	NTG 60
	REAL NP,NM	NTG 70
C		NTG 80
C	PRIMARY ELECTRONS	NTG 90
C		NTG 100
	DO 101 I=1,21	NTG 110
	SX(I)=SIGMA(1,I)	NTG 120
101	SE(I)=SIGNRG(1,I)	NTG 130
	CALL AITKEN (SE,SX,21,2,PRINRG,RX)	NTG 140
	PSUM=NP*PROP*RX	NTG 150
C		NTG 160

C	MAXWELLIAN ELECTRONS	NTG	170
C		NTG	180
	DO 102 I=1,21	NTG	190
	SX(I)=SIGMA(2,I)	NTG	200
102	SE(I)=SIGNRG(2,I)	NTG	210
	CALL AITKEN (SE,SX,21,2,T,TR)	NTG	220
	TSUM=PROP*NM*TR	NTG	230
	SUM=TSUM+PSUM	NTG	240
	PRSUM=PSUM/SUM	NTG	250
	RETURN	NTG	260
C	END	NTG	270
		NTG	280
	SUBROUTINE SUMIT (SIG,SGE,N,PROP,TSUM,SUMS,PRSUMS)	SUM	10
C		SUM	20
C	TRANSFER ROUTINE FOR EXCITED STATES	SUM	30
C		SUM	40
	COMMON /A/ NP,NM,TEMP,PRINRG	SUM	50
	DIMENSION SIG(N,2,21), SGE(N,2,21), PROP(N), SUMS(N), PRSUMS(N),	SSUM	60
	1X(2,25), SF(2,25)	SUM	70
	REAL NP,NM	SUM	80
		SUM	90
C	CALCULATES THE SUM OF INTERGALS	SUM	100
C		SUM	110
	TSUM=0.	SUM	120
	DO 102 I=1,N	SUM	130
	DO 101 J=1,2	SUM	140
	DO 101 K=1,21	SUM	150
	SX(J,K)=SIG(I,J,K)	SUM	160
101	SF(J,K)=SGE(I,J,K)	SUM	170
	CALL YINTEG (SX,SE,PROP(I),SUMS(I),PRSUMS(I))	SUM	180
102	TSUM=TSUM+SUMS(I)	SUM	190
	RETURN	SUM	200
C	END	SUM	210
		SUM	220
	SUBROUTINE AITKEN (X,Y,N,K,XR,YR)	AIT	10
C		AIT	20
C	*****	AIT	30
C		AIT	40
C	AITKEN INTERPOLATION SURROUTINE	AIT	50
C	CALLING SEQUENCE...	AIT	60
C	CALL AITKEN(X,Y,N,K,XR,YR)	AIT	70
C	X IS A ONE DIMENSIONAL ARRAY OF INDEPENDENT	AIT	80
C	VARIABLE(INCREASING OR DECREASING)	AIT	90
C	Y IS A ONE DIMENSIONAL ARRAY OF DEPENDENT	AIT	100
C	VARIABLE	AIT	110
C	N IS NO. OF X,Y PAIRS	AIT	120
C	K IS DEGREE OF INTERPOLATING POLYNOMIAL (MAX = 10)	AIT	130
C	XR IS INDEP. VARIABLE ARGUMENT	AIT	140
C	YR IS INTERPOLATED RESULT	AIT	150
C		AIT	160
C	*****	AIT	170
C		AIT	180
C	TYPE, DIMENSION AND LABELED COMMON STATEMENTS	AIT	190
C		AIT	200
	DIMENSION X(N), Y(N), XX(11), YY(11)	AIT	210
	K1=K+1	AIT	220
	IF (X(N)-X(1)) 110,101,101	AIT	230
101	IF (XR-X(1)) 102,102,103	AIT	240
102	LL=0	AIT	250
	GO TO 119	AIT	260
C		AIT	270
103	IF (X(N)-XR) 104,104,105	AIT	280
104	LL=N-K1	AIT	290
	GO TO 119	AIT	300

C	105 LL=1	AIT 310			
	LU=N	AIT 320			
	106 IF (LU-LL-1) 117,117,107	AIT 330			
	107 LI=(LL+LU)/2	AIT 340			
	IF (X(LI)-XB) 108,108,109	AIT 350			
	108 LL=LI	AIT 360			
	GO TO 106	AIT 370			
C		AIT 380			
	109 LU=LI	AIT 390			
	GO TO 106	AIT 400			
C		AIT 410			
	110 IF (XB-X(1)) 111,102,102	AIT 420			
	111 IF (X(N)-XB) 112,104,104	AIT 430			
	112 LL=1	AIT 440			
	LU=N	AIT 450			
	113 IF (LU-LL-1) 117,117,114	AIT 460			
	114 LI=(LL+LU)/2	AIT 470			
	IF (X(LI)-XB) 115,116,116	AIT 480			
	115 LU=LI	AIT 490			
	GO TO 113	AIT 500			
C		AIT 510			
	116 LL=LI	AIT 520			
	GO TO 113	AIT 530			
C		AIT 540			
	117 LL=LL-(K1+1)/2	AIT 550			
	IF (LL) 102,119,118	AIT 560			
	118 IF (LL+K1-N) 119,119,104	AIT 570			
	119 DO 120 I=1,K1	AIT 580			
	JI=LL+I	AIT 590			
	XX(I)=X(JI)-XB	AIT 600			
	120 YY(I)=Y(JI)	AIT 610			
	DO 121 I=1,K	AIT 620			
	DO 121 J=I,K	AIT 630			
	IF (XX(J+1).EQ.XX(I)) GO TO 122	AIT 640			
	121 YY(J+1)=(1./(XX(J+1)-XX(I)))*(YY(I)*XX(J+1)-YY(J+1)*XX(I))	AIT 650			
	YF=YY(K1)	AIT 660			
	RETURN	AIT 670			
	122 WRITE (6,123) (X(I),I=1,N)	AIT 680			
	WRITE (6,123) (Y(I),I=1,N)	AIT 690			
	WRITE (6,124)	AIT 700			
	A=1./(XX(J+1)-XX(I))	AIT 710			
	CCC=3.*A	AIT 720			
	RETURN	AIT 730			
C		AIT 740			
	123 FORMAT (10(2X,F10.3))	AIT 750			
	124 FORMAT (10X,17HTROUBLE IN AITKEN)	AIT 760			
C		AIT 770			
	END	AIT 780			
		AIT 790			
&					
	5.0000 0.	6.0000 0.	7.0000 0.	HG-HG+	1
	8.0000 0.	9.0000 0.	10.0000 0.	HG-HG+	2
	11.0000 .624E-14	12.0000 .164E-13	14.0000 .339E-13HG-HG+		3
	16.0000 .506E-13	18.0000 .673E-13	20.0000 .837E-13HG-HG+		4
	23.5000 .111E-12	27.0000 .136E-12	30.0000 .153E-12HG-HG+		5
	33.5000 .172E-12	37.0000 .188E-12	40.0000 .198E-12HG-HG+		6
	42.0000 .205E-12	44.0000 .211E-12	50.0000 .230E-12HG-HG+		7
	3.0000 .225E-14	4.0000 .633E-14	4.3000 .792E-14HG-HG+		1
	4.7000 .103E-13	5.0000 .121E-13	5.3000 .141E-13HG-HG+		2
	5.7000 .169E-13	6.0000 .191E-13	6.3000 .214E-13HG-HG+		3
	6.7000 .244E-13	7.0000 .268E-13	7.5000 .308E-13HG-HG+		4
	8.0000 .348E-13	8.5000 .388E-13	9.0000 .429E-13HG-HG+		5
	9.5000 .469E-13	10.0000 .509E-13	10.5000 .549E-13HG-HG+		6
	11.0000 .589E-13	12.0000 .666E-13	13.0000 .740E-13HG-HG+		7
	5.0000 0.	6.0000 0.	7.0000 0.	HG-HG++	1
	8.0000 0.	9.0000 0.	10.0000 0.	HG-HG++	2

11.0000	0.	12.0000	0.	14.0000	0.	HG-HG++	3
16.0000	0.	18.0000	0.	20.0000	0.	HG-HG++	4
23.5000	0.	27.0000	0.	30.0000	.617E-15	HG-HG++	5
33.5000	.190E-14	37.0000	.306E-14	40.0000	.434F-14	HG-HG++	6
42.0000	.536E-14	44.0000	.648E-14	50.0000	.103E-13	HG-HG++	7
3.0000	.322E-18	4.0000	.429E-17	4.3000	.743F-17	HG-HG++	1
4.7000	.139E-16	5.0000	.210E-16	5.3000	.304F-16	HG-HG++	2
5.7000	.470E-16	6.0000	.629E-16	6.3000	.922F-16	HG-HG++	3
6.7000	.114E-15	7.0000	.142E-15	7.5000	.197E-15	HG-HG++	4
8.0000	.265F-15	8.5000	.346E-15	9.0000	.439E-15	HG-HG++	5
9.5000	.546E-15	10.0000	.665E-15	10.5000	.797E-15	HG-HG++	6
11.0000	.942E-15	12.0000	.127E-14	13.0000	.164F-14	HG-HG++	7
5.	-3. E-30	7.	-2.5 E-30	8.5	-2. F-30	HG+ - HG++	1
10.	-1.5 E-30	12.	-1.25E-30	14.	-1. F-30	HG+ - HG++	2
16.	-.5 E-30	18.6	0. E-30	19.25	.162 E-13	HG+ - HG++	3
20.	.443 E-13	20.5	.47 E-13	22.	.529 E-13	HG+ - HG++	4
25.	.657 E-13	27.5	.766 E-13	30.	.854 E-13	HG+ - HG++	5
33.	.941 E-13	37.	1.02 E-13	40.	1.1 E-13	HG+ - HG++	6
42.	1.15 E-13	46.	1.24 E-13	50.	1.33 F-13	HG+ - HG++	7
3.0000	.267F-15	4.0000	.127E-14	4.3000	.177E-14	HG+ - HG++	1
4.7000	.257E-14	5.0000	.327E-14	5.3000	.405E-14	HG+ - HG++	2
5.7000	.521E-14	6.0000	.616E-14	6.3000	.717E-14	HG+ - HG++	3
6.7000	.860E-14	7.0000	.973E-14	7.5000	.117E-13	HG+ - HG++	4
8.0000	.138E-13	8.5000	.159E-13	9.0000	.181F-13	HG+ - HG++	5
9.5000	.203F-13	10.0000	.226E-13	10.5000	.249E-13	HG+ - HG++	6
11.0000	.272E-13	12.0000	.318F-13	13.0000	.364E-13	HG+ - HG++	7
5.0000	.988F-14	6.0000	.121E-13	7.0000	.107F-13	HG-HGM 3P0	1
8.0000	.907F-14	9.0000	.744E-14	10.0000	.576F-14	HG-HGM 3P0	2
11.0000	.441E-14	12.0000	.333E-14	14.0000	.228F-14	HG-HGM 3P0	3
16.0000	.191E-14	18.0000	.123E-14	20.0000	.103F-14	HG-HGM 3P0	4
23.5000	.827E-15	27.0000	.720E-15	30.0000	.579E-15	HG-HGM 3P0	5
33.5000	.423E-15	37.0000	.286E-15	40.0000	.188E-15	HG-HGM 3P0	6
42.0000	0.	44.0000	0.	50.0000	0.	HG-HGM 3P0	7
3.0000	.318E-14	4.0000	.378E-14	4.3000	.387E-14	HG-HGM 3P0	1
4.7000	.395E-14	5.0000	.398E-14	5.3000	.399E-14	HG-HGM 3P0	2
5.7000	.398E-14	6.0000	.396E-14	6.3000	.393F-14	HG-HGM 3P0	3
6.7000	.388E-14	7.0000	.384E-14	7.5000	.376E-14	HG-HGM 3P0	4
8.0000	.367E-14	8.5000	.358E-14	9.0000	.348E-14	HG-HGM 3P0	5
9.5000	.339F-14	10.0000	.330E-14	10.5000	.321F-14	HG-HGM 3P0	6
11.0000	.312E-14	12.0000	.294E-14	13.0000	.278E-14	HG-HGM 3P0	7
5.0000	0.	6.0000	.437E-13	7.0000	.482E-13	HG-HGM 3P2	1
8.0000	.404E-13	9.0000	.329E-13	10.0000	.260F-13	HG-HGM 3P2	2
11.0000	.212F-13	12.0000	.185E-13	14.0000	.136F-13	HG-HGM 3P2	3
16.0000	.105E-13	18.0000	.799E-14	20.0000	.655E-14	HG-HGM 3P2	4
23.5000	.433F-14	27.0000	.312E-14	30.0000	.227E-14	HG-HGM 3P2	5
33.5000	.168E-14	37.0000	.144E-14	40.0000	.131F-14	HG-HGM 3P2	6
42.0000	.113E-14	44.0000	.916E-15	50.0000	.365E-15	HG-HGM 3P2	7
3.0000	.963E-14	4.0000	.125E-13	4.3000	.130F-13	HG-HGM 3P2	1
4.7000	.135E-13	5.0000	.138F-13	5.3000	.140E-13	HG-HGM 3P2	2
5.7000	.142E-13	6.0000	.143E-13	6.3000	.143E-13	HG-HGM 3P2	3
6.7000	.143E-13	7.0000	.142E-13	7.5000	.141F-13	HG-HGM 3P2	4
8.0000	.139F-13	8.5000	.137E-13	9.0000	.134F-13	HG-HGM 3P2	5
9.5000	.132E-13	10.0000	.129E-13	10.5000	.126E-13	HG-HGM 3P2	6
11.0000	.123F-13	12.0000	.118E-13	13.0000	.112F-13	HG-HGM 3P2	7
5.0000	.948F-14	6.0000	.961E-14	7.0000	.462E-14	HG-HGR 3P1	1
8.0000	.410E-14	9.0000	.694E-14	10.0000	.719F-14	HG-HGR 3P1	2
11.0000	.708E-14	12.0000	.606E-14	14.0000	.628F-14	HG-HGR 3P1	3
16.0000	.640E-14	18.0000	.641E-14	20.0000	.633E-14	HG-HGR 3P1	4
23.5000	.595E-14	27.0000	.527E-14	30.0000	.444E-14	HG-HGR 3P1	5
33.5000	.319E-14	37.0000	.161E-14	40.0000	0.	HG-HGR 3P1	6
42.0000	0.	44.0000	0.	50.0000	0.	HG-HGR 3P1	7
3.0000	.234E-14	4.0000	.315E-14	4.3000	.334F-14	HG-HGR 3P1	1
4.7000	.356F-14	5.0000	.371E-14	5.3000	.384E-14	HG-HGR 3P1	2
5.7000	.398E-14	6.0000	.408E-14	6.3000	.416E-14	HG-HGR 3P1	3
6.7000	.426E-14	7.0000	.432E-14	7.5000	.439E-14	HG-HGR 3P1	4
8.0000	.445E-14	8.5000	.449E-14	9.0000	.451E-14	HG-HGR 3P1	5

9.5000	.452E-14	10.0000	.451E-14	10.5000	.450E-14HG-HGR	3P1	6
11.0000	.448E-14	12.0000	.441E-14	13.0000	.433E-14HG-HGR	3P1	7
5.0000	0.	6.0000	0.	7.0000	.132E-13HG-HGR	1P1	1
8.0000	.349E-13	9.0000	.579E-13	10.0000	.818E-13HG-HGR	1P1	2
11.0000	.106E-12	12.0000	.130E-12	14.0000	.162E-12HG-HGR	1P1	3
16.0000	.179E-12	18.0000	.189E-12	20.0000	.199E-12HG-HGR	1P1	4
23.5000	.209E-12	27.0000	.216E-12	30.0000	.220E-12HG-HGR	1P1	5
33.5000	.223E-12	37.0000	.224E-12	40.0000	.224E-12HG-HGR	1P1	6
42.0000	.224E-12	44.0000	.224E-12	50.0000	.222E-12HG-HGR	1P1	7
3.0000	.166E-13	4.0000	.323E-13	4.3000	.372E-13HG-HGR	1P1	1
4.7000	.437E-13	5.0000	.485E-13	5.3000	.532E-13HG-HGR	1P1	2
5.7000	.594E-13	6.0000	.638E-13	6.3000	.682E-13HG-HGR	1P1	3
6.7000	.737E-13	7.0000	.777E-13	7.5000	.841E-13HG-HGR	1P1	4
8.0000	.901E-13	8.5000	.957E-13	9.0000	.101E-12HG-HGR	1P1	5
9.5000	.106E-12	10.0000	.111E-12	10.5000	.115E-12HG-HGR	1P1	6
11.0000	.119E-12	12.0000	.127E-12	13.0000	.133E-12HG-HGR	1P1	7
5.0000	0.	6.0000	.951E-15	7.0000	.865E-14HGM-HG+3P0		1
8.0000	.233E-13	9.0000	.355E-13	10.0000	.477E-13HGM-HG+3P0		2
11.0000	.590E-13	12.0000	.701E-13	14.0000	.916E-13HGM-HG+3P0		3
16.0000	.110E-12	18.0000	.130E-12	20.0000	.157E-12HGM-HG+3P0		4
23.5000	.205E-12	27.0000	.247E-12	30.0000	.278E-12HGM-HG+3P0		5
33.5000	.309E-12	37.0000	.335E-12	40.0000	.354E-12HGM-HG+3P0		6
42.0000	.365E-12	44.0000	.376E-12	50.0000	.400E-12HGM-HG+3P0		7
3.0000	.103E-13	4.0000	.210E-13	4.3000	.247E-13HGM-HG+3P0		1
4.7000	.298E-13	5.0000	.338E-13	5.3000	.378E-13HGM-HG+3P0		2
5.7000	.433E-13	6.0000	.476E-13	6.3000	.518E-13HGM-HG+3P0		3
6.7000	.575E-13	7.0000	.618E-13	7.5000	.690E-13HGM-HG+3P0		4
8.0000	.762E-13	8.5000	.834E-13	9.0000	.904E-13HGM-HG+3P0		5
9.5000	.974E-13	10.0000	.104E-12	10.5000	.111E-12HGM-HG+3P0		6
11.0000	.118E-12	12.0000	.131E-12	13.0000	.143E-12HGM-HG+3P0		7
5.0000	.682E-15	6.0000	.958E-14	7.0000	.312E-13HGM-HG+3P2		1
8.0000	.484E-13	9.0000	.652E-13	10.0000	.798E-13HGM-HG+3P2		2
11.0000	.929E-13	12.0000	.106E-12	14.0000	.129E-12HGM-HG+3P2		3
16.0000	.149E-12	18.0000	.169E-12	20.0000	.197E-12HGM-HG+3P2		4
23.5000	.244E-12	27.0000	.285E-12	30.0000	.316E-12HGM-HG+3P2		5
33.5000	.346E-12	37.0000	.371E-12	40.0000	.390E-12HGM-HG+3P2		6
42.0000	.400E-12	44.0000	.410E-12	50.0000	.433E-12HGM-HG+3P2		7
3.0000	.176E-13	4.0000	.327E-13	4.3000	.376E-13HGM-HG+3P2		1
4.7000	.442E-13	5.0000	.492E-13	5.3000	.542E-13HGM-HG+3P2		2
5.7000	.610E-13	6.0000	.661E-13	6.3000	.711E-13HGM-HG+3P2		3
6.7000	.778E-13	7.0000	.828E-13	7.5000	.911E-13HGM-HG+3P2		4
8.0000	.992E-13	8.5000	.107E-12	9.0000	.115E-12HGM-HG+3P2		5
9.5000	.123E-12	10.0000	.130E-12	10.5000	.138E-12HGM-HG+3P2		6
11.0000	.145E-12	12.0000	.159E-12	13.0000	.172E-12HGM-HG+3P2		7
5.0000	0.	6.0000	0.	7.0000	0.	HGM+ HG++5	1
8.0000	0.	9.0000	0.	10.0000	0.	HGM+ HG++5	2
11.0000	0.	12.0000	0.	14.0000	0.	HGM+ HG++5	3
16.0000	0.	18.0000	0.	20.0000	.625E-15HGM+ HG++5		4
23.5000	.722E-14	27.0000	.238E-13	30.0000	.396E-13HGM+ HG++5		5
33.5000	.576E-13	37.0000	.744E-13	40.0000	.877E-13HGM+ HG++5		6
42.0000	.959E-13	44.0000	.104E-12	50.0000	.124E-12HGM+ HG++5		7
3.0000	.370E-16	4.0000	.261E-15	4.3000	.397E-15HGM+ HG++5		1
4.7000	.642E-15	5.0000	.879E-15	5.3000	.116E-14HGM+ HG++5		2
5.7000	.162E-14	6.0000	.202E-14	6.3000	.247E-14HGM+ HG++5		3
6.7000	.315E-14	7.0000	.372E-14	7.5000	.477E-14HGM+ HG++5		4
8.0000	.594E-14	8.5000	.722E-14	9.0000	.860E-14HGM+ HG++5		5
9.5000	.101E-13	10.0000	.116E-13	10.5000	.133E-13HGM+ HG++5		6
11.0000	.149E-13	12.0000	.185E-13	13.0000	.221E-13HGM+ HG++5		7
5.0000	0.	6.0000	0.	7.0000	0.	HGM+-HG++3	1
8.0000	0.	9.0000	0.	10.0000	0.	HGM+-HG++3	2
11.0000	0.	12.0000	0.	14.0000	0.	HGM+-HG++3	3
16.0000	0.	18.0000	0.	20.0000	.625E-15HGM+-HG++3		4
23.5000	.722E-14	27.0000	.238E-13	30.0000	.396E-13HGM+-HG++3		5
33.5000	.576E-13	37.0000	.744E-13	40.0000	.877E-13HGM+-HG++3		6
42.0000	.959E-13	44.0000	.104E-12	50.0000	.124E-12HGM+-HG++3		7
3.0000	.370E-16	4.0000	.261E-15	4.3000	.397E-15HGM+-HG++3		1

4.7000	.642E-15	5.0000	.879E-15	5.3000	.116E-14HGM+-HG++3	2
5.7000	.162E-14	6.0000	.202E-14	6.3000	.247E-14HGM+-HG++3	3
6.7000	.315E-14	7.0000	.372E-14	7.5000	.477E-14HGM+-HG++3	4
8.0000	.594E-14	8.5000	.722E-14	9.0000	.860E-14HGM+-HG++3	5
9.5000	.101E-13	10.0000	.116E-13	10.5000	.133E-13HGM+-HG++3	6
11.0000	.149E-13	12.0000	.185E-13	13.0000	.221E-13HGM+-HG++3	7
5.0000	0.	6.0000	.221E-14	7.0000	.129E-13HGR-HG+3P1	1
8.0000	.289E-13	9.0000	.423E-13	10.0000	.553E-13HGR-HG+3P1	2
11.0000	.670E-13	12.0000	.787E-13	14.0000	.101E-12HGR-HG+3P1	3
16.0000	.119E-12	18.0000	.140E-12	20.0000	.167E-12HGR-HG+3P1	4
23.5000	.214E-12	27.0000	.256E-12	30.0000	.288E-12HGR-HG+3P1	5
33.5000	.318E-12	37.0000	.344E-12	40.0000	.363E-12HGR-HG+3P1	6
42.0000	.374E-12	44.0000	.384E-12	50.0000	.409E-12HGR-HG+3P1	7
3.0000	.119E-13	4.0000	.237E-13	4.3000	.276E-13HGR-HG+3P1	1
4.7000	.331E-13	5.0000	.373E-13	5.3000	.416E-13HGR-HG+3P1	2
5.7000	.475E-13	6.0000	.519E-13	6.3000	.563E-13HGR-HG+3P1	3
6.7000	.623E-13	7.0000	.668E-13	7.5000	.743E-13HGR-HG+3P1	4
8.0000	.817E-13	8.5000	.890E-13	9.0000	.963E-13HGR-HG+3P1	5
9.5000	.103E-12	10.0000	.111E-12	10.5000	.117E-12HGR-HG+3P1	6
11.0000	.124E-12	12.0000	.137E-12	13.0000	.150E-12HGR-HG+3P1	7
5.0000	0.	6.0000	0.	7.0000	.793E-15HGR-HG+1P1	1
8.0000	.628E-14	9.0000	.161E-13	10.0000	.246E-13HGR-HG+1P1	2
11.0000	.338E-13	12.0000	.435E-13	14.0000	.625E-13HGR-HG+1P1	3
16.0000	.793E-13	18.0000	.988E-13	20.0000	.126E-12HGR-HG+1P1	4
23.5000	.173E-12	27.0000	.215E-12	30.0000	.247E-12HGR-HG+1P1	5
33.5000	.279E-12	37.0000	.305E-12	40.0000	.375E-12HGR-HG+1P1	6
42.0000	.336E-12	44.0000	.347E-12	50.0000	.372E-12HGR-HG+1P1	7
3.0000	.585E-14	4.0000	.134E-13	4.3000	.162E-13HGR-HG+1P1	1
4.7000	.201E-13	5.0000	.233E-13	5.3000	.265E-13HGR-HG+1P1	2
5.7000	.311E-13	6.0000	.346E-13	6.3000	.382E-13HGR-HG+1P1	3
6.7000	.431E-13	7.0000	.468E-13	7.5000	.531E-13HGR-HG+1P1	4
8.0000	.595E-13	8.5000	.659E-13	9.0000	.722E-13HGR-HG+1P1	5
9.5000	.786E-13	10.0000	.849E-13	10.5000	.912E-13HGR-HG+1P1	6
11.0000	.974E-13	12.0000	.109E-12	13.0000	.121E-12HGR-HG+1P1	7
5.0000	.174E-13	6.0000	.188E-13	7.0000	.200E-13HG+-HGM+ 5	1
8.0000	.210E-13	9.0000	.219E-13	10.0000	.277E-13HG+-HGM+ 5	2
11.0000	.235E-13	12.0000	.241E-13	14.0000	.250E-13HG+-HGM+ 5	3
16.0000	.216E-13	18.0000	.190E-13	20.0000	.168E-13HG+-HGM+ 5	4
23.5000	.137E-13	27.0000	.113E-13	30.0000	.967E-14HG+-HGM+ 5	5
33.5000	.817E-14	37.0000	.697E-14	40.0000	.613E-14HG+-HGM+ 5	6
42.0000	.564E-14	44.0000	.521E-14	50.0000	.416E-14HG+-HGM+ 5	7
3.0000	.806E-14	4.0000	.108E-13	4.3000	.114E-13HG+-HGM+ 5	1
4.7000	.122E-13	5.0000	.126E-13	5.3000	.130E-13HG+-HGM+ 5	2
5.7000	.135E-13	6.0000	.138E-13	6.3000	.140E-13HG+-HGM+ 5	3
6.7000	.143E-13	7.0000	.144E-13	7.5000	.146E-13HG+-HGM+ 5	4
8.0000	.147E-13	8.5000	.148E-13	9.0000	.148E-13HG+-HGM+ 5	5
9.5000	.148E-13	10.0000	.148E-13	10.5000	.147E-13HG+-HGM+ 5	6
11.0000	.146E-13	12.0000	.144E-13	13.0000	.141E-13HG+-HGM+ 5	7
5.0000	0.	6.0000	0.	7.0000	.154E-13HG+-HGM+ 3	1
8.0000	.164E-13	9.0000	.173E-13	10.0000	.181E-13HG+-HGM+ 3	2
11.0000	.188E-13	12.0000	.196E-13	14.0000	.208E-13HG+-HGM+ 3	3
16.0000	.180E-13	18.0000	.157E-13	20.0000	.138E-13HG+-HGM+ 3	4
23.5000	.112E-13	27.0000	.922E-14	30.0000	.789E-14HG+-HGM+ 3	5
33.5000	.664E-14	37.0000	.565E-14	40.0000	.496E-14HG+-HGM+ 3	6
42.0000	.456E-14	44.0000	.421E-14	50.0000	.335E-14HG+-HGM+ 3	7
3.0000	.413E-14	4.0000	.633E-14	4.3000	.688E-14HG+-HGM+ 3	1
4.7000	.754E-14	5.0000	.797E-14	5.3000	.636E-14HG+-HGM+ 3	2
5.7000	.882E-14	6.0000	.911E-14	6.3000	.937E-14HG+-HGM+ 3	3
6.7000	.967E-14	7.0000	.985E-14	7.5000	.101E-13HG+-HGM+ 3	4
8.0000	.103E-13	8.5000	.105E-13	9.0000	.106E-13HG+-HGM+ 3	5
9.5000	.106E-13	10.0000	.107E-13	10.5000	.107E-13HG+-HGM+ 3	6
11.0000	.107E-13	12.0000	.106E-13	13.0000	.105E-13HG+-HGM+ 3	7
1	1	6	1			
1.	1.	800.	2.3	3.1		
.014	4.2	27.5	.034	9.8	E16	

APPENDIX B

The computer program "PROP" is listed below. It can be used to determine the values of the volume averaged plasma properties and the uniformity factors needed by the computer program "HG." The data needed to determine these quantities is obtained from a Langmuir probe survey of the discharge chamber in which the plasma properties are determined at many different locations within the chamber. This data is used to numerically evaluate Equations (10) to (15) and (21) yielding the volume averaged plasma properties and the uniformity factors. Comment cards are included in the computer program to indicate the purpose of each section. A CDC 6400 computer will use approximately thirty seconds of Central Processor time to evaluate five sets of data obtained from five Langmuir probe surveys.

```

PROGRAM PROP (INPUT,OUTPUT,TAPE5=INPUT,TAPE6=OUTPUT) PRP 10
C PRP 20
C THIS PROGRAM CALCULATES THE AVERAGE PROPERTIES PRP 30
C PLS-RADIAL POSITION OF LANGMUIR PROBE POINTS (1-CENTERLINE) PRP 40
C POS-POS. OF DESIRED DATA POINTS IF NR .NE. 4 PRP 50
C POSZ-AXIAL POSITION OF LANGMUIR PROBE POSITIONS (1-UPSTREAM PNT.) PRP 60
C NT-NO. OF TRACFS PER SET NR-NO. OF RADIAL POINTS PRP 70
C IFLAG=1 IF ONE WANTS TO PRODUCE A SET OF POINTS UPSTREAM PRP 80
C IFLAG=2 POINTS PRODUCED AT THE BAFFLE PRP 90
C DIS-DISTANCE FROM SCREEN TO POINT WHERE THE GENERATED SET IS TO PRP 100
C BE PLACFD PRP 110
C RCATH-CATHODE RADIUS PRP 120
C ENP-LENGTH OF PRIMARY ELECTRON REGION AT CENTERLINE PRP 130
C PRP 140
  DIMENSION XNP(72), XNM(72), T(70), Z(70), V(50), ZI(21), G(21), F( PRP 150
121), TE(21), AA(5), HH(5), CC(5), DD(5), EF(5), FF(5), END(11), POPRP 160
2S(5), W(11), POSZ(11), YT(11), YP(11), YM(11), YZ(11), POR(10), AAPRP 170
3A(10), VE(51) PRP 180
  DIMENSION AT(70), AZ(70), ANP(70), ANM(70), A(11), B(11), C(11), DPRP 190
1(11), E(11), VT(11), PLS(5) PRP 200
  DATA AA,RR,CC,DD,EE/25*0./ PRP 230
  DATA POS /0.,1.1,2.2,3.3,4./ PRP 210
  DATA PLS /0.,1.,2.,3.,3.5/ PRP 220
C PRP 240
C INTEGRATED CROSS SECTIONS FOR + TO ++ PRP 250
C PRP 260
  READ (5,129) (ZI(I),F(I),I=1,21) PRP 270
  READ (5,129) (TE(I),G(I),I=1,21) PRP 280
  WRITE (6,133) (ZI(I),F(I),I=1,21) PRP 290
  WRITE (6,133) (TE(I),G(I),I=1,21) PRP 300
  PI=6.2832 PRP 310
101 READ (5,126) NR,NT,IFLAG,DIS,RCATH,ENP PRP 320
  IF (EOF(5)) 125,102,125 PRP 330
102 ND=NT/NR PRP 340
  NN=ND PRP 350
  IF (IFLAG.NE.0) NN=ND+1 PRP 360
  READ (5,127) (POSZ(I),I=1,ND) PRP 370
C PRP 380
C RADIAL DISTANCE TO CRITICAL FIELD LINE PRP 390
C PRP 400
  READ (5,127) (FND(I),I=1,NN) PRP 410
C PRP 420
C READ IN THE PROPERTIES PRP 430
C PRP 440
  DO 103 I=1,NT PRP 450
103 READ (5,130) T(I),Z(I),XNP(I),XNM(I) PRP 460
  IF (NR.EQ.4) GO TO 108 PRP 470
  IS=0 PRP 480
  DO 106 I=1,NT,NR PRP 490
    NND=I+NR-1 PRP 500
    DO 104 J=I,NND PRP 510
      K=J+1-I PRP 520
      YT(K)=T(J) PRP 530
      YP(K)=XNP(J) PRP 540
      YM(K)=XNM(J) PRP 550
104 YZ(K)=Z(J) PRP 560
    DO 105 J=1,4 PRP 570
      L=J+IS PRP 580
      CALL AITKEN (PLS,YT,NR,1,POS(J),AT(L)) PRP 590
      CALL AITKEN (PLS,YP,NR,1,POS(J),ANP(L)) PRP 600
      CALL AITKEN (PLS,YM,NR,1,POS(J),ANM(L)) PRP 610
105 CALL AITKEN (PLS,YZ,NR,1,POS(J),AZ(L)) PRP 620
106 IS=IS+4 PRP 630
  NT=NT*4/NR PRP 640
  ND=NT/4 PRP 650

```

DO 107 J=1,NT	PRP 660
T(J)=AT(J)	PRP 670
Z(J)=AZ(J)	PRP 680
XNP(J)=ANP(J)	PRP 690
107 XNM(J)=ANM(J)	PRP 700
WRITE (6,130) (T(N),Z(N),XNP(N),XNM(N),N=1,NT)	PRP 710
108 IF (IFLAG.EQ.0) GO TO 114	PRP 720
C	PRP 730
C	PRP 740
C	PRP 750
N=1	PRP 760
DO 110 I=1,4	PRP 770
L=0	PRP 780
DO 109 J=I,NT,4	PRP 790
L=L+1	PRP 800
YT(L)=T(J)	PRP 810
YP(L)=XNP(J)	PRP 820
YM(L)=XNM(J)	PRP 830
109 YZ(L)=Z(J)	PRP 840
K=NT+I	PRP 850
CALL AITKEN (POSZ,YT,ND,N,DIS,AT(K))	PRP 860
K=NT+I	PRP 850
CALL AITKEN (POSZ,YT,ND,N,DIS,AT(K))	PRP 860
CALL AITKEN (POSZ,YZ,ND,N,DIS,AZ(K))	PRP 870
CALL AITKEN (POSZ,YP,ND,N,DIS,ANP(K))	PRP 880
CALL AITKEN (POSZ,YM,ND,N,DIS,ANM(K))	PRP 890
IF (AT(K).LT.0.) AT(K)=0.0	PRP 900
IF (AZ(K).LT.0.) AZ(K)=0.0	PRP 910
IF (ANP(K).LT.0.) ANP(K)=0.0	PRP 920
IF (ANM(K).LT.0.) ANM(K)=0.0	PRP 930
WRITE (6,128) AT(K),AZ(K),ANP(K),ANM(K)	PRP 940
110 CONTINUE	PRP 950
C	PRP 960
C	PRP 970
C	PRP 980
ND=ND+1	PRP 990
NNN=ND-1	PRP 1000
XK=FND(ND)	PRP 1010
DO 111 J=1,NNN	PRP 1020
J=ND+1-I	PRP 1030
END(J)=END(J-1)	PRP 1040
111 POSZ(J)=POSZ(J-1)	PRP 1050
END(1)=XK	PRP 1060
POSZ(1)=DIS	PRP 1070
NT=NT+4	PRP 1080
ND=NT/4	PRP 1090
DO 112 I=5,NT	PRP 1100
K=NT+5-I	PRP 1110
J=K-4	PRP 1120
T(K)=T(J)	PRP 1130
Z(K)=Z(J)	PRP 1140
XNP(K)=XNP(J)	PRP 1150
112 XNM(K)=XNM(J)	PRP 1160
NTM=NT-3	PRP 1170
DO 113 I=NTM,NT	PRP 1180
J=I-NTM+1	PRP 1190
T(J)=AT(I)	PRP 1200
Z(J)=AZ(I)	PRP 1210
XNP(J)=ANP(I)	PRP 1220
113 XNM(J)=ANM(I)	PRP 1230
C	PRP 1240
C	PRP 1250
C	PRP 1260
114 DO 123 I=1,ND	PRP 1270
L=4*(I-1)+1	PRP 1280
K=L+3	PRP 1290

C		PRP 1300
C	THIS PRODUCES AN ARRAY OF F(R) AT CONSTANT Z POINTS	PRP 1310
C		PRP 1320
	DO 117 J=L,K	PRP 1330
	M=J-L+1	PRP 1340
	R=POS(M)*PI	PRP 1350
	CALL AITKEN (TE,G,21,2,T(J),GI)	PRP 1360
	CALL AITKEN (ZI,F,21,2,Z(J),FI)	PRP 1370
	XT=XNP(J)+XNM(J)	PRP 1380
	IF (XNM(J).EQ.0.0) GO TO 115	PRP 1390
	TERM=1.0*XNP(J)/XNM(J)	PRP 1400
	GO TO 116	PRP 1410
115	TERM=1.0	PRP 1420
116	VF(J)=SQRT(T(J)*4.803E9*TERM)	PRP 1430
	AA(M)=XNP(J)*XT*FI*R	PRP 1440
	RR(M)=XT*R	PRP 1450
	CC(M)=XT*R*XNP(J)	PRP 1460
	DD(M)=XNM(J)*XT*GI*R	PRP 1470
	EE(M)=XNM(J)*XT*R	PRP 1480
117	FF(M)=R	PRP 1490
C		PRP 1500
C	INTEGRATION OF F YIELDING G(Z)	PRP 1510
C		PRP 1520
	M=4	PRP 1530
	NM=19	PRP 1540
	CALL INTR (POS,AA,M,NM,2,END(I),H)	PRP 1550
	A(I)=H	PRP 1560
	IF (IFLAG.NE.1.OR.I.NE.1) GO TO 118	PRP 1570
	CALL INTR (POS,AA,M,NM,2,RCATH,HM)	PRP 1580
	A(I)=A(I)-HM	PRP 1590
118	CALL INTR (POS,PB,M,NM,2,END(I),H)	PRP 1600
	R(I)=H	PRP 1610
	IF (IFLAG.NE.1.OR.J.NE.1) GO TO 119	PRP 1620
	CALL INTR (POS,RR,M,NM,2,RCATH,HM)	PRP 1630
	R(I)=R(I)-HM	PRP 1640
119	CALL INTR (POS,CC,M,NM,2,END(I),H)	PRP 1650
	C(I)=H	PRP 1660
	IF (IFLAG.NE.1.OR.I.NE.1) GO TO 120	PRP 1670
	CALL INTR (POS,CC,M,NM,2,RCATH,HM)	PRP 1680
	C(I)=C(I)-HM	PRP 1690
120	CALL INTR (POS,DD,M,NM,2,END(I),H)	PRP 1700
	D(I)=H	PRP 1710
	IF (IFLAG.NE.1.OR.I.NE.1) GO TO 121	PRP 1720
	CALL INTR (POS,DD,M,NM,2,RCATH,HM)	PRP 1730
	D(I)=D(I)-HM	PRP 1740
121	CALL INTR (POS,EE,M,NM,2,END(I),H)	PRP 1750
	E(I)=H	PRP 1760
	IF (IFLAG.NE.1.OR.I.NE.1) GO TO 122	PRP 1770
	CALL INTR (POS,EE,M,NM,2,RCATH,HM)	PRP 1780
	E(I)=E(I)-HM	PRP 1790
122	CALL INTR (POS,FF,M,NM,2,END(I),H)	PRP 1800
	VT(I)=H	PRP 1810
	IF (IFLAG.NE.1.OR.I.NE.1) GO TO 123	PRP 1820
	CALL INTR (POS,FF,M,NM,2,RCATH,HM)	PRP 1830
	VT(I)=VT(I)-HM	PRP 1840
123	CONTINUE	PRP 1850
C		PRP 1860
C	INTEGRATION IN Z DIRECTION	PRP 1870
C		PRP 1880
	M=ND	PRP 1890
	CALL QTFG (POSZ,A,V,ND)	PRP 1900
	CALL AITKEN (POSZ,V,ND,2,ENP,QA)	PRP 1910
	CALL AITKEN (POSZ,V,ND,2,0.0,RA)	PRP 1920
	QA=QA-RA	PRP 1930
	CALL QTFG (POSZ,R,V,ND)	PRP 1940
	CALL AITKEN (POSZ,V,ND,2,ENP,QR)	PRP 1950

	CALL AITKEN (POSZ,V,ND,2,0,0,RH)	PRP 1960
	QB=QB-RR	PRP 1970
	CALL QTFG (POSZ,C,V,ND)	PRP 1980
	CALL AITKEN (POSZ,V,ND,2,ENP,QC)	PRP 1990
	CALL AITKEN (POSZ,V,ND,2,0,0,RC)	PRP 2000
	QC=QC-RC	PRP 2010
	CALL QTFG (POSZ,D,V,ND)	PRP 2020
	CALL AITKEN (POSZ,V,ND,2,ENP,QD)	PRP 2030
	CALL AITKEN (POSZ,V,ND,2,0,0,RD)	PRP 2040
	QD=QD-RD	PRP 2050
	CALL QTFG (POSZ,E,V,ND)	PRP 2060
	CALL AITKEN (POSZ,V,ND,2,ENP,QE)	PRP 2070
	CALL AITKEN (POSZ,V,ND,2,0,0,RE)	PRP 2080
	QE=QE-RE	PRP 2090
	CALL QTFG (POSZ,VT,V,ND)	PRP 2100
	CALL AITKEN (POSZ,V,ND,2,ENP,QVT)	PRP 2110
	CALL AITKEN (POSZ,V,ND,2,0,0,RVT)	PRP 2120
	QVT=QVT-RVT	PRP 2130
C		PRP 2140
C	CALCULATION OF PROPERTIES	PRP 2150
C		PRP 2160
	FZI=QA/QC	PRP 2170
	GTE=QD/QE	PRP 2180
	ANE=QB/QVT	PRP 2190
	AP=QC/QB	PRP 2200
	AM=QE/QB	PRP 2210
	Q=QC/QE	PRP 2220
	XP=SQRT((AP*ANE)/(1.+1./Q))	PRP 2230
	XM=SQRT((AM*ANE)/(1.+G))	PRP 2240
	XNE=XP+XM	PRP 2250
	CALL AITKEN (G,TE,21,1,GTE,TE)	PRP 2260
	CALL AITKEN (F,ZI,21,1,FZI,ZIS)	PRP 2270
	R=XP/XM	PRP 2280
	WRITE (6,133) QA,QB,QC,QD,QE	PRP 2290
	WRITE (6,131) XP,XM,R,TE,ZIS	PRP 2300
	WRITE (6,132) XNE,QVT	PRP 2310
	VEA=SQRT(TFS*4.803E9*(1.+R))	PRP 2320
C		PRP 2330
C	FIND NONUNIFORMITY FACTORS	PRP 2340
C		PRP 2350
	CALL AREA (XNP,XNM,XNE,POS,POSZ,ND,KCATH,VE,VEA)	PRP 2360
	IF (IFLAG.EQ.0) GO TO 124	PRP 2370
	NT=NT-4	PRP 2380
	ND=NT/4	PRP 2390
124	CONTINUE	PRP 2400
	GO TO 101	PRP 2410
125	STOP	PRP 2420
C		PRP 2430
	126 FORMAT (3I5,4F10.4)	PRP 2440
	127 FORMAT (8F10.6)	PRP 2450
	128 FORMAT (10X,2F10.4,2E10.3)	PRP 2460
	129 FORMAT (3(F10.4,F10.3),20X)	PRP 2470
	130 FORMAT (10X,2F10.4,2F10.3)	PRP 2480
	131 FORMAT (2X, 11HNP (CM-3) =,E11.4,3X, 11HNM (CM-3) =,E11.4,3X, 6HNPRP 2490	
	1P/NM=,F10.4,3X, 8HT (EV) =,F10.4,3X, 13HPKI. EN.(EV)=,F10.4)	PRP 2500
	132 FORMAT (10X, 13HELECT. DFNS.=,E11.4,5X, 9HVT (CM3)=,F10.4/)	PRP 2510
	133 FORMAT (/8(E11.4,2X))	PRP 2520
C		PRP 2530
	END	PRP 2540
	SUBROUTINE INTR (X,Y,NIN,NUSED,INT,XP,YP)	NTG 10
C		NTG 20
C	THIS SUBROUTINE INTEGRATES Y(X) AND THEN FINDS THE VALUE OF THE	NTG 30
C	INTEGRAL AT XP	NTG 40
C		NTG 50
C	DIMENSION X(NIN), Y(NIN), A(100), H(100), C(100)	NTG 60

	CALL XINTERP (X,Y,A,R,NIN,NUSED,INT)	NTG	70
	CALL QTFG (A,B,C,NUSED)	NTG	80
	CALL AITKEN (A,C,NUSED,INT,XP,YP)	NTG	90
	RETURN	NTG	100
C	END	NTG	110
		NTG	120
	SUBROUTINE AREA (XNP,XNM,XNEE,DTR,DTY,NLN,R,VE,VEA)	ARA	10
C		ARA	20
C	THIS SUBROUTINE CALCULATES THE PLASMA NONUNIFORMITY FACTORS	ARA	30
C	PRY-POINTS (7) DEFINING PRIMARY FIELD LINE (FROM SCREEN GRID)	ARA	40
C	PRR-POINTS (P) DEFINING PRIMARY FIELD LINE (FROM CENTER LINE)	ARA	50
C	NPRF-NO. OF PRIMARY FIELD LINE POINTS	ARA	60
C	IFLAG=1 IF LOSSES ARE ALLOWED TO THE CATHODE POLE PIECE	ARA	70
C	DI- DISTANCE TO BAFFLE FROM SCREEN	ARA	80
C	CZU-POINT WHERE PRIMARY FIELD LINE INTERSECTS CATHODE POLE PIECE	ARA	90
C	(IF IFLAG=1)	ARA	100
C		ARA	110
	DIMENSION DTR(5), DTY(10), XI1(11), XI2(11), XI3(11), XI4(11), PRRARA	ARA	120
	1(10), PRY(10), P(5), Z(5), XNP(51), XNM(51), Q(5), VE(51), V(5), VARA	ARA	130
	2E1(11), VE2(11), VE3(11), VE4(11)	ARA	140
	REAL I1,I2	ARA	150
	NFLAG=0	ARA	160
	MFLAG=0	ARA	170
	READ (5,107) NPRF,IFLAG,DI,CZU	ARA	180
	CZD=DI	ARA	190
	READ (5,111) (PRR(I),PRY(I),I=1,NPRF)	ARA	200
	NR=NLN*4	ARA	210
C		ARA	220
C	BEGIN CALCULATIONS	ARA	230
C	SHUFFLE NO. DENSITIES INTO CORRECT ARRAYS	ARA	240
C		ARA	250
	DO 101 I=1,NP*4	ARA	260
	J=I+1	ARA	270
	K=I+2	ARA	280
	L=I+3	ARA	290
	M=I/4+1	ARA	300
	VF1(M)=VE(I)	ARA	310
	VF2(M)=VE(J)	ARA	320
	VF3(M)=VE(K)	ARA	330
	VE4(M)=VE(L)	ARA	340
	XI2(M)=XNP(J)+XNM(J)	ARA	350
	XI3(M)=XNP(K)+XNM(K)	ARA	360
	XI4(M)=XNP(L)+XNM(L)	ARA	370
	101 XI1(M)=XNP(I)+XNM(I)	ARA	380
C		ARA	390
C	WRITE OUT THESE ARRAYS	ARA	400
C		ARA	410
	WRITE (6,110) (XI1(I),I=1,NLN)	ARA	420
	WRITE (6,110) (XI2(I),I=1,NLN)	ARA	430
	WRITE (6,110) (XI3(I),I=1,NLN)	ARA	440
	WRITE (6,110) (XI4(I),I=1,NLN)	ARA	450
	AZ=0.	ARA	460
	DY=PRY(NPRF)/200.	ARA	470
	AN=0.	ARA	480
	AR=0.	ARA	490
	YZ=DY/2.	ARA	500
C		ARA	510
C	BEGIN CALCULATION OF THE SURFACE INTEGRAL	ARA	520
C	PRIMARY FIELD LINE SECTION	ARA	530
C		ARA	540
	DO 102 I=1,300	ARA	550
	IF (I.EQ.100) DY=DY/2.	ARA	560
	YP=YZ+DY/2.	ARA	570
	YM=YZ-DY/2.	ARA	580
	CALL AITKEN (PRY,PRR,NPRF,1,YZ,XP)	ARA	590

CALL AITKEN (PRY,PRR,NPRF,1,YP,DP)	ARA 600
CALL AITKEN (PRY,PRR,NPRF,1,YM,DM)	ARA 610
DX=DP-DM	ARA 620
N=1	ARA 630
IF (I.GT.225) N=1	ARA 640
CALL AITKEN (DTY,XI1,NLN,N,YZ,P(1))	ARA 650
CALL AITKEN (DTY,XI2,NLN,N,YZ,P(2))	ARA 660
CALL AITKEN (DTY,XI3,NLN,N,YZ,P(3))	ARA 670
CALL AITKEN (DTY,XI4,NLN,N,YZ,P(4))	ARA 680
CALL CHECK (P,4,NFLAG)	ARA 690
J=4	ARA 700
P(5)=P(4)/5.	ARA 710
CALL AITKEN (DTY,VE1,NLN,N,YZ,V(1))	ARA 720
CALL AITKEN (DTY,VE2,NLN,N,YZ,V(2))	ARA 730
CALL AITKEN (DTY,VE3,NLN,N,YZ,V(3))	ARA 740
CALL AITKEN (DTY,VE4,NLN,N,YZ,V(4))	ARA 750
CALL CHECK (V,4,MFLAG)	ARA 760
V(5)=V(4)/5.	ARA 770
CALL AITKEN (DTP,P,J,N,XP,XNE)	ARA 780
CALL AITKEN (DTR,V,J,N,XP,VEE)	ARA 790
YZ=YZ+DY	ARA 800
AR=AR+SQRT(DX**2+DY**2)*6.2832*XP	ARA 810
AZ=AZ+SQRT(DX**2+DY**2)*6.2832*XP*XNE**2*VEE	ARA 820
102 AN=AN+SQRT(DX**2+DY**2)*6.2832*XP*XNE*VEE	ARA 830
C	ARA 840
C SECTION FOR GRIDS	ARA 850
C	ARA 860
P(1)=6.2832*DTR(1)*XI1(NLN)	ARA 870
P(2)=6.2832*DTR(2)*XI2(NLN)	ARA 880
P(3)=6.2832*DTR(3)*XI3(NLN)	ARA 890
P(4)=6.2832*DTR(4)*XI4(NLN)	ARA 900
CALL CHECK (P,4,NFLAG)	ARA 910
P(5)=0.	ARA 920
V(1)=VE1(NLN)	ARA 930
V(2)=VE2(NLN)	ARA 940
V(3)=VE3(NLN)	ARA 950
V(4)=VE4(NLN)	ARA 960
V(5)=0.	ARA 970
DO 103 IK=1,5	ARA 980
103 Q(IK)=V(IK)*P(IK)	ARA 990
CALL QTFG (DTR,Q,Z,5)	ARA 1000
WRITE (6,108) Z(5)	ARA 1010
I1=Z(5)	ARA 1020
AN=AN+Z(5)	ARA 1030
DO 104 JK=2,5	ARA 1040
104 Q(IK)=Q(IK)*P(IK)/(6.2832*DTR(IK))	ARA 1050
CALL QTFG (DTR,Q,Z,5)	ARA 1060
I2=Z(5)	ARA 1070
AZ=AZ+Z(5)	ARA 1080
Z(5)=Z(5)*2.2828	ARA 1090
WRITE (6,108) Z(5)	ARA 1100
AR=AR+3.14159*DTR(5)**2	ARA 1110
Q(5)=0.	ARA 1120
C	ARA 1130
C SECTION FOR RAFFLE	ARA 1140
C	ARA 1150
C	ARA 1160
N=1	ARA 1170
CALL AITKEN (DTY,XI1,NLN,N,DI,P(1))	ARA 1180
CALL AITKEN (DTY,XI2,NLN,N,DI,P(2))	ARA 1190
CALL AITKEN (DTY,XI3,NLN,N,DI,P(3))	ARA 1200
CALL AITKEN (DTY,XI4,NLN,N,DI,P(4))	ARA 1210
CALL CHECK (P,4,NFLAG)	ARA 1220
CALL AITKEN (DTY,VE1,NLN,N,DI,V(1))	ARA 1230
CALL AITKEN (DTY,VE2,NLN,N,DI,V(2))	ARA 1240
CALL AITKEN (DTY,VE3,NLN,N,DI,V(3))	ARA 1250
CALL AITKEN (DTY,VE4,NLN,N,DI,V(4))	ARA 1250

	CALL CHECK (V,4,MFLAG)	ARA 1260
	Q(1)=6.2832*DTR(1)*P(1)*V(1)	ARA 1270
	Q(2)=6.2832*DTR(2)*P(2)*V(2)	ARA 1280
	Q(3)=6.2832*DTR(3)*P(3)*V(3)	ARA 1290
	Q(4)=6.2832*DTR(4)*P(4)*V(4)	ARA 1300
	CALL QTFG (DTR,Q,Z,5)	ARA 1310
	CALL AITKEN (DTR,Z,5,1,R,EC)	ARA 1320
	DO 105 IJ=1,4	ARA 1330
105	Q(IJ)=Q(IJ)*P(IJ)	ARA 1340
	CALL QTFG (DTR,Q,Z,5)	ARA 1350
	CALL AITKEN (DTR,Z,5,1,R,ED)	ARA 1360
	AR=AR+3.1416*R**2	ARA 1370
	AN=AN+EC	ARA 1380
	AZ=AZ+ED	ARA 1390
	IF (IFLAG.NE.1) GO TO 106	ARA 1400
C		ARA 1410
C	CATHODE POLE PIECE SECTION	ARA 1420
C		ARA 1430
	CALL AITKEN (DTY,XI1,NLN,N,CZU,P(1))	ARA 1440
	CALL AITKEN (DTY,XI2,NLN,N,CZU,P(2))	ARA 1450
	CALL AITKEN (DTY,XI3,NLN,N,CZU,P(3))	ARA 1460
	CALL AITKEN (DTY,XI4,NLN,N,CZU,P(4))	ARA 1470
	CALL CHECK (P,4,NFLAG)	ARA 1480
	P(5)=P(4)/5.	ARA 1490
	CALL AITKEN (DTR,P,5,N,R,XN1)	ARA 1500
	CALL AITKEN (DTY,VE1,NLN,N,CZU,V(1))	ARA 1510
	CALL AITKEN (DTY,VE2,NLN,N,CZU,V(2))	ARA 1520
	CALL AITKEN (DTY,VE3,NLN,N,CZU,V(3))	ARA 1530
	CALL AITKEN (DTY,VE4,NLN,N,CZU,V(4))	ARA 1540
	CALL CHECK (V,4,MFLAG)	ARA 1550
	V(5)=V(4)/5.	ARA 1560
	CALL AITKEN (DTR,V,5,N,R,VN1)	ARA 1570
	CALL AITKEN (DTY,XI1,NLN,N,CZD,P(1))	ARA 1580
	CALL AITKEN (DTY,XI2,NLN,N,CZD,P(2))	ARA 1590
	CALL AITKEN (DTY,XI3,NLN,N,CZD,P(3))	ARA 1600
	CALL AITKEN (DTY,XI4,NLN,N,CZD,P(4))	ARA 1610
	CALL CHECK (P,4,NFLAG)	ARA 1620
	P(5)=P(4)/5.	ARA 1630
	CALL AITKEN (DTR,P,5,N,R,XN2)	ARA 1640
	CALL AITKEN (DTY,VE1,NLN,N,CZD,V(1))	ARA 1650
	CALL AITKEN (DTY,VE2,NLN,N,CZD,V(2))	ARA 1660
	CALL AITKEN (DTY,VE3,NLN,N,CZD,V(3))	ARA 1670
	CALL AITKEN (DTY,VE4,NLN,N,CZD,V(4))	ARA 1680
	CALL CHECK (V,4,MFLAG)	ARA 1690
	V(5)=V(4)/5.	ARA 1700
	CALL AITKEN (DTR,V,5,N,R,VN2)	ARA 1710
	XL=CZU-CZD	ARA 1720
	AR=AR+XL*6.2832*R	ARA 1730
	XN=(XN1+XN2)/2.	ARA 1740
	VN=(VN1+VN2)/2.	ARA 1750
	AN=AN+6.2832*R*XL*XN*VN	ARA 1760
	AZ=AZ+6.2832*R*L*XN**2*VN	ARA 1770
C		ARA 1780
C	WRITE OUT RESULTS	ARA 1790
C		ARA 1800
106	WRITE (6.113) AR	ARA 1810
	WRITE (6.112) AN	ARA 1820
	WRITE (6.114) AZ	ARA 1830
	F1=AR*XNEE/AN*VEA	ARA 1840
	F2=AR*XNEE**2/AZ*VEA	ARA 1850
	BPR=2.828*I2/(I1*XNEE)	ARA 1860
	WRITE (6.115) F1,F2,BPR	ARA 1870
	WRITE (6.116) NFLAG	ARA 1880
	WRITE (6.109) MFLAG	ARA 1890
	RETURN	ARA 1900
C		ARA 1910

107	FORMAT (2I5,4F10.4)	ARA	1920
108	FORMAT (2X, 9HI (CM-1)=,E11.4)	ARA	1930
109	FORMAT (2X, 40HNEGATIVE VELOCITY EXTRAPOLATION OCCURRED,IS, 7H TARA 1940 1IMES)	ARA	1950
110	FORMAT (10X,8(E10.3,2X))	ARA	1960
111	FORMAT (8F10.6)	ARA	1970
112	FORMAT (3X, 13HAN (CM2/CM3)=,E11.4)	ARA	1980
113	FORMAT (3X, 9HAR (CM2)=,E11.4)	ARA	1990
114	FORMAT (3X, 13HAZ (CM2/CM6)=,E11.4)	ARA	2000
115	FORMAT (2X, 3HF1=,F10.4,2X, 3HF2=,F10.4,2X, 13HI++/I+ FACTOR,F10ARA 2010 1.4)	ARA	2020
116	FORMAT (2X, 39HNEGATIVE DENSITY EXTRAPOLATION OCCURRED,IS, 8H TARA 2030 1IMES)	ARA	2040
C		ARA	2050
	END	ARA	2060
	SUBROUTINE CHECK (P,N,NFLAG)	CK	10
	DIMENSION P(N)	CK	20
	DO 101 I=1,N	CK	30
	IF (P(I).GE.0.0) GO TO 101	CK	40
	P(I)=0.0	CK	50
	NFLAG=NFLAG+1	CK	60
101	CONTINUE	CK	70
	RETURN	CK	80
C		CK	90
	END	CK	100
#			

